Piezoelectric Energy Harvesting From Water Droplet Impact

Mohammad Adnan Ilyas

Submitted for the degree of Doctor of Philosophy

Heriot-Watt University

School of Engineering and Physical Sciences

NOVEMBER 2020

ABSTRACT

In recent years there has been an increased interest in scavenging energy from ambient sources such as precipitation which is a freely available source occurring mainly in the form of raindrops. This work investigates the design analysis of a piezoelectric system, capable of converting the mechanical energy generated by the impact of water droplets into electrical energy. The system is not designed for any specific rain type and responds to the whole range of raindrops to provide energy to low-powered devices or applications. An off-the-shelf piezoelectric transducer with Polyvinylidene Difluoride (PVDF) polymer film was used as a water droplet impact harvester for this research.

Detailed analysis of water droplet impact harvester shows two distinct stages in the voltage output, first a logarithmic growth, then an exponential decay during a single droplet impact event. The energy of the growth stage was found to be much higher than that of the decay stage. Thus, growth stage of the impact process has a significant contribution to the overall output of the harvester. The experimental results show a power output of 2.5 µW with a 4 mm diameter droplet at a maximum height attained of 47 cm, which resulted in a low energy conversion efficiency of 0.12 %. A Harvester Array Model (HAM) then developed to characterise the output power of a single unit harvester, which is then applied to an array of rain impact harvesters.

An energy harvesting module is then developed consisting of multiple units where only one unit was excited. The module was tested during a single droplet impact event which generated a power of 3.6 µW and giving the energy conversion efficiency of 0.67 %. A technique was also presented which was able to identify the efficiency of the impact conversion mechanism as the droplet interacts with the device and the efficiency of the mechano-electric conversion mechanism due to internal losses.

Furthermore, a prototype is developed with multiple units and multiple impact events which resulted in an average power of 0.05 µW, over a light rain shower of 2.5 seconds with an array area of 0.003 m^2. A mathematical model of the prototype was presented to predict design parameters for different rainstorms. Harvested power in this research was found to be in the µW region. Nevertheless, with suitable energy technology it can provide power to specialist application for low-powered devices.

ACKNOWLEDGEMENTS

First and foremost, I would like to thank Almighty Allah for providing me the ability and strength to undertake this research study.

I would like to express my gratitude to my supervisor, Dr Jonathan Swingler for his continued support and guidance throughout this work. He truly has been a great mentor which has helped me develop as a researcher and provided me various opportunities to develop my skills and knowledge. I am extremely grateful that without his support this research would not have been possible.

I am grateful to School of Engineering and Physical Sciences for awarding me the EPS Scholarship which funded this research project. A special thanks to all the staff in Electrical, Electronic and Computer Engineering department for their constant support and encouragement over the years, particularly Dr Keith Brown, Dr Matt Dunnigan and Dr Umar Khan.

I would also like to thank all my friends who have had to put up with me during the highs and lows of last few years. Finally, I would like to thank all my family members for their love and support especially my mum, dad and little brother.

Research Thesis Submission

Please note this form should be bound into the submitted thesis.

Name*:*	Mohammad Adnan Ilyas		
School:	Engineering and Physical Sciences		
Version:*(i.e.First, Resubmission, Final)*	Final	Degree Sought:	PhD in Electrical Engineering

Declaration

In accordance with the appropriate regulations I hereby submit my thesis and I declare that:

1. The thesis embodies the results of my own work and has been composed by myself
2. Where appropriate, I have made acknowledgement of the work of others
3. The thesis is the correct version for submission and is the same version as any electronic versions submitted*.
4. My thesis for the award referred to, deposited in the Heriot-Watt University Library, should be made available for loan or photocopying and be available via the Institutional Repository, subject to such conditions as the Librarian may require
5. I understand that as a student of the University I am required to abide by the Regulations of the University and to conform to its discipline.
6. I confirm that the thesis has been verified against plagiarism via an approved plagiarism detection application e.g. Turnitin.

ONLY for submissions including published works

Please note you are only required to complete the Inclusion of Published Works Form (page 2) if your thesis contains published works)

7. Where the thesis contains published outputs under Regulation 6 (9.1.2) or Regulation 43 (9) these are accompanied by a critical review which accurately describes my contribution to the research and, for multi-author outputs, a signed declaration indicating the contribution of each author (complete)
8. Inclusion of published outputs under Regulation 6 (9.1.2) or Regulation 43 (9) shall not constitute plagiarism.

**Please note that it is the responsibility of the candidate to ensure that the correct version of the thesis is submitted*

Signature of Candidate*:*		Date:	

Submission

Submitted By *(name in capitals):*	
Signature of Individual Submitting:	
Date Submitted:	

For Completion in the Student Service Centre (SSC)

Limited Access	Requested	Yes		No		Approved	Yes		No	
E-thesis Submitted **(mandatory for final theses**)										
Received in the SSC by *(name in capitals):*						Date:				

Inclusion of Published Works

Please note you are only required to complete the Inclusion of Published Works Form if your thesis contains published works under Regulation 6 (9.1.2)

Declaration

This thesis contains one or more multi-author published works. In accordance with Regulation 6 (9.1.2) I hereby declare that the contributions of each author to these publications is as follows:

Citation details	M. A. Ilyas and J. Swingler, "Piezoelectric energy harvesting from raindrop impacts," Energy, vol. 90, pp. 796-806, 2015.
Author 1	Conducted literature review, carried out experimental work, analysed data and development of a MATLAB model.
Author 2	As the supervisor provided guidance for experimental work and data analysis, supported with the development of MATLAB model and proofread the paper.
Signature:	
Date:	

Citation details	M. A. Ilyas and J. Swingler, "Towards a prototype module for piezoelectric energy harvesting from raindrop impacts," Energy, vol. 125, pp. 716-725, 2017.
Author 1	Conducted literature review, produced CAD drawings for the test bench, carried out experimental work, analysed data and produced efficiency model.
Author 2	As the supervisor provided guidance for experimental work and data analysis, supported with the development of efficiency model and proofread the paper.
Signature:	
Date:	

Citation details	M. A. Ilyas, “Piezoelectric Energy Harvesting: Methods, Progress, and Challenges,” Energy Physics and Engineering Collection, Momentum Press, 2018.
Author 1	Conducted literature review, explored challenges, added more background information and wrote the book.
Author 2	N/A
Signature:	
Date:	

TABLE OF CONTENTS

ABSTRACT ..... **ii**

ACKNOWLEDGEMENTS ..... **iii**

TABLE OF CONTENTS ..... **vi**

LIST OF TABLES ..... **x**

LIST OF FIGURES ..... **xi**

NOMENCLATURE ..... **xv**

PUBLICATION LIST ..... **xvii**

1 Introduction **1**

1.1 Raindrop Energy Harvesting 1

1.1.1 Motivation 1

1.1.2 Scope 4

1.1.3 Application 6

1.2 Aims & Objectives 8

1.3 Thesis Structure 9

1.4 Major Contributions 10

1.5 Summary 11

2 Literature Review **13**

2.1 Mechanical to Electrical Generators 13

2.1.1 Electromagnetic 14

2.1.2 Electrostatic 15

2.1.3 Piezoelectric 16

2.1.4 Summary of Generators 18

2.2 Water Droplet Impact Harvesters 20

2.2.1 Fluid Impact Dynamics 20

2.2.2 Surface Interaction 24

2.2.3 Impact Force and Velocity 26
2.3 Behaviour and Distribution of Rain 27
2.3.1 Rain Types 27
2.3.2 Behaviour and Distribution of Rain 29
2.4 Review of Existing Rain Impact Harvesters 33
2.5 Performance of Rain Impact Harvesters 38
2.6 Summary 42
3 Piezoelectricity & Transducers 43
3.1 Piezoelectric Fundamentals 43
3.2 Piezoelectric Material Classification 47
3.2.1 PZT & PVDF 49
3.2.2 Material Selection and Structural Configurations 52
3.3 Single Degree of Freedom System 53
3.3.1 Free Vibrations of SDOF System under Impulse 53
3.3.2 Mechanical and Electrical Behaviour 55
3.4 Interface Circuit to Harvester 56
3.4.1 Full Bridge Rectifier 57
3.4.2 Voltage Doubler 57
3.4.3 Circuit Selection 58
3.5 Device Specification 60
3.6 Summary 62
4 Impact of Water Droplet on a Piezoelectric Transducer 64
4.1 Experimental Arrangement 64
4.2 Experimental Results 65
4.2.1 Initial Impact 65
4.2.2 Growth Stage 68
4.2.3 Decay Stage 70

4.3 Discussion of Implementation 73
4.3.1 Harvesting System Model 73
4.3.2 One Unit Harvester 76
4.3.3 An Array of Harvesters 77
4.3.4 Experimental Limitations and Assumptions 80
4.4 Summary 81
5 Single and Multiple Unit Module 83
5.1 Experimental Arrangement 83
5.1.1 Test Facility 83
5.1.2 Experimental Set-up 85
5.2 Single Unit 86
5.2.1 Voltage Measurements 86
5.2.2 Power and Energy Calculations 90
5.3 Multiple Unit Module 91
5.3.1 Voltage Measurements 91
5.3.2 Power and Energy Calculations 94
5.4 Analysis of Module Experiments 95
5.5 Energy Conversion Efficiency 97
5.5.1 Impact Mechanism 97
5.5.2 Mechano-Electric Mechanism 98
5.5.3 Overall Device and Module 99
5.6 Summary 100
6 Prototype Device & Final Discussion 101
6.1 Experimental Arrangement 101
6.2 Empirical Results 103
6.2.1 Voltage Measurements 103
6.2.2 Power Calculations 104

6.3 Comparison of Empirical Results with HAM 106
6.3.1 Empirical Data Analysis 106
6.3.2 Discussion of HAM 107
6.4 Log-Log Investigation 109
6.4.1 Empirical Data Analysis 109
6.4.2 Empirical Data Modelling 113
6.4.3 Log-log Discussion 115
6.5 Final Discussion 116
6.5.1 Single Event 116
6.5.2 Harvester Array Model 118
6.5.3 Power Output Comparison 118
7 Conclusion 121
7.1 Achievements 121
7.1.1 Investigation of a Single PEH Device 122
7.1.2 Investigation of a Harvester Module 123
7.1.3 Investigation of Prototype Device 123
7.1.4 Harvester Array Model 124
7.2 Objectives Achieved 124
7.3 Future Work 125
REFERENCES 128
APPENDICES 139
Appendix A 139

LIST OF TABLES

Table 1.1 : Harvested power from vibration/motion [33] 7
Table 1.2 : Power consumption of various battery-operated devices [36] 7
Table 2.1 : Comparison of energy densities [40] 18
Table 2.2 : Advantages and disadvantages of generators 20
Table 2.3 : Rain types along with terminal velocity and estimated impact force 28
Table 2.4 : Comparison of energy conversion efficiency of REH 39
Table 2.5 : Comparison of maximum output of water droplet energy harvesters 41
Table 3.1 : Piezoelectric constants 45
Table 3.2 : Piezoelectric parameters for PZT and PVDF [155, 156] 52
Table 3.3 : Comparison of PZT and PVDF 53
Table 3.4 : Model frequency of piezoelectric unimorph cantilever [163] 55
Table 3.5 : Piezo transducer specification 61
Table 4.1 : Kinetic energy of water droplets 74
Table 5.1 : Peak voltage at various surface conditions 88
Table 6.1 : Prototype device specification 101
Table 6.2 : Storm type characterisation 107
Table 6.3 : Power law parameters for distribution function 110
Table 6.4 : Power law parameters for CDF 113
Table 6.5 : Power output of the research study 119

LIST OF FIGURES

Figure 1.1 Representation of a self-powered energy system 2
Figure 1.2 (Left) Energy harvesting using an oscillating human index figure [22] and (Right) Flexible piezoelectric device attached to fish-aggregating device [23]. 4
Figure 1.3: Annual UK rainfall data for 2019 [29] 5
Figure 1.4: Summary of work conducted in this thesis 10
Figure 2.1: Selection of harvesting sources and potential applications using piezoelectric devices [38] 13
Figure 2.2: Model of a single degree-of-freedom electromagnetic vibration energy harvester [39] 14
Figure 2.3: Equivalent circuit diagram of electrostatic generator [41] 15
Figure 2.4: Model of a single degree-of-freedom piezoelectric vibration energy harvester [39] 17
Figure 2.5: Circuit representation of a piezoelectric generator [53] 18
Figure 2.6: Power density versus voltage for batteries and regenerative power supplies [57] 19
Figure 2.7: Depiction of contact angle on a homogenous surface [64] 21
Figure 2.8: Depiction of water droplet impact on solid surface 22
Figure 2.9: Depiction of water droplet impact on a liquid layer surface 22
Figure 2.10: Beam-tip displacement of a cantilever for hydrophobic and hydrophilic surfaces [75] 25
Figure 2.11: Impact force of water droplet on solid surface against (a) velocity and (b) diameter [83] 27
Figure 2.12: Average annual rainfall data for 24 tropical regions [87] 29
Figure 2.13: Set of 1 million random numbers described in the text which have a power-law distribution (a) normal scale and (b) logarithmic scales [93] 31
Figure 2.14: Cumulative distribution of the number of hits received on a website [95] 32
Figure 2.15: Examples of parabolic fractal law number versus concentration [97] 32
Figure 2.16: Example of cumulative distribution showing exponential power law [100] 33
Figure 2.17: System design of the randrop energy harveter [102] 34
Figure 2.18: Voltage and enrgy profiles as a function of mechanical energy [102] 34

Figure 2.19: Arrangements for PVDF transducers (a) Single cantilever and (b) Collecting diaphragm [106] 35
Figure 2.20: (a) Design of hardware circuit and (b) System design of plate [107] 36
Figure 2.21: (a) Fabrication steps for the design and (b) Meshed model of piezoelectric harvester [108] 37
Figure 2.22: Rain event (a) experimental setup and (b) raindrop count and instantaneous energy graphs over time duration 38
Figure 3.1: Simple molecular model to explain piezoelectric effect [129] 44
Figure 3.2: Piezoelectric material in relation to direction of polarization [130] 45
Figure 3.3: Representation of piezoelectric material in (a) 31 mode and (b) 33 mode [136] 47
Figure 3.4: Classification of piezoelectric materials 47
Figure 3.5: Schematic of Heel Strike generator [152] 50
Figure 3.6: Output voltage at no load over mass for PZT arrangement [153] 50
Figure 3.7: Output power against resistive load [153] 51
Figure 3.8: Polymerisation and structure of PVDF [84] 51
Figure 3.9: (a) EMFi and (b) PVDF sensor structures [154] 52
Figure 3.10: Cantilever beam under free vibrations 54
Figure 3.11: Cantilever beam under impulse 54
Figure 3.12: Equivalent circuit model for harvester 56
Figure 3.13: Circuit diagram of full bridge rectifier 57
Figure 3.14: Circuit diagram of voltage doubler 57
Figure 3.15: Schematic for (a) Rectifier circuit and (b) Trigger circuit for microgenerator [168] 58
Figure 3.16: Voltages on the load for single droplet using different rectifying circuits [106] 59
Figure 3.17: Output of full-bridge rectifier and voltage doubler with and without ideal diodes [169] 60
Figure 3.18: Schematic of Pro-Wave FS-2513P 61
Figure 3.19: Schematic of cantilever beam 62
Figure 4.1: Experimental setup to measure impact of single droplet 65
Figure 4.2: Voltage output and sensor position profiles of the device 66
Figure 4.3: Voltage output of harvester for one event (Raw data) 67
Figure 4.4: Peak voltage from harvester 68

Figure 4.5: (a) Power, (b) Duration and (c) Energy output of the log growth stage of one event 70
Figure 4.6: (a) Decay constant and (b) Time constant for one event 71
Figure 4.7: (a) Power, (b) Duration & (c) Energy output of the exponential decay stage of one event 72
Figure 4.8: Relating droplet fall height to velocity 74
Figure 4.9: (a) Peak voltage from raindrop velocity and (b) Volt per impact characteristic of the harvester 75
Figure 4.10: Output of the device 76
Figure 4.11: Mean power found from model 78
Figure 4.12: Power output for HAM at (a) $1m^2$ and (b) $10m^2$ 79
Figure 4.13: Power output from an array for different droplet impact velocity 80
Figure 5.1: Impact of water droplets on PEH device 84
Figure 5.2: Schematic of test facility 84
Figure 5.3: Impact region on the PEH device 85
Figure 5.4: Circuit diagram of parallel connection with n number of units (a) non-rectified module and (b) rectified module 86
Figure 5.5: Parameters of single PEH device (a) peak voltage, (b) power output from harvester, (c) energy output 87
Figure 5.6: Device output in different conditions (a) Dry device and (b) Wet device with frequency of oscillation of 250 Hz 89
Figure 5.7: Non-rectified voltage output of Unit 1 with six additional units added in parallel 92
Figure 5.8: Rectified voltage output of Unit 1 with six additional units added in parallel 93
Figure 5.9: Parameters of the module (a) peak power, (b) RMS voltage, (c) energy delivered 94
Figure 5.10: Equivalent circuit model of the module with multiple units 96
Figure 5.11: Finding the excitation voltage $Vstm(0)$ 98
Figure 5.12: Finding the internal resistance (losses) $R0$ of a harvester 99
Figure 6.1: Prototype device (a) and (b) Rectifying circuit 102
Figure 6.2: Experimental equipment and set-up 102
Figure 6.3: One experimental run voltage profiles for (a) 0.5 second, (b) 1 second and (c) 2.5 seconds 104

Figure 6.4: One experimental run peak power profiles for (a) 0.5 second, (b) 1 second and (c) 2.5 seconds 105
Figure 6.5: Empirical data for prototype device with all experimental runs 107
Figure 6.6: Power output from HAM 108
Figure 6.7: Example distributive profile of data gathered in a time period of 0.5 seconds 109
Figure 6.8: Distribution function of empirical data for 0.5 second, 1 second and 2.5 seconds 111
Figure 6.9: CDF of empirical data for 0.5 second, 1 second and 2.5 seconds 112
Figure 6.10: Modelled plot of P_{ref} 115
Figure 6.11: Proposed use of HAM 118
Figure 7.1: Harvester system with a spoon [184] 126
Figure 7.2: Large harvesting system with advanced Arduino-based measuring system [108] 127

NOMENCLATURE

Abbreviations

Acronym	Description
AI	Artificial intelligence
CDF	Cumulative distribution function
CEH	Combined energy harvesting
DSD	Drop size distribution
EH	Energy harvesting
EMF	Electromotive force
FAD	Fish-aggregating device
FPED	Flexible piezoelectric device
HAM	Harvester array model
HT	Heavy thunderstorms
IoT	Internet of Things
K-H	Kelvin-Helmholtz
LSR	Light stratiform rain
MEMS	Micro-electromechanical systems
MOSFET	Metal Oxide Semiconductor Field Effect Transistor
MSR	Moderate stratiform rain
PDF	Probability distraction function
PDMS	Polydimethylsiloxane
PEH	Piezoelectric energy harvesting
PL	Power law
PP	Polypropylene
PV	Photovoltaic
PVC	Polyvinyl chloride
PZT	Lead zicronate titanate
PVDF	Polyvinylidene flouride
RF	Radio frequency
REH	Raindrop energy harvesting
RL	Circuit with resistor and inductor
RLC	Circuit with resistor, inductor and capacitor

RMS	Root mean square
ST	Splashing threshold
SDOF	Single degree of freedom
STM	Simplified theoretical model
SWL	Sea water level

PUBLICATION LIST

A) Published

1. Ilyas MA, and Swingler J, "Piezoelectric energy harvesting from raindrop impacts," *Energy*, vol. 90, pp. 796-806, 2015.

2. Ilyas MA, and Swingler J, "Towards a prototype module for piezoelectric energy harvesting from raindrop impacts," *Energy*, vol. 125, pp. 716-725, 2017.

3. Ilyas, MA, "Piezoelectric Energy Harvesting: Methods, Progress, and Challenges," *Energy Physics and Engineering Collection*, Momentum Press, 2018.

B) Pending publications

1. Ilyas MA, and Swingler J, "Analysis of prototype module using water droplet impacts on piezoelectric energy harvesting," – To be submitted to the *International Journal of Energy Conversion and Management*, end of 2020.

CHAPTER 1

1 Introduction

Making better use of energy resources is just as important as finding alternative sources of supply. Advancement in technology becomes more important with ever-growing energy demand. Conventional technologies may have the potential and high efficiencies in meeting this ever-growing demand but have a significant impact on the environment and finite resources. Energy harvesting (EH) techniques can be used to scavenge energy using ambient sources which have the potential to provide electrical power to electronic systems with various applications in hand-held devices [1], implantable medical devices [2], health monitoring systems [3] and sensors [4, 5].

The use of fossil fuels in conventional technologies is likely to continue for the foreseeable future particularly in underdeveloped countries where there is no legislation to reduce the carbon footprint. Even though significant progress has been made in decreasing carbon dioxide (CO_2) emissions from conventional fossil fuel technologies, the need for development of novel technologies harvesting energy from ambient sources has become important than ever. The work in this thesis, investigating the design analysis of piezoelectric energy harvesting (PEH) system scavenging energy from raindrops will help better understand the feasibility and effectiveness of such methods.

1.1 Raindrop Energy Harvesting

1.1.1 Motivation

The growth of the global energy sector is constantly under review to ensure new energy technologies are developed with an emphasis on multi-disciplinary research. Smart, flexible and clean energy technologies have been identified as one of the key areas to solve the energy challenge of supplying sustainable and affordable energy securely to ever more-demanding societies around the world.

A self-powered energy system can be defined as consisting of 3 distinct stages; generation, conversion and consumption as represented in Figure 1.1. Energy generation stage requires a harvester system and energy source. Energy conversion stage requires power management circuitry and system that trades and optimises the energy harvested in the energy generation block to energy consumption. Energy conversion could also integrate storage technology that could be used to accumulate energy from the harvester and provide it to the system whenever sufficient energy is available or needed.

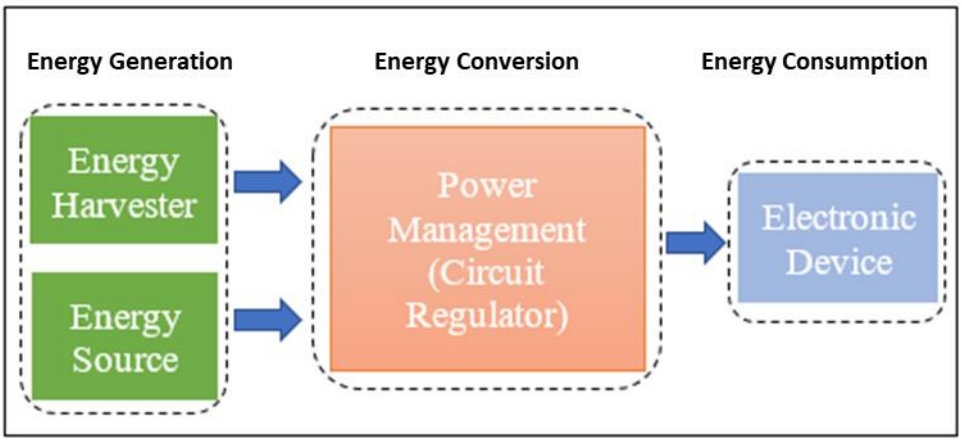

Figure 1.1 Representation of a self-powered energy system

Self-powered energy systems or machines are increasingly being commercialised due to low power electronics. The idea of harvesting energy from ambient sources attracts new harvesting techniques and novel applications. These systems come in various shapes and sizes, ranging from a tiny device to a large-scale system. These devices can operate without any human intervention which makes it a valuable proposal. With the rise in automation and artificial intelligence (AI), applications for these self-powered devices are vast. Some of the applications of such a system includes; autonomous vehicles [6] , delivery robots [7] and self-sustainable energy harvesting systems [8].

In a traditional context, there are many energy fields available [9] that can be harvested to provide electrical energy. Solar, wind and tidal sources are generally known for higher energy outputs that can power our growing demand for electrical energy. A significant amount of research has been devoted to developing and over-coming challenges faced by renewable energy technologies.

A few approaches to EH with significant results include:

- Solar energy is free and rather available in abundance in many parts of the world. There are various methods by which energy can be harvested which include solar thermal collectors [10] or photovoltaic (PV) technology [11], by absorbing sunlight to convert it into electrical energy.
- Thermal gradient (or temperature difference) exists around us either naturally present or manmade. Two main methods by which we can utilise this thermal gradient include pyroelectric energy harvesting capabilities [12] or thermoelectric energy harvesting [13], for converting this wasted heat into electrical energy.
- Combined energy harvesting (CEH) system utilising PV and Thermoelectric devices [14-16] using hybrid systems to scavenge more than one energy.
- Vibrational energy is available just about everywhere in the urban and industrial environment, but it is often overlooked as a source of power to be scavenged. Researchers have been successful in testing such piezoelectric generators embedded in a highway [17], transducers embedded in pavements [18] or triboelectric generator [19], for converting mechanical energy into electrical energy under the action of mechanical stress.
- Electromagnetic radiation carries radiant energy which can be used to power devices by using systems such as radio frequency (RF) energy harvesting [20] or an acoustic metamaterial harvester [21].

Over the last few years, the focus of providing energy has drifted more towards low-powered devices and electronics, such as mobile/handheld devices, sensors etc. With this new focus towards low-powered devices that rely on regenerative source, various approaches to EH particularly vibration and motion can be utilised to power such electronic devices.

Mechanical energy in the form of motion or vibration opens new applications and innovative approaches using PEH techniques to power various devices. PEH devices use vibrations, motion, or acoustic noise as the source of external energy which can be converted to electrical energy. Various harvester systems are being developed to utilise untapped energy sources to provide electrical energy using PEH techniques. Figure 1.2 shows two such examples where energy is being harvested from ambient sources. Firstly, using motion from an index finger [22] which has the potential to use flexible and

stretchable harvester that can convert the muscle movement to electrical charges by using a piezoelectric nanogenerator. Secondly, a larger system of flexible piezoelectric device (FPED) developed [23] is integrated on to a fish-aggregating device (FAD) that was floated near the sea water level (SWL) moored by a chain to harvest wave motion to produce electricity. Both harvesting systems showcase the potential of vibration/motion as novel applications.

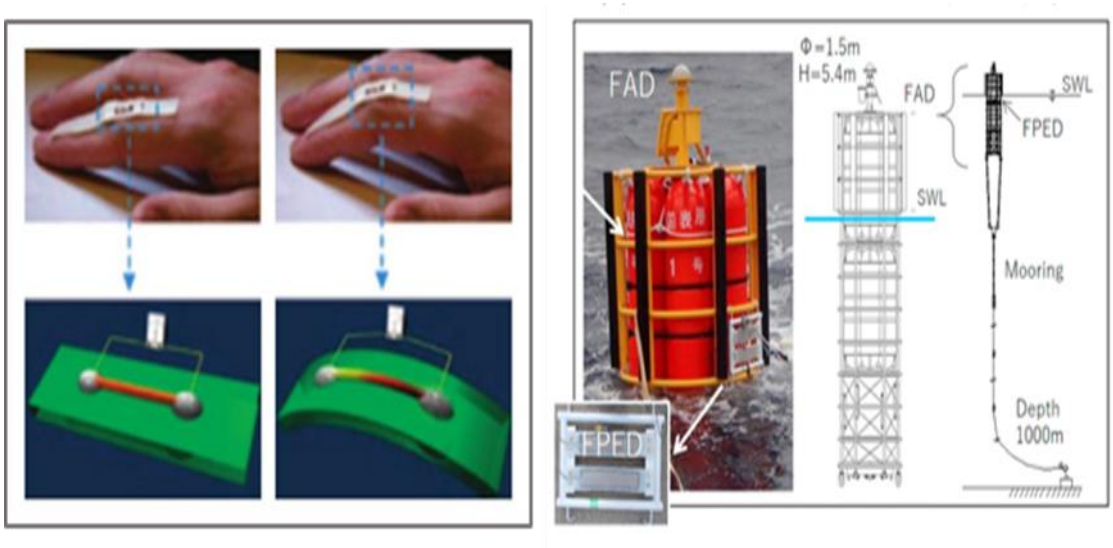

Figure 1.2 (Left) Energy harvesting using an oscillating human index figure [22] and (Right) Flexible piezoelectric device attached to fish-aggregating device [23].

1.1.2 Scope

Research within the energy sector has attracted tremendous attention as clean energy becomes a hot issue. In 2008, the UK government passed the 'Climate Change Act 2008' to ensure that the net UK carbon account by the year 2050 is at least 80% lower than the 1990 baseline [24] . In 2019 due to changing public perception, a new legislation commits to net zero greenhouse gas emissions by the year 2050 [25]. Energy has been the biggest contributor to CO_2 emissions from the combustion of fossil fuels [26] but over the last decade a shift towards renewable energy sources has meant the contribution from energy sector towards these emissions has been reduced significantly in comparison to other sectors [27]. Whilst research advancements are made on large-scale power generation the focus of this research is on small-scale power generation.

EH from the impact of raindrops has been gaining significant research interest over recent years by a handful of groups, but the potential has yet to fully unlocked. It is this raindrop

energy harvesting (REH) that is the focus of this study. Many geographical locations receive a moderate to heavy rainfall which can then be utilised to generate electricity as an alternative method to conventional fossil fuel generation and other mainstream renewable energy technologies.

One of the earliest studies conducted [28] recommended the use of harvesting devices based on impact of raindrops for remote areas and cities not connected to the grid system in Bangladesh. The emphasis in the country has been on renewable energy primarily in the form of solar systems to address the problem of connecting these remote locations to electricity network. Solar systems are effective during a sunny spell but prove ineffective during monsoon season. Bangladesh as an example, routinely has around 4 months of monsoon season, which could find the implementation of a REH system to be very beneficial. Rain pattern of Bangladesh highlights this as a very favourable source for energy output using EH techniques to harness the power of raindrops, depending on the location and time of the year.

United Kingdom is known for being wet and windy, which makes it an ideal location for using renewable energy technologies that harvest these ambient sources. The Metropolitan Office published data which gives a total provisional rainfall of 1210 mm in 2019. Figure 1.3 depicts the rainfall data of 2019 compared to the average of rainfall recorded from 1981-2010, with the highest and lowest rainfall recorded as 1460 mm and 820 mm, respectively.

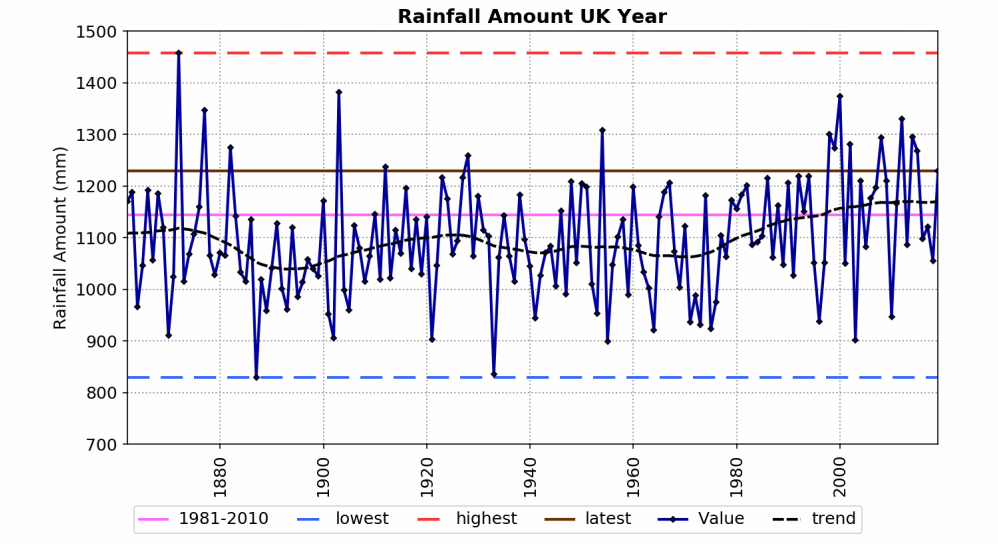

Figure 1.3: Annual UK rainfall data for 2019 [29]

Based on the data published by the Metropolitan Office of the UK, which gave a modest average rainfall amount of 1210 mm. Therefore, we can make a theoretical estimation of the recoverable energy of rainfall within the UK:

- UK's land area is around 243,305 km^2 [30]
- Volume of rainfall deposited in 2019 is estimated as 2.94×10^8 m^3
- Total body of water is estimated as 2.94×10^{11} (assuming 1 m^3 water is equivalent to 1000 kg of mass)
- Cloud height above ground level for low level clouds is estimated at around 2000 m [31]
- Maximum velocity of raindrops (typical diameter of 5 mm) can be calculated as around 9 m/s [32]

$$Potential\ Energy = mgh \tag{1.1}$$

$$Kinetic\ Energy = \frac{1}{2}mv^2 \tag{1.2}$$

By using Equation 1.1, potential energy can be calculated as 5.8×10^{15} J and by using Equation 1.2, kinetic energy can be calculated as 1.2×10^{13} J. It is understood that this estimated available energy is considerably higher than what is practically possible but highlights a major untapped energy source. There are various factors which have an impact on the output of implementing such a harvester to scavenge raindrop energy some of them include factors such as the design of harvester, energy conversion and losses of the harvester system, and behaviour of rainstorms. These factors are discussed in subsequent chapters in more depth, along with presenting an optimal harvesting model based on an off-the-shelf piezoelectric transducer.

1.1.3 Application

There is a lot of scope for developing harvesters based on vibration or motion due to the great potential identified. Raindrop or water droplet impact can provide kinetic energy to such a harvesting system powering up low-powered devices or electronic systems. The challenge is to provide efficient and sustainable power for micro to macro level applications. Table 1.1 represents a comparison of harvested power using vibration or motion which has great potential.

Table 1.1 : Harvested power from vibration/motion [33]

Energy Source	Harvested Power
Human	4 μW/cm^2
Industry	100 μW/cm^2

Currently batteries are in wide use for many electronic devices or systems depending on their functionality which makes us highly dependent on batteries as the power source to these devices. Even though batteries have proven to be a good source of power but have many disadvantages mainly due to their size, weight, safety, and service life. Emerging applications like wireless micro-sensor networks [34] and micro electromechanical systems (MEMS) [35] are a couple of such examples that can integrate EH techniques to provide power needed for their operation. Replacing batteries in such devices becomes difficult because of the complexity and size but a favourable solution to power up such devices would be to have a battery-less operation by which can scavenge energy from the environment through EH techniques.

Many portable or handheld devices such as MP3 players, hearing aids and pacemakers are all operated by household batteries. Types of batteries used in such devices can vary from lithium-ion to alkaline. In many cases the battery life is limited to either days or months which is not always ideal for operation. Even though the shift to rechargeable batteries has reduced the environmental impact, the challenge of reliability, size and life of batteries remains a big issue. Table 1.2 shows the typical power consumption of such devices which generally can be as little as in the μW range.

Table 1.2 : Power consumption of various battery-operated devices [36]

Device	Power consumption	Energy autonomy
Smartphone	1 W	5 hours
MP3 player	50m W	15 hours
Hearing aid	1 mW	5 days
Wireless sensor node	100 μW	Lifetime
Cardiac pacemaker	50 μW	7 years
Quartz watch	5 μW	5 years

Research within the field of PEH has attracted a lot of attention in recent years as scavenging low grade ambient energy sources such as environmental vibrations and human power into usable electrical energy. Such devices are therefore potentially attractive as replacements for primary batteries in low power electronics or integrated with other harvesters to explore combined energy harvesting (CEH), which has the potential to improve the power output.

The growing field of EH is envisaged to support systems in new ways that have not been explored before on a commercial basis. IDTechEx research study has predicted that investment in energy harvesting technologies will grow to a substantial amount and will create billion-dollar businesses in the sector over the next decade. It is estimated that the market for piezoelectric energy harvesters will reach over $1 billion by 2029 [37].

1.2 Aims & Objectives

This work investigates the design analysis of a PEH system, capable of converting the kinetic energy generated by the impact of raindrops into electrical energy. Specialist application for such a harvesting system paves way to utilising this concept at providing energy to low-powered devices or electronics.

Main objectives include the following:

1. **Review**

   Critically review state-of-the-art publications on piezoelectric energy harvesting using impact of water droplets and outline parameters that describe the performance of such an approach.
2. **Investigate**

   Conduct experimental work on a piezoelectric device using single impact of droplet, multiple units with single impact of droplet and multiple units with multiple impacts of droplet.
3. **Model**

   Development of an empirical energy harvesting model based on the impact of water droplet on a piezoelectric device and develop a technique to explore the energy conversion efficiency.

4. **Build**

   Construct a prototype capable of harvesting power from a whole range of raindrops and present a mathematical behaviour to predict design parameter

5. **Evaluate**

   Assess the feasibility of this study and recommend future work for the areas of implementation.

1.3 Thesis Structure

The methodology of this research study is mainly based on four main parts, which include the following:

- Review of literature and mechanical/electrical behaviour of water droplet impact harvesters.
- Proof of concept through empirical study of single droplet impact on an off-the-shelf piezoelectric transducer and developing a harvestor model in MATLAB.
- Conducting experimental tests on multiple piezoelectric devices and developing a prototype capable of operating with multiple impacts (responds to whole range of raindrops).
- Presenting a mathematical behaviour of the developed prototype harvester which can predict parameters for a variety of rainstorms.

Firstly, a literature review is conducted in Chapter 2 with a particular focus on water droplet impact harvestors. Chapter 3 provides background in piezoelectricity, materials used for PEH devices, reviews the mechanical and electrical behaviour of a piezoelectric device and presents the experimental arrangement. The subsequent chapters provide the key contributions of this research. Chapter 4 investigates the power output of a single piezoelectric transducer, develops an empirical model for the harvester and presents the idea of an array of harvesters. Chapter 5 further explores this concept of harvesting energy from raindrops by conducting further experimental work using PEH devices in various formations; single transducer with single droplet impact with different surface conditions, multiple transducers with single droplet impact with and without rectification to explore

the coupling effect. This chapter also presents the energy conversion efficiency which relates to the impact mechanism and mechano-electric mechanism. Chapter 6 studies the implementation of a prototype with multiple PEH devices undergoing multiple events replicating a rainstorm and presents a mathematical model for the design of a harvesting system based on water droplet impacts. Chapter 7 concludes the work carried out in this research and proposes future work in this field.

Figure 1.4 presents the summary of the main work carried out in this research where the rainstorm and harvester type are parameters that can't be changed, however work is carried out to explore the impact mechanism, develop a model for the harvester, conduct experimental work on single and multiple units of piezoelectric transducer, development of a prototype based on the learnings from single and multiple units which feeds in to developing a mathematical behaviour to predict expected power characteristics of this prototype.

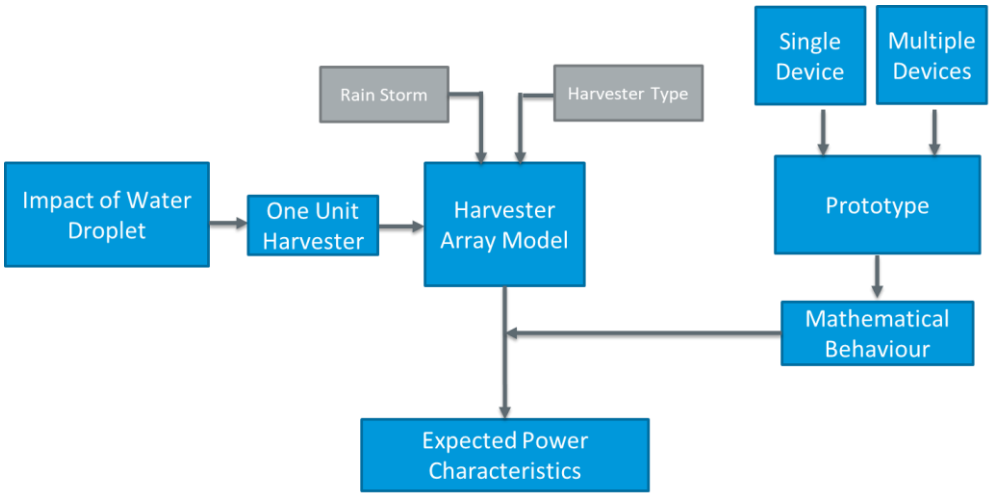

Figure 1.4: Summary of work conducted in this thesis

1.4 Major Contributions

The thesis presents novel work carried out in piezoelectric energy harvesting using water droplet impacts.

- Detailed analysis of raindrop impact on a piezoelectric transducer showing an oscillating profile which consists the impact (log growth) and decay (exponential) stages.

- Development of an energy harvesting model using a single piezoelectric transducer.
- Presentation of techniques to identify the efficiency of piezoelectric transducer which can be classified in to two main stages: the impact mechanism and mechano-electric conversion mechanism.
- Development of a working prototype device tested in replicated rain shower and presentation of mathematical behaviour to predict harvesting parameters with various rainstorm types.

Some of the findings of this research have been published in the International Journal of Energy (Elsevier) with an impact factor of over 5.5. The two peer reviewed journal articles were published in 2015 and 2017 and monograph was published in 2018. A fourth publication is currently being drafted which is aimed to be submitted by the end of 2020.

List of publications include:

1) M. A. Ilyas and J. Swingler, "Piezoelectric energy harvesting from raindrop impacts," *Energy*, vol. 90, pp. 796-806, 2015.
2) M. A. Ilyas and J. Swingler, "Towards a prototype module for piezoelectric energy harvesting from raindrop impacts," *Energy*, vol. 125, pp. 716-725, 2017.
3) M. A. Ilyas, "Piezoelectric Energy Harvesting: Methods, Progress, and Challenges," *Energy Physics and Engineering Collection*, Momentum Press, 2018.

1.5 Summary

This chapter outlined the key objectives of this research, methodology and major contributions. EH from ambient sources has become incredibly important as the focus from large-scale power generation moves to providing electrical energy to low-powered devices. PEH techniques have shown great potential and can power devices and electronics using mechanical energy which is converted to electrical energy. A successful integration of such harvesters will diminish the use of batteries which have a harmful impact to the environment. Energy output using such a system is very low in comparison to other forms of renewable power generation but may be sufficient to power electronic devices in specialist low power applications where use of batteries is not considered a

feasible option. Additionally, the battery-less application is becoming more frequent because of the limitations due to size, weight, environmental impact and life of the battery.

It has been established that it rains a lot in the UK which is an untapped energy resource that could be utilised to power electronics. A theoretical estimate shows that we can harvest up to 11 TJ of kinetic energy using a PEH system based on the kinetic energy available from raindrops. However, it is understood that this value of kinetic energy relates to capturing all the raindrops, which is not a practically possible. The estimated energy does provide the starting point to focus this research on scavenging ambient source of raindrops. The energy output in REH devices, broadly depends on fluid dynamics (impact and surface interaction), velocity at which the droplet impacts the harvester and distribution/behaviour of rain which will be explored further in subsequent chapters. This leads to Chapter 2, which will present an in-depth background study and review of harvesting technique using water droplet impact harvesters.

CHAPTER 2

2 Literature Review

There are various methods to develop EH systems that utilise the conversion from mechanical energy to electrical energy. REH systems use kinetic energy from the impact of raindrops on a PEH device to harvest power. This chapter covers literature review for mechanical to electrical generators, fluid dynamics associated with water droplet impacts and provides an overview of existing harvesters.

2.1 Mechanical to Electrical Generators

A significant amount of research has been devoted to developing and understanding EH systems. Mechanical energy can be found almost anywhere, and vibration sources such as ocean waves and human motion makes converting mechanical energy to electrical energy an attractive approach. Figure 2.1 shows such possible vibrational ambient sources available within manufacturing industry, transport and precipitation in the form of a rain, and highlights some potential applications which range from biomedicine to defence.

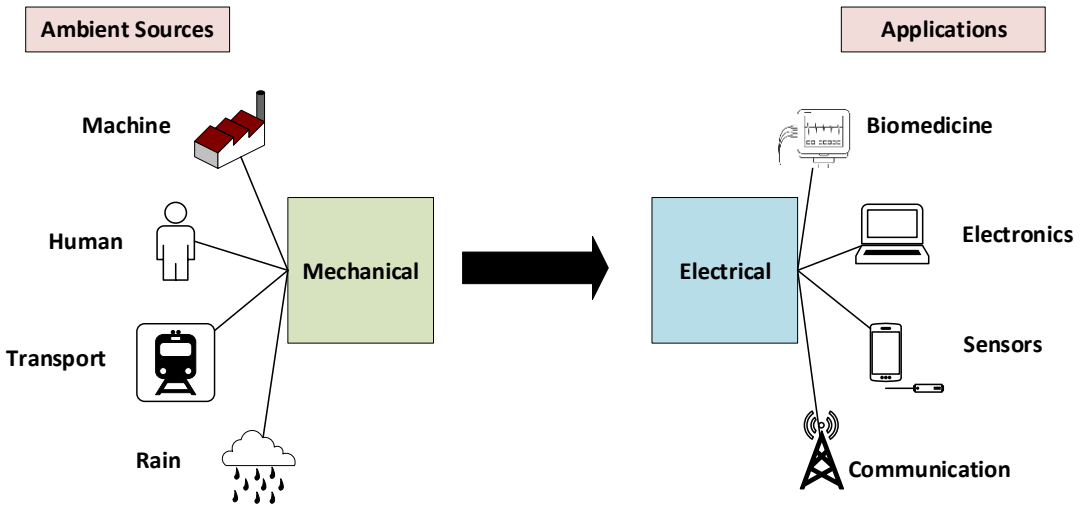

Figure 2.1: Selection of harvesting sources and potential applications using piezoelectric devices [38]

There are three categories within mechanical to electrical generators: electromagnetic, electrostatic and piezoelectric.

2.1.1 Electromagnetic

In 1831, electromagnetic induction was discovered by Michael Faraday. Faraday's law of electromagnetic induction pretty much defines the working principle of most electrical motors, generators, and transformers. Faraday's law states that any change in the magnetic field of a coil will cause voltage to be induced which is referred to as electromotive force (EMF). EMF in the coil can be determined by Faraday's law, which is the rate of change of magnetic flux, where φ is the magnetic flux:

$$emf = -\frac{d\varphi}{dt} \qquad 2.1$$

The direction of EMF is determined by Lenz's law which states that magnetic field created by induced current opposes the changing magnetic field and the negative sign in Equation 2.1 comes from Lenz's law.

A single degree-of-freedom (SDOF) model of an electromagnetic vibration energy harvester presented in Figure 2.2 can be described as a simple RL circuit (which contains the impedance of the coil connected in series with a resistive load). A mass is connected by means of a spring where k is the elastic modulus (stiffness of the spring), $\ddot{y}$ is the acceleration applied to the base, z is the displacement of mass and B is the magnetic field. Vibrations cause a translational movement of the magnet which in turn causes a change of magnetic flux inside the coil due to the oscillating movement.

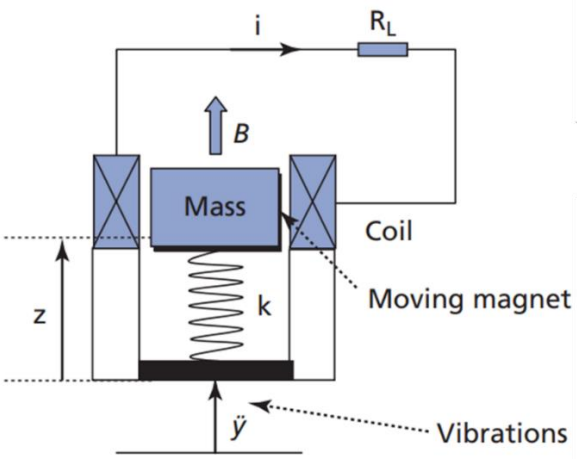

Figure 2.2: Model of a single degree-of-freedom electromagnetic vibration energy harvester [39]

Open circuit voltage (V_{oc}) in Figure 2.2 can be determined where N is the number of turns in the coil, B is the magnetic induction, l is the length of windings and z is the relative displacement between the magnet and the coil [40]:

$$V_{oc} = NBl\frac{dz}{dt} \tag{2.2}$$

2.1.2 Electrostatic

An electrostatic generator relies on the variable capacitor which is driven by mechanical vibrations. As the charge in the capacitor gets constrained it moves from the capacitor to the load. This way the mechanical energy is converted into electrical energy.

An adaptation of the circuit diagram representation of an electrostatic generator is shown in Figure 2.3 where C_V is the variable capacitor and C_L is the load. The maximum voltage across the load can be determined but we need to define other parameters first.

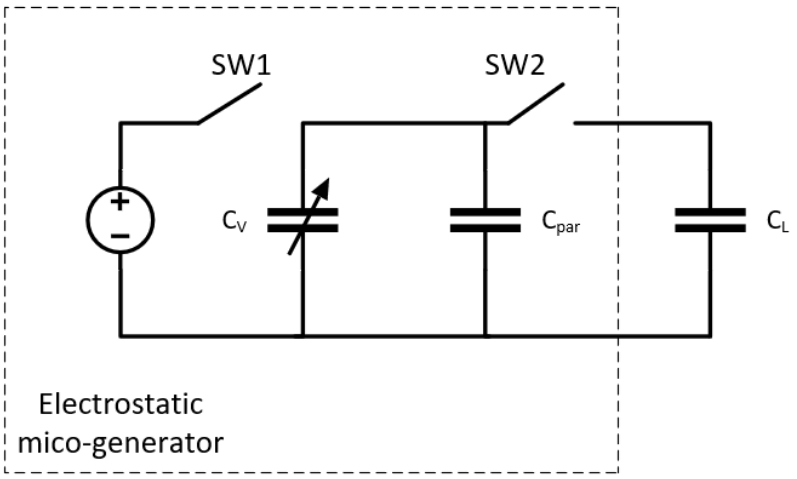

Figure 2.3: Equivalent circuit diagram of electrostatic generator [41]

Generally, capacitance can be defined by Equation 2.3, where Q is the charge on the plates and V is the voltage on the plates.

$$C = \frac{Q}{V} \tag{2.3}$$

For a parallel plate capacitor the expression can be re-written as Equation 2.4, where ε_0 is the dielectric permittivity of free space, ε_r is the relative dielectric permittivity of the

material between the capacitor plates, A is the area of the capacitor plates, and d_s is the distance between the plates.

$$C = \frac{\varepsilon_0 \varepsilon_r A}{d_s} \quad 2.4$$

Electrostatic generators consist of a capacitor related to the displacement. Equation 2.5 can be deduced for current in an electrostatic generator [42] , where V is the voltage when capacitor is charged, V_o is the initial voltage and C is the capacitance.

$$I = V_o \frac{dC(z)}{dt} + C(z)\frac{dV}{dt} \quad 2.5$$

2.1.3 Piezoelectric

Piezoelectric harvesters consist of an active dielectric material, the piezoelectric, which is plated with a conductor or has an arrangement of a conductor to capture the electric charge developed due to mechanical displacement.

PEH devices use vibrations, motion or acoustic noise as the source of external energy which can be converted to electrical energy. These are typically used for application with low power requirements such as powering sensor equipment from ambient vibrations [43], MEMS application [44], wireless sensor [45], and military applications [46]. Although significant progress has been made in this field in the development of micro-scale power supplies, power management and consumption, there remains a need to improve these further with the advent of the Internet of Things (IoT).

A piezoelectric material can produce an electric charge when the material undergoes mechanical stress. There are many materials such as quartz and tourmaline crystals that exhibit this piezoelectric effect. Such materials have in the past been actively used as electromechanical transducers [47]. The ferroelectric group of materials which exhibit the piezoelectric effect are also known as piezoelectric materials. Ferroelectric ceramics such as lead zirconate titanate (PZT) are widely used in EH due to their favourable properties and much discussion can be found in the literature on these [48, 49]. PZT harvesters have been considered to be a prospective replacement for batteries in some applications due to their high piezoelectric character and energy output. Polymers such as polyvinylidene

fluoride (PVDF) are mainly used in applications requiring a higher degree of mechanical flexibility and optical transparency. These polymers are relatively cheap and can be easily integrated into various applications; in garments [50] or shoes [51]. These polymers also exhibit unique features such as demonstrating excellent mechanical behaviour, being corrosion resistant, having the ability to withstand stress without structural fatigue and illustrating ease of processability on dielectric thin films. In particular, these polymers have the potential to be integrated into flexible devices [52].

A SDOF model of a piezoelectric vibration energy harvester presented in Figure 2.4. A mass is connected by means of a spring where k is the elastic modulus (stiffness of the spring), $\ddot{y}$ is the acceleration applied to the base, z is the displacement of mass. Vibrations cause a movement of the magnet which in turn applies force on the piezoelectric element due to the oscillating movement.

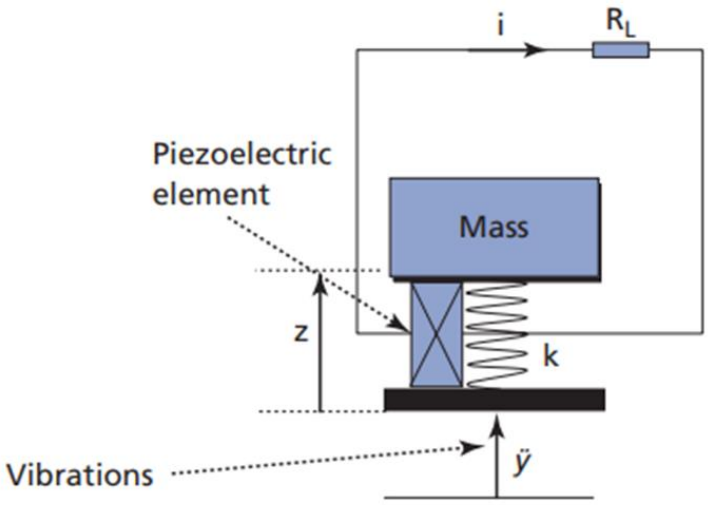

Figure 2.4: Model of a single degree-of-freedom piezoelectric vibration energy harvester [39]

Figure 2.5 represents the circuit representation of a piezoelectric generator where both the mechanical and electrical components of the circuit are shown. This is modelled as a transformer where L_m is mass of generator, R_b is mechanical damping, C_k is mechanical stiffness, n equivalent turns ratio of the transformer, C_b is capacitance of piezoelectric and V is the voltage across the piezoelectric generator.

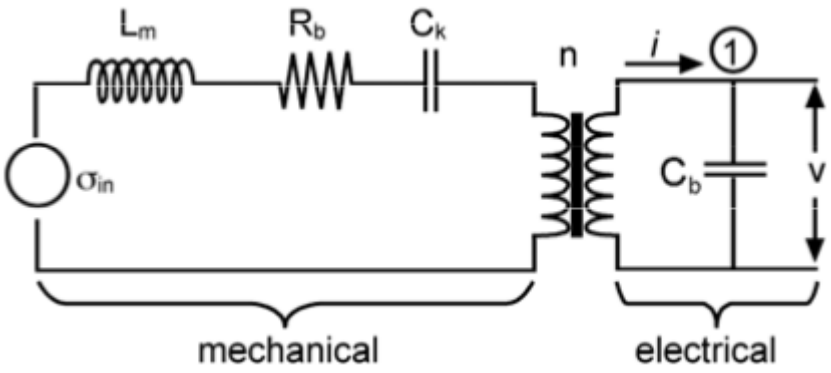

Figure 2.5: Circuit representation of a piezoelectric generator [53]

2.1.4 Summary of Generators

Previous studies [54] have found that piezoelectric generators are by far the most advantageous and can yield up to 35.4 mJ/cm^3 of energy. Table 2.1 gives a comparison of the energy densities of the three vibration-based generators achieved practically and theoretically which indicates a 6-10 % efficiency range of such harvesters.

Table 2.1 : Comparison of energy densities [40]

	Practical (mJ/cm^3)	**Theoretical (mJ/cm^3)**
Piezoelectric	35.4	335
Electrostatic	4	44
Electromagnetic	24.8	400

Three main generators capable of scavenging ambient sources capable of converting mechanical to electrical energy have been looked at earlier in this section. A comparison of typical power densities versus volatge for energy sources must be considered with other competing technologies such as photovoltaic and thermoelectric, which should then be compared with materials used to make commercial batteries which can help us fully explore the potential of PEH devices. Firstly, voltages produced by solar cells [55] require significant processing in comparison to battery technologies. Secondly, power generation through thermoelectric generators require large temperature gradients [56] and requires complex material optimization. Finally, piezoelctric sources provides high power density in comparison to other vibrational generators thus making it a favourable option. Figure 2.6 shows this comparison of power density for various power supplies. The plot indicates

that the bandwidth of power density values of piezoelectric systems are comparable with batteries such as lithium-ion yielding good voltage range and power density for varius applications.

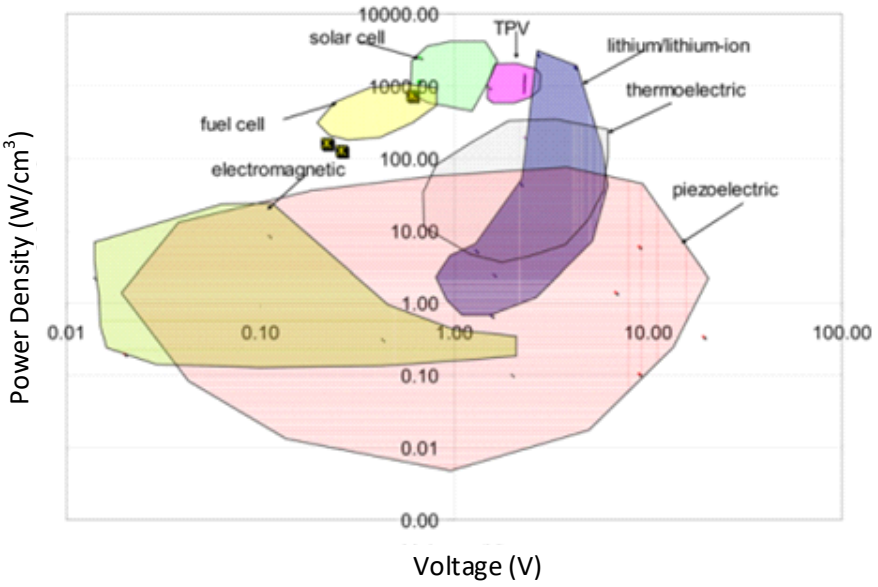

Figure 2.6: Power density versus voltage for batteries and regenerative power supplies [57]

Piezoelectric generators in comparison to electrostatic and electromagnetic have several advantages which include a simple design, low cost of transducers and small sizes suitable for integration with various versatile applications. However, some of the disadvantages of piezoelectric generators include high frequency requirements (which is an important issue as low energy excitations may not give a high output for specialist application requiring high power) and has limited material selection. Overall, piezoelectric generators are considered to be a far better option for REH devices. The disadvantages of electromagnetic and electrostatic vary from complex design to requiring a separate voltage source. Therefore, it is reasonable to select piezoelectric generators or transducers as the EH system for application with raindrops. Table 2.2 gives an overview of the advantages and disadvantages of the three mechanical to electrical generators; electrostatic, electromagnetic and piezoelectric as published by researchers [53, 58, 59].

Table 2.2 : Advantages and disadvantages of generators

	Advantages	**Disadvantages**
Electrostatic	Small size Control of mechanical resonance	Requires separate voltage source Higher frequency than piezoelectric is needed. Low output current
Electromagnetic	No voltage source required Higher power output	Complex design Difficult to integrate into microsystems
Piezoelectric	Simple design No voltage source required Small size Precise mechanical control	Needs higher frequency Limited material selection Poor mechanical properties Low output current

2.2 Water Droplet Impact Harvesters

The key factors that influence the output of water droplet impact harvesters include volumetric size of rainfall, mass of droplet (relates to impact force), velocity of impact of droplets, fluid dynamics and surface interaction [60]. In this section these factors will be explored which will help in the development of a PEH system capable of harnessing power from raindrops, which is the ultimate aim of this research.

2.2.1 Fluid Impact Dynamics

The study of water droplet interaction with various surfaces must be briefly discussed before we can understand how the water droplet interacts with PEH devices. In 1805, Thomas Young and Pierre Simon de Laplace had developed an insight that an interface has a specific energy, interfacial energy, which can be described as proportional to the molecules at a given surface and subsequently also proportional to the surface area of this interface [61-63]. Raindrops are generally spherical in air as they are generally tiny neglecting the impact of gravity on them. However, when these droplets interact with surfaces, surface forces have an impact on them.

Let us consider an example of homogenous solid surface (a single solid surface which cannot be split into simpler compounds), the impact of droplet forms a disc with a radius ℓ and a contact angle of θ which is depicted in Figure 2.7. The contact angle describes the radius of the disc formed by the droplet [64] and is used as a measure of the surface's

wettability which can be described as the droplets ability to maintain contact with a solid surface. Surface material can generally be classed as hydrophobic (wettable) when $\theta > 90°$ or hydrophilic (non-wettable) when $\theta < 90°$ [65]. Moreover, surface material can also be described as superhydrophobic when $\theta > 150°$ and such materials could be characterised as having a very high resistance to wetting [66].

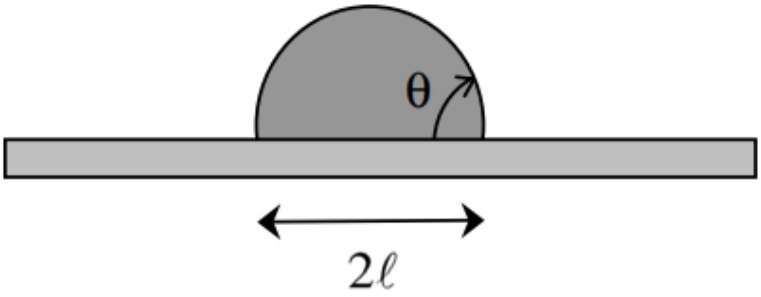

Figure 2.7: Depiction of contact angle on a homogenous surface [64]

The impact dynamics is one of the main factors which will significantly influence the energy transfer function of the harvesting device and its power output. Water droplets can impact a REH device either on a solid surface or liquid surface. The impact of a droplet on a harvesting device is expected to demonstrate a variety of mechanisms ranging from floating, bouncing to splashing. It is important to study how the droplet behaves when impacted with both solid and liquid surfaces.

Solid Surface

The impact mechanism of a droplet falling onto a solid surface can be divided into three main categories: bouncing, spreading and splashing as depicted in Figure 2.8. The water droplet can either fully bounce leaving no water residue on the solid surface, or partially bounce leaving some water residue. The second category of the water droplet is spreading on impact, when the water adheres to the surface at impact as the shape of droplet deteriorates. The third category of the water droplet is splashing, when the droplet breaks into many parts and adheres to the surface, the droplet will then be distributed on the surface.

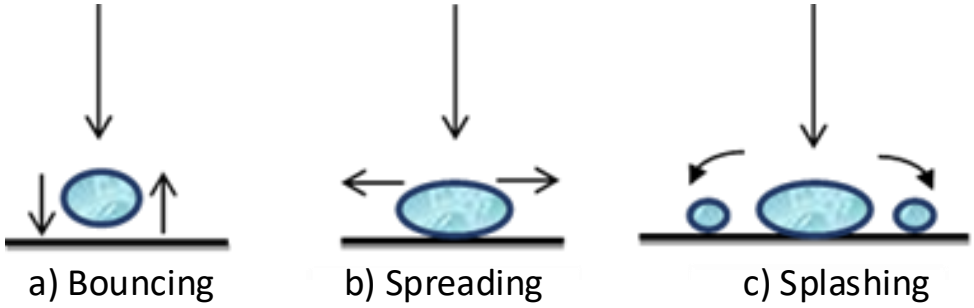

Figure 2.8: Depiction of water droplet impact on solid surface

Liquid Layer

The impact mechanism of a droplet falling onto a liquid layer surface can be divided into four main categories; floating, bouncing, coalescence and splashing as indicated in Figure 2.9. The droplet can float on the surface for a few seconds and then disappear. Similarly, to a solid surface, the water droplet can either fully bounce or partially bounce. The third category representing coalescence is when a small carter is formed but with no production of secondary droplets, and the liquid layer it impacts on is hardly disturbed. The last category of splashing is when secondary droplets are produced due to the impact as the liquid layer below is greatly disturbed.

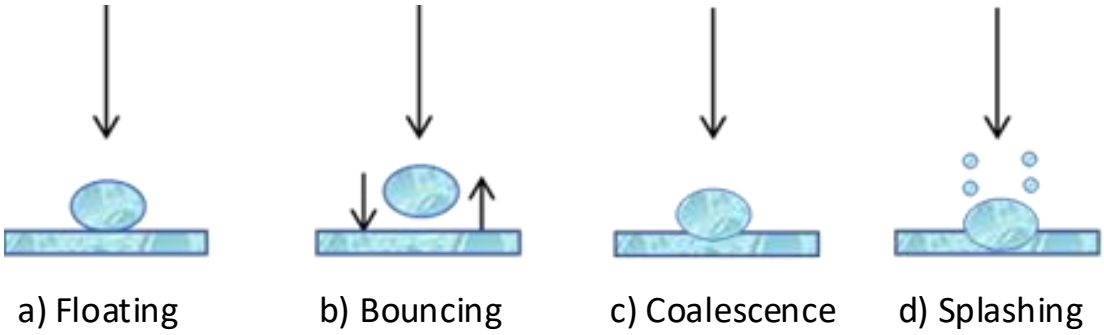

Figure 2.9: Depiction of water droplet impact on a liquid layer surface

Overall Impact

An expression can be developed for harvested energy through such mechanisms focusing on the impact on solid surfaces and then on liquid surfaces. Studies show the dominant impact mechanism of a water droplet is one that involves splashing [67, 68] depending on the surface. An empirical relation as represented in Equation 2.6 is developed [69, 70] from experiments, where R_e is the Reynolds number (a dimensionless number defined as the ratio of inertial forces to viscous forces), W_e is the Weber number (a dimensionless

number with relative importance of fluids inertia compared to surface tension) and K_m is defined as the impact parameter (which depends on the roughness of solid surface and thickness of layer).

$$K_m = W_e^{\frac{1}{2}} \times R_e^{\frac{1}{4}} \quad 2.6$$

The Reynold's and Webber's numbers are found from Equation 2.7 where ρ_w is the density of fluid, μ_a is the viscosity, σ is the surface tension of the fluid and v is the velocity:

$$Re = \frac{\rho_w v\, d}{\mu_a}; \quad We = \frac{\rho_w v\, d}{\sigma} \quad 2.7$$

It is proposed that the behaviour of the water droplet can be determined using Equation 2.6, which will either deposit on the surface or splash. If K_m is found to be smaller than a threshold value (K_c), then only deposition will occur. On the other hand if K_m is found to be greater than K_c then a splash will develop [71].

A study of the impact of water droplet should also consider whether the impact surface is horizontal or inclined. Investigations conducted [72, 73] analysed the theoretical and experimental results of horizontal and inclined surfaces. The effect on horizontal surface was found to be mainly due to surface material properties, impact velocity, droplet viscosity, droplet surface tension and droplet size. The surface of impact plays an important role where the maximum spread is large on a glass surface in comparison to wax and polyvinyl chloride (PVC). The maximum spread and spreading velocity increases with increasing the impact velocity. Water, isopropanol and glycerine droplets were used in some of the experiments with nearly the same Webber and Reynolds numbers. The results of the experimental study formulated the empirical model of impacting droplet-surface interaction. The maximum spread increases with increasing Reynolds number and Weber number. The impact onto an inclined surface is dependent on droplet material properties such as viscosity, density and surface tension. The rebound effect could only be achieved on a dry smooth glass and on wetted surfaces. There was no rebound on wax and rough glass.

One of the objectives of this research is to investigate the conversion of water droplet kinetic energy using a piezoelectric transducer, to convert the impact and vibrational

energy into electrical energy. As the droplet falls from standstill, it accelerates along a path increasing in velocity. The water droplet can reach equilibrium at a certain stage. The kinetic energy of the droplet is then dependant on to the volume which relates to droplet size and velocity as shown in Equation 2.8 where ρ_w is the density of water, D_{drop} is the droplet diameter and v is the velocity of the droplet.

$$\mathrm{KE} = \frac{1}{2}\rho_w \left(\frac{4}{3}\pi \left(\frac{D_{drop}}{2}\right)^3\right) v^2 \qquad 2.8$$

REH devices are not expected to be able to extract all this energy, even if it is an optimised harvester, however, a Betz type limit is expected to apply as deposits on the harvester need energy to be removed.

2.2.2 Surface Interaction

The fluid mechanics of droplet impact with a surface is of importance in a variety of different fields. The fluid flow associated with impinging drops is non-trivial and not fully described in detail in the scientific literature. As demonstrated before, a raindrop impact on a liquid surface can splash, bounce or merge with any surface liquid whereas a raindrop impact on a solid surface will mainly either splash or spread out on the surface. Splashing phenomenon is the dominant one [74].

A leaf-raindrop system study [75] shows that hydrophilic surfaces with remains of water droplet on a piezoelectric cantilever beam yields higher energy in comparison to hydrophobic surfaces. This can be explained by Figure 2.10 where two beams (80 mm and 140 mm in length) are used as hydrophilic (wetting) and hydrophobic (non-wetting) surfaces. For a hydrophilic surface, the torque produced by the droplet is proportional to droplet weight and beam length. The displacement is not centred around the zero deflection which indicates there is additional weight exerted on the beam as the droplet sticks to the surface, therefore increasing the bending energy giving a higher output. However, for a hydrophobic surface as the droplet bounces off, it undergoes zero average torque over time. The displacement is centred around the zero deflection which indicates there is no additional weight as the droplet does not stick to the surface.

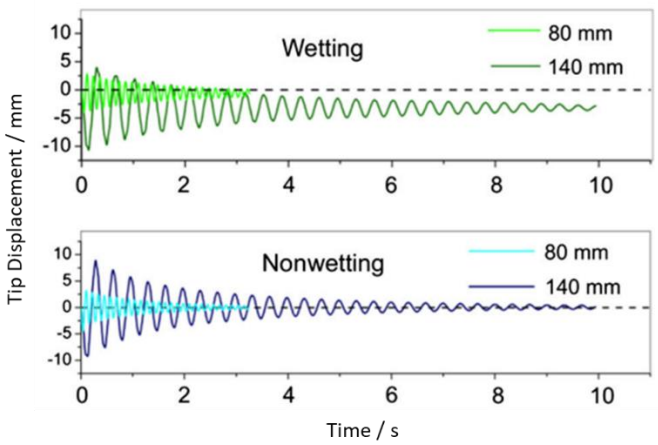

Figure 2.10: Beam-tip displacement of a cantilever for hydrophobic and hydrophilic surfaces [75]

It has been reported that superhydrophobic surfaces could potentially enable the droplet to bounce multiple times [76], which could potentially provide an opportunity to fabricate a piezoelectric transducer with high output as this would allow elastic impact behaviour.

By reviewing different scenarios of droplet impact [77] the liquid can be described by its thermodynamic state, surface tension, viscosity and compressibility. Most theoretical and numerical calculations assume that the drops are spherical, and experimental work carried out in this research study will maintain this assumption. Due to aerodynamic forces the shape of drops moving through air will always be rendered slightly ellipsoidal [78].

Another feature to take into consideration is that the harvester surface can generally be either smooth or rough. It is reported [79] that splashing is reduced when highly polished surface are used. At small surface roughness the splashing threshold depends strongly on the roughness, whereas the threshold is little influenced by the surface roughness when it is large. In many problems the elastic response of the surface is insignificant. However, the elasticity of the surface can no longer be neglected when high speed drops collide with a surface.

During the initial stage of impact, the drop is merely deformed and compressed at its base. Hence, surface tension forces and the viscosity of the liquid do not enter the scenario at this stage. The important parameters are density and compressibility of the liquid, impact velocity and diameter of the droplet. In the contact zone between the drop and the surface, pressure is not uniform. It is highest at the contact edge where it exceeds the water

hammer (defined as the pressure when a fluid either stops or changes direction), and is lowest at the centre due to the spherical geometry of the drop [79]. Splashing is a phenomenon often observed during liquid droplet impact onto a solid surface. The threshold of splashing is known to be related to droplet size, impact velocity, and physical properties of the liquid, but the mechanisms that initiate splashing are not understood completely.

2.2.3 Impact Force and Velocity

A raindrop in freefall towards the ground experiences two forces that are exerted vertically on it; a force acting upwards (drag force), and the force acting downwards (gravitational force resulting in the weight of the droplet). Equations related to raindrop in freefall were proposed by Warude *et al.* [80].

The drag force on the droplet is represented in Equation 2.9, where ρ_a is the density of air, A is the projected frontal area of the droplet, v is the velocity of the droplet and C is the coefficient of drag.

$$F_{air} = \frac{1}{2}\rho_a A C v^2 \qquad 2.9$$

The weight of the droplet is represented in equation 2.10, where ρ_w is the density of the water droplet, r is the radius of the droplet and g is the acceleration of the droplet due to gravity.

$$F_{gravity} = \frac{4}{3}\pi r^3 \rho_w g \qquad 2.10$$

When these forces are in balance the droplet reaches its terminal velocity, v_T, the maximum velocity if no other forces act on the raindrop. This is shown in equation 2.11, where D_{drop} is the diameter of the droplet.

$$v_T = \sqrt{\frac{\pi {D_{drop}}^3 \rho_w g}{6\rho_a A C}} \qquad 2.11$$

Estimated maximum impact force (F_0) of rain drops can be presented by Equation 2.12 [81]:

$$F_0 = \pi \rho_w r^2 v^2 \qquad 2.12$$

where ρ_w is the density of the water droplet, r is the radius of the droplet and v is the velocity of the droplet.

Water droplets are defined as compressible in nature and produce sharp, pulse loading events during impact [82]. Figure 2.11 shows the impact force of water droplet gradually increases, firstly with an increase in velocity and secondly with an increase in diameter of the droplet. These two parameters are crucial for a higher power output.

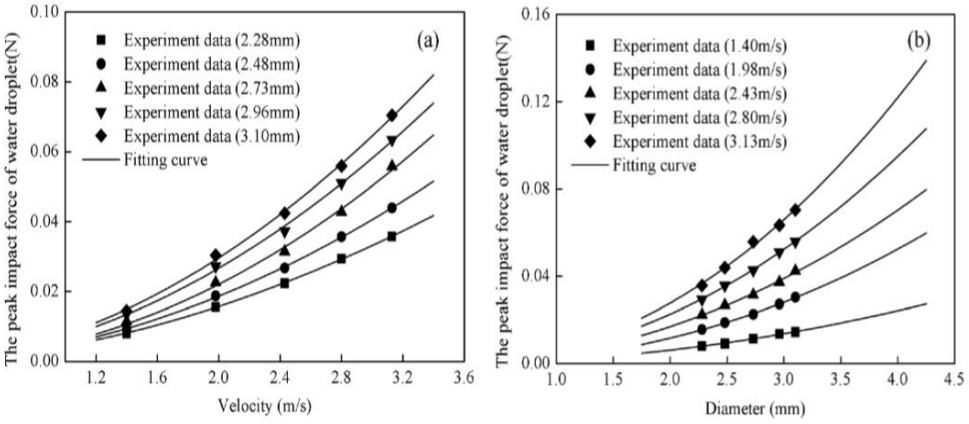

Figure 2.11: Impact force of water droplet on solid surface against (a) velocity and (b) diameter [83]

2.3 Behaviour and Distribution of Rain

2.3.1 Rain Types

Rain and other forms of precipitation occur when warm moist air cools and condenses. This happens as a result of moisture condensing to liquid, as warm air can hold more water than cool air. Also, rain can be categorised into convection or stratiform. The cycle of convection mostly occurs in regions closer to the equator where the moisture in the ground is heated above the temperature of the surrounding areas, leading to an increase in evaporation. As the water vapour rises, this condenses into clouds which then subsequently can produce rain. The resulting convective shower mostly occurs for a short period of time over a limited area. Areas surrounding the equator are most likely to

receive regular convective showers. For example, in the UK this phenomenon is referred to as ‘sunshine and showers’ as it rains in a smaller area followed by clear spells [84].

Stratiform rain occurs when warm and cold air meet, but do not mix easily since they have different densities. Normally under these conditions the warm air rises over the cold air creating a ‘front’. When air is forced up a mountainside, the water vapour in that air then condenses and falls as raindrops. Generally warm fronts are followed by light showers. The duration of stratiform rainfall is less but the intensity can be high [85].

Stratiform rain is further categorised into 3 types: light stratiform rain (LSR), moderate stratiform rain (MSR) and heavy thunderstorm (HT). Typical rain rate for LSR is between 2-4 mm/h, MSR are is 5-9 mm/h and for HT is 10-40 mm/h [86] Some typical values of raindrop size and velocity measured by [67] and estimated impact force calculations are presented in Table 2.3 using Equation 2.12.

Table 2.3 : Rain types along with terminal velocity and estimated impact force

Rain Type	**Droplet Size (mm)**	**Terminal Velocity (m/s)**	**Estimated Impact Force (N)**
Light stratiform rain			
Small	0.5	2.06	8.3×10^{-4}
Large	2.0	6.49	0.13
Moderate stratiform rain			
Small	1.0	4.03	3.2×10^{-3}
Large	2.6	7.57	0.30
Heavy thundershower			
Small	1.2	4.64	0.02
Large	4.0	8.83	0.98
Largest	5.0	9.09	1.62

Researchers in Malaysia gathered data over a nine year period for tropical countries known for heavy rain as shown in Figure 2.12. Some of these countries included Malaysia, Nigeria and Kenya to showcase the distribution of rain in these vast regions. This study has been particularly helpful to showcase the potential of REH devices and their application of generating electricity directly from raindrops, but the full potential is yet to be covered. There is a good range of rainfall accumulated, where regions only

received precipitation up to 1000 mm whereas some regions received precipitation up to 4500 mm. These are typical average values for annual rain date and it is understood the average year on year may be different, but it gives a good estimation of kinetic energy available through rainstorms.

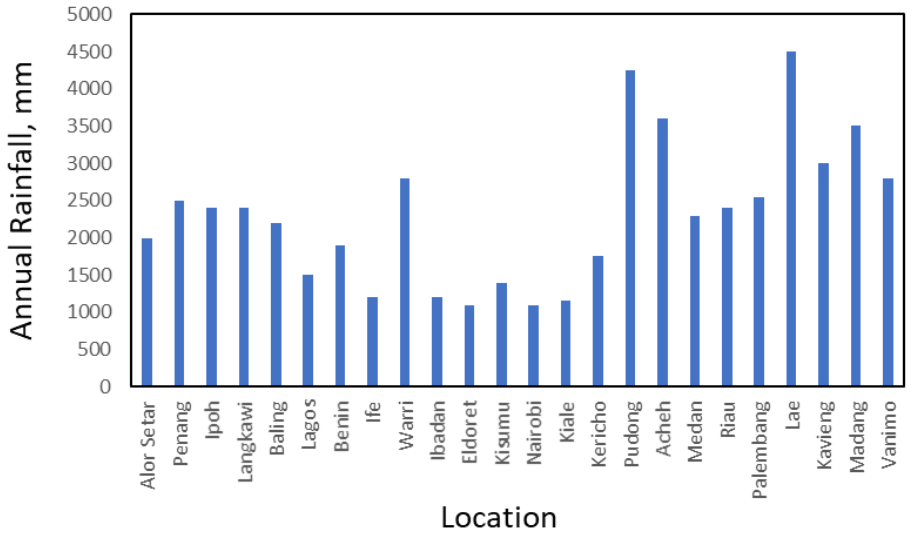

Figure 2.12: Average annual rainfall data for 24 tropical regions [87]

2.3.2 Behaviour and Distribution of Rain

Rain behaviour is random, and is hard to predict using a single deterministic parameter [88]. Rain can be characterised by rain rate (mm/hr) and drop size distribution (DSD) which shows the total amount of raindrop count with a particular droplet diameter. A study conducted by Wong *et al.* [89] characterised the performance of a PEH device under real rain by collecting data using disdrometer (an instrument used to measure the drop size distribution and velocity of falling droplets) over long periods. The device was able to harvest 2076 µJ of energy over a long period of 301 minutes. The study concluded that the total energy harvested after a duration of time was not influenced by the duration of rain but was dependant on the rain rate.

Natural phenomenon generally shows two types of behaviour; Gaussian distribution with an average sized parameter which is scale critical, and Fractal distribution, which is independent of scale (whatever scale we look at we see the same distribution of that parameter). Fractal and multi-fractal methods get used to describe various natural or physical distributions with large numbers. This research can utilise a variety of techniques to understand and mathematically describe the distribution of water droplets on a PEH

device as one of the objectives of this research is to present a mathematical behaviour of a PEH device undergoing various impacts or hits resulting in power. Such a behaviour has been described as multi-fractal system previously [90] and to fully explore the relationship behaviour around any point is described by a power law.

Fractal behaviour can be simply explained in terms of self-similarity where little pieces are smaller copies of larger pieces. The values measured and average size depends on the resolution used to make the measurement (also referred as scaling). Fractals have unique statistical properties as there is no defined range that can describe it accurately, but the important element is how this range depends upon the resolution that we use to measure it. Fractals are important as they help analyse and understand experimental data [91].

Power law (PL) is present in natural or manmade systems. In most cases, single PL distribution holds for the entire range but in some cases more than one PL feature is observed known as multi-fractals. If we observe a straight line or a linear behaviour on log-log scale plot of a quantity, it is generally described by power law distribution. This distribution can be written as Equation 2.13 [92]:

$$P(x) = Ax^{-\propto} \tag{2.13}$$

The cumulative distribution can be described as Equation 2.14:

$$\mathbb{P}(x) = Cx^{-(\propto-1)} \tag{2.14}$$

where $\propto$ is the maximum likelihood estimator.

Figure 2.13 shows an example of PL distribution of random numbers described in a specific text using normal and logarithmic scale on both axes respectively. The linear behaviour power law form asserts only for higher values and such a quantity is often referred to as having a power-law tail.

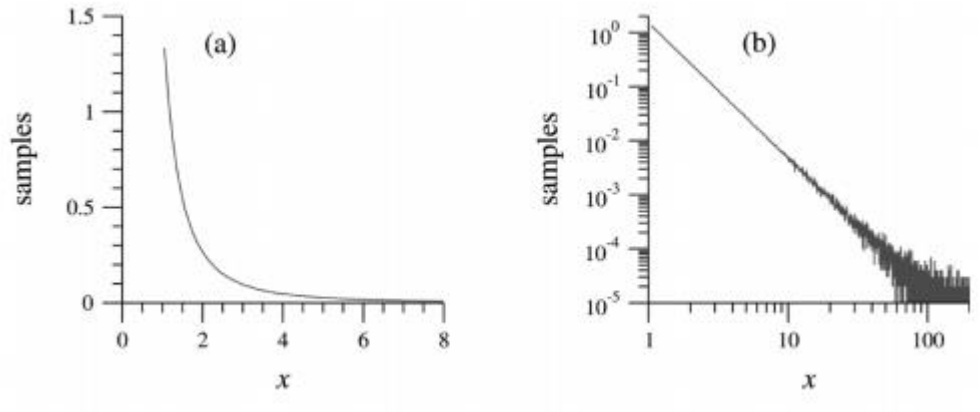

Figure 2.13: Set of 1 million random numbers described in the text which have a power-law distribution (a) normal scale and (b) logarithmic scales [93]

For most cases PL distribution holds for the entire range but in some cases more than one PL feature is observed known as multi-fractals. Estimations for fractal behaviour are often tricky, therefore we will explore 3 forms of multi-fractals in this section that will be relevant to the empirical data presented in this thesis.

Double Power Law

Behaviour of some data can be described as broken power law in which case two or more PL is observed. Some examples of experimental data described by a dual or double PL include; exact solutions to Schrodinger's equation (defining the saturation of the nonlinear refractive index) [94], and cumulative distribution of hits received by a website [95]. An example of double PL is illustrated in Figure 2.14 where the rank/frequency log-log plot of hits received by a website is shown. The distribution on the plot clearly shows two features which can be further explained and analysed using double PL or fractal analysis.

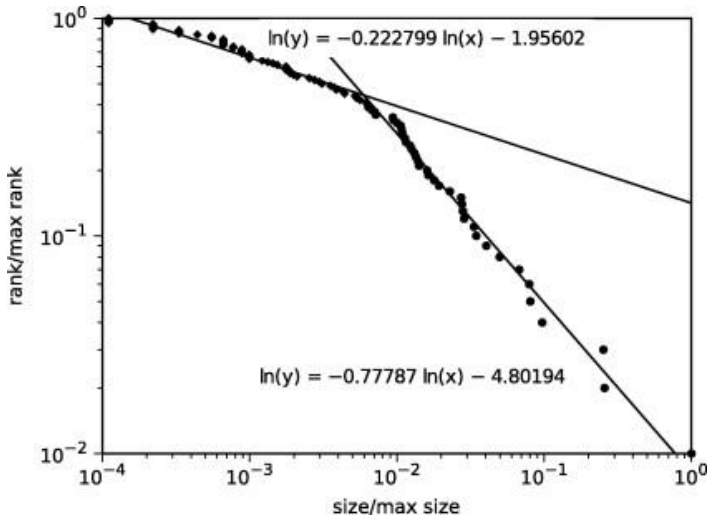

Figure 2.14: Cumulative distribution of the number of hits received on a website [95]

Parabolic Fractal Law

Parabolic fractal law (PFL) [96] concept defines non-linear relationships where the behaviour of data is described by an unperfect self-similarity. An example of concentration data gathered by simulation is shown in Figure 2.15, which shows the parabolic fractal distribution based on the best fit.

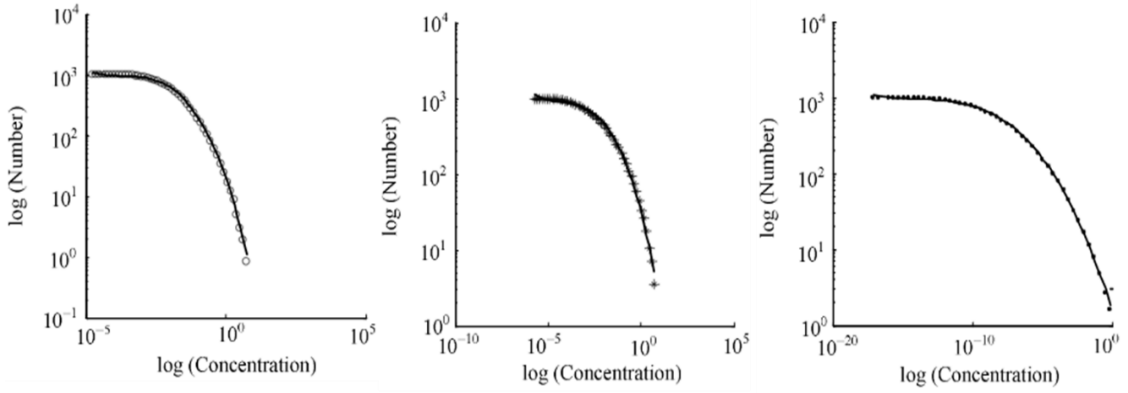

Figure 2.15: Examples of parabolic fractal law number versus concentration [97]

Exponential Power Law

A power law with an exponential cut-off is known as an exponential PL. Some experimental data described as exponential PL include wetting kinetics of partial drop spreading [98] and reservoir models of tight gas [99]. Figure 2.16 shows an example comparing 4 exponential PL distribution with varying likelihood estimator.

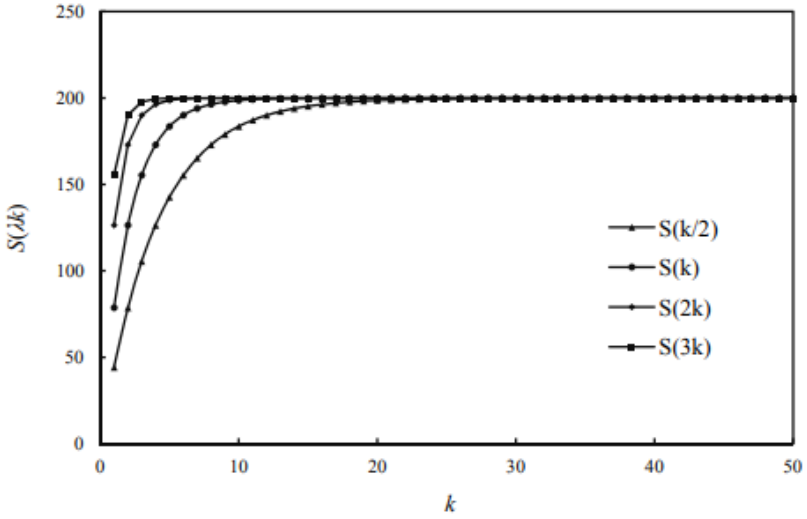

Figure 2.16: Example of cumulative distribution showing exponential power law [100]

2.4 Review of Existing Rain Impact Harvesters

The scope of this research has identified that one of the specialist applications for piezoelectric transducers is harvesting power from the untapped energy source of raindrops. To date, limited number of researchers have conducted study in this field and this section reviews such harvester systems that can produce energy using water droplet impact. Systems able to scavenge rain energy by impact of droplets can be divided in to two categories; stand-alone systems that can only capture droplet impact energy and CEH systems that are able to integrate techniques that can use two or more ambient sources. Focus of this research is a stand-alone system capable of producing energy for low-powered devices.

One of the earliest study that has inspired many researchers to focus their attention on REH system based on a PEH device as a water droplet impact harvester was carried out by Guigon *et al.* in 2008 [101, 102], in which the authors conducted work on theoretical and experimental basis. Theoretical investigation outlined the changes in elastic deformation with size variations (width and thickness of active layer of PVDF) of the harvester design. It was proposed an optimal harvester should have a very thin layer of piezoelectric material in the region of µm and the width of such a layer be slightly smaller than the diameter of the droplet. Simulations of such a design system based on 25 µm thickness of PVDF membrane produced a maximum output energy output of 25 µJ and

peak instantaneous power of 12 mW with a HT (with droplet diameter of 5 mm and impact velocity of 5.7 m/s). It was proposed that if the impact were slightly off-centre the electrical energy recovered could be maximised as the setup is less rigid at the centre. The theoretical design can be seen as a bridge arrangement where the transducer is fixed on both ends with support and the PVDF sheet is encapsulated in electrodes as shown in Figure 2.17.

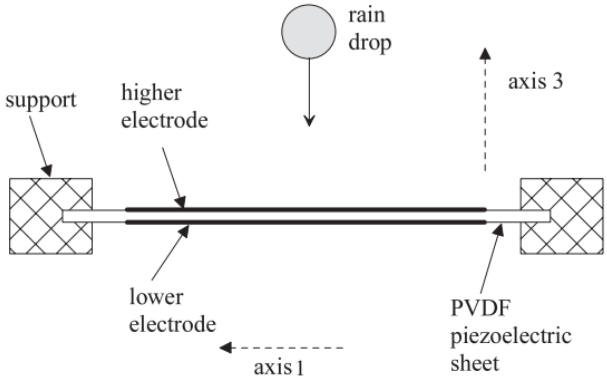

Figure 2.17: System design of the randrop energy harveter [102]

The experimental study firstly demonstrated that voltage is proportional to the mechanical energy transferred to the material, whilst the electrical energy is proportional to the square of mechanical energy delivered which can be seen in Figure 2.18. The experimental values showed that electrical energy recovered was approximately 1nJ and instantaneous power was 1 µW. The study concluded that splash leads to reduction in experimental whereas the simulations did not take this inelastic collision into account which results in loss of energy.

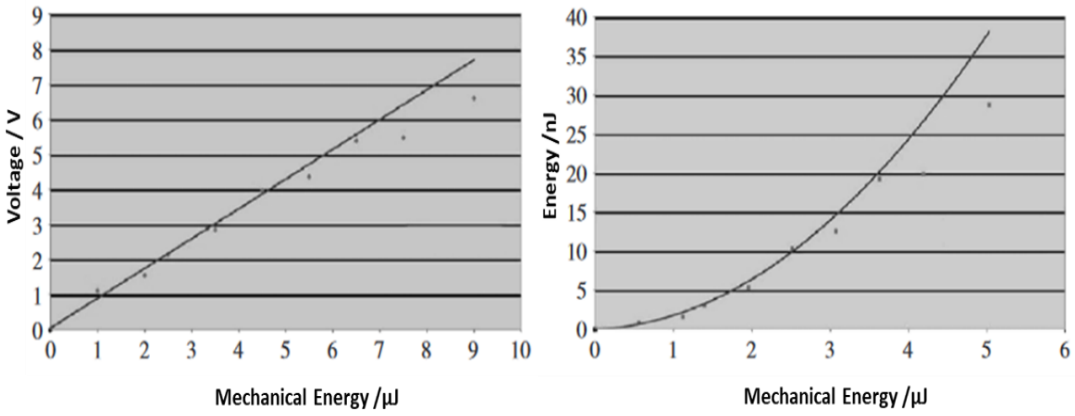

Figure 2.18: Voltage and enrgy profiles as a function of mechanical energy [102]

A study looking at harvesting energy from water droplets using an off-the-shelf transducer was conducted by Viola *et al.* [103-106], using PZT (Mide Volture V22B/L) and PVDF (MEAS LDT1-028K) transducers as a means of drawing a beneficial comparison between the two piezoelectric materials. Initial study concluded higher output with single droplet impact with PVDF transducer (cantilever arrangement) of 4 µW in comparison to PZT transducer (bridge arrangement) of 0.9 µW. The transducers were exposed to water droplets to determine the voltage levels generated by the impact and as the study recommended the use of cantilever arrangement for droplet impact as the optimum arrangement. This gives us a good understanding of the performance of such water droplet impact harvesters indicating the focus for REH devices should be on cantilever arrangements. Two design arrangements are discussed, first a single cantilever with one edge of the cantilever bound, and second with one edge of the cantilever was bound but a floating circle (collecting diaphragm) was placed on the other edge of the cantilever. The droplet impact region for the single cantilever design is the surface of that transducers whereas for the collecting diaphragm arrangement the impact region is the floating circle. Approximate peak voltage values for an impact height of 0.5 m was measured as 9 V in the first arrangement and 2 V in the second arrangement for a single drop. These two arrangements are shown in Figure 2.19.

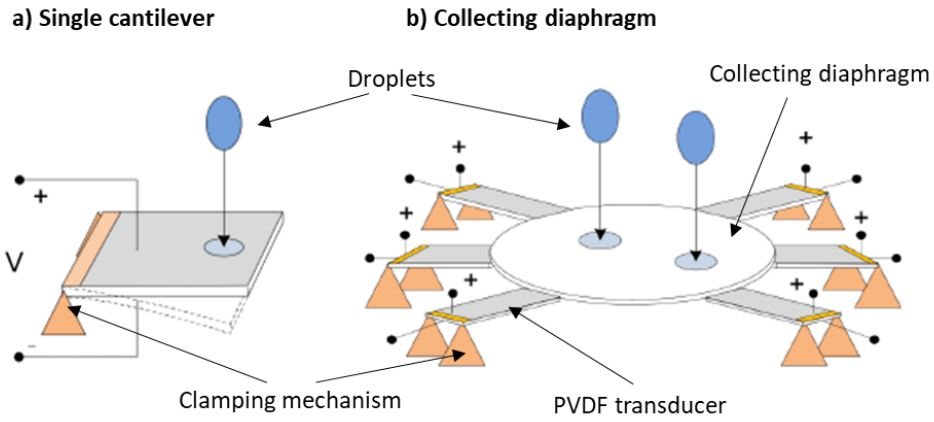

Figure 2.19: Arrangements for PVDF transducers (a) Single cantilever and (b) Collecting diaphragm [106]

A study conducted by Nayan *et al.* [107] showcased the need for developing a rain harvester due to the favourable rainy condition in Malaysia and focused on transducers

connected in series, parallel or mixed arrangement. The proposed design was in the form of a piezoelectric plate which had several circular piezoelectric discs of diameter 50 mm and hardware circuit with rectification, battery bank and voltage regulator. The voltage output was measured for different droplet heights (ground, first and second floor) and experimental data gathered resulted in an output of 1 V for series configuration with 8 transducers, 8 V for parallel configurations with 8 transducers, and 14 V with mixed series-parallel configuration of 28 transducers. The output of the piezoelectric device was found to be dependent on the impact force on the piezoelectric body where droplets were released from different heights; ground, first and second floor. Figure 2.20 shows the harvester system design and the design of the plates.

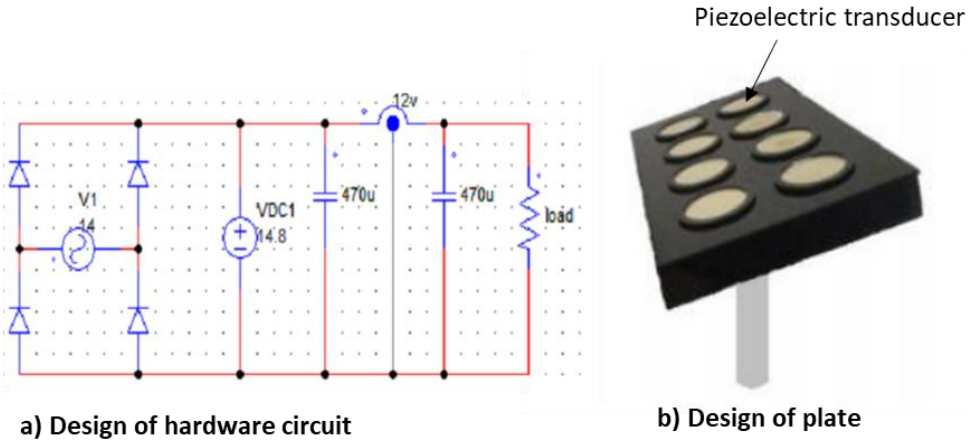

Figure 2.20: (a) Design of hardware circuit and (b) System design of plate [107]

A simulative study conducted by Chin-Hong *et al.* [108], focused on a harvester design comprised of a circular diaphragm with a diameter of 10 mm surrounded by 20 cantilever beams with dimensions of 3 × 1.2 mm. The harvester prototype developed consisted of several layers which included silicon (Si), polyamide, aluminium (Al) bottom, PVDF active layer and Al top. Finite Elements Analysis (FEA) simulations were performed to investigate maximum displacement caused by the droplet impact. To achieve optimum results, thinner Al and PVDF layers are used, as thickness is presented to be inversely proportional to maximum displacement. At the cantilever, PVDF thickness of 150 µm and Al thickness of 35 µm results in a maximum displacement of 2800 µm whereas at these thicknesses the maximum displacement on the centre of the diaphragm is relatively small. These thicknesses can withstand the impact pressure of a large droplet of 13.718

Mpa and gives some insight into the design parameters of a harvester. Figure 2.21 shows the design process of these layers and presents the meshed model of the harvester.

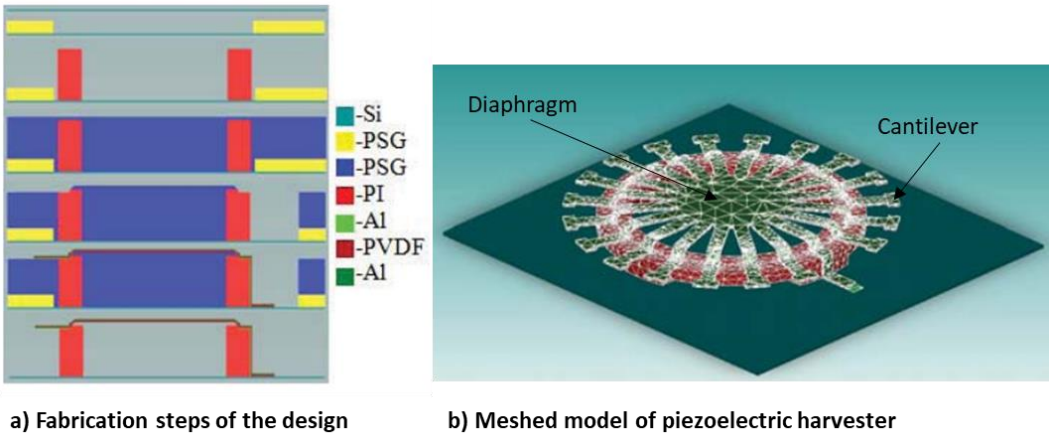

Figure 2.21: (a) Fabrication steps for the design and (b) Meshed model of piezoelectric harvester [108]

Performance evaluations were presented by Wong *et al.* [89, 109], which compared simulated and real rainfall. In simulated study, an off-the-shelf PZT transducer (Mide Volture V25W) was used with an impact height of 2.5 m with 4 different rain rates ranging from 33-99 mm/h. Maximum power of 0.2 µW was generated with droplet diameter of 0.73 mm, rain rate of 99 mm/hr and rain duration was 300 s. Experiments conducted in real rainfall yielded maximum energy of 0.2 mW with a time duration of 301 minutes. Based on the experimental data there were times when only slight rain activity happened and then there are times when the raindrop count was very high. This feature highlights one of the drawbacks of REH devices where we cannot rely on these devices to directly power the load, energy storage will need to be integrated. Energy storage will not be explored in this research as it is out of scope but highlights the importance of one. Figure 2.22 shows the experimental setup where the piezoelectric transducer was positioned below the laser precipitation sensor (to measure the raindrop count) and also shows the raindrop count and energy plots are shown which show the times when the device was harvesting power and times when either low or no power was harvested.

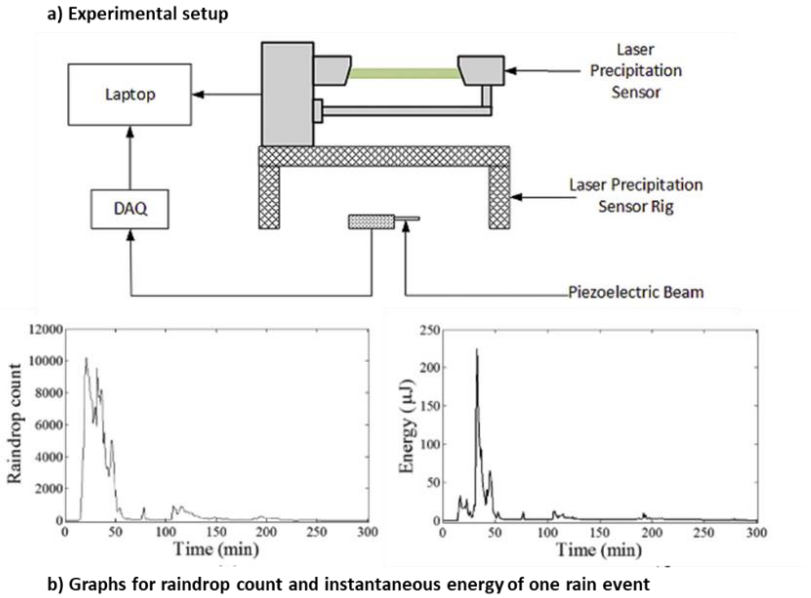

Figure 2.22: Rain event (a) experimental setup and (b) raindrop count and instantaneous energy graphs over time duration

Another approach to harvest from vibration energy is using flow-induced vibration such as water vortex. As this approach does not use the impact of water droplet it has not been presented in this section in detail, but some harvested power values have been mentioned for reference. An example using water vortex [110] on a macro fibre composite piezoelectric energy harvester was found to generate around 1.32 μW of maximum power with a water velocity of 0.5 m/s at the cylindrical diameter of 30mm. A different example of using an upright vortex-induced piezoelectric energy harvester [111] generated a maximum power output of around 84.49 μW using a velocity of 0.35 m/s. These power values are also within the μW range and do not present a better alternative of water droplet impact harvesters.

2.5 Performance of Rain Impact Harvesters

Energy conversion efficiency of a REH device is based on the harvested energy of the harvester in comparison to the kinetic energy of the droplet. As highlighted in the literature, the typical harvested power is in the μW range for different arrangements. However, none of the published papers have explicitly included a value for this energy conversion efficiency. As a reference to compare such values we can compute the maximum energy conversion efficiency of a few experimental studies as shown in Table 2.4.

Table 2.4 : Comparison of energy conversion efficiency of REH

Authors	**Harvester**	**Parameters**	**Harvested Energy**	**Kinetic Energy**	**η (%)**
Guigon *et al.* **[102]**	Bridge (PVDF)	$D_{drop} = 3$ mm $v = 4.5$ m/s	147 nJ	0.143 mJ	0.1 %
Wong *et al.* **[109]**	Cantilever (PZT)	$m = 47.7$ mg $v = 3.7$ m/s	23 µJ	5.88 mJ	0.39 %
Al Ahmad **[112]**	Cantilever (PZT)	$m = 0.23$ g $v = 3.7\ m/s$	1.73 µJ	1.35 mJ	0.128 %

D_{drop} is the droplet diameter, v is the fall velocity and m is the mass of the droplet.

Typical power density value for rain harvesters using direct impact techniques with PEH have been experimentally reported to range from 10^{-5} W/m^3 for a light rain shower (with droplet size of 1 mm and impact velocity of 2.8 m/s) to 10 W/m^3 a heavy rain shower (with droplet size of 5 mm and impact velocity of 5.7 m/s) [102]. A watermill setup using piezoelectric transducers yielded average power density value ranging from 10 W/m^3 to 100 W/m^3 [113]. When compared to solar and wind [114], which can yield power density in the range 10-100 W/m^2 (with solar irradiance ranging between 100 W/m^2 to 1 kW/m^2 and wind velocity of 2-10 m/s), we can conclude rain fares reasonably. Electricity produced by REH would cost more in comparison with traditional fossil fuels as the payback period of such a plan is large [115].

There are several factors that affect the output and efficiency of the REH device. Some these key factors have been summarised here:

Rain Pattern & Distribution

Rain pattern is unpredictable and random in nature which makes it difficult to control certain parameters such as the size of the droplet and impact position/area on the harvester. External factors such as temperature and wind can further play a part in changing the power output which relies on these parameters to be consistent.

Piezoelectric Material

Most of the research conducted has been on either PZT or PVDF but there is further scope to fabricate organic materials which are less toxic and provide more favourable outputs but is out of scope for this research.

Size of the Harvester

Most of the previous experimental studies conducted do date have used small piezoelectric harvesters with smaller dimensions which being an advantage for PEH devices but can be seen as a disadvantage for REH. However, as the size of the harvester is increased the trend demonstrates that the output power can be increased which can be achieved using an array of harvesters.

Output

As it has been demonstrated in the review, PEH gives low output in comparison to other harvesting systems. It is proposed output could be further enhanced by using combined energy harvesting technique to explore hybrid harvester [116] but is out of scope for this research.

Commercial Viability

Published data suggests that REH devices produce lower output which raises the question of how viable such devices are an economic level. Research has progressed where various other techniques are being explored to enhance the output and improve the efficiency. Even though power output may have low values but it sufficient for low-power electronics which is what this study is aimed to look at.

Some of the significant research conducted by PEH using water droplet impact has been identified in Table 2.5 which covers a period from 2008 to 2020. In that period various harvesting methods were investigated but the dominating method has been one with a cantilever arrangement which has produced power in the μW region with various loads connected. Most of the studies conducted on the cantilever arrangement used small devices or small active areas. The output presented has either been reported as peak voltage, peak power or average power generated in that arrangement but it is difficult to carry out a like-for-like analysis of all the harvester types as each publication has data in a different format.

Table 2.5 : Comparison of maximum output of water droplet energy harvesters

Year	Material	Source	Dimensions / Area	Output	Load	Ref
2008	PVDF	Droplet with $D_{drop} = 5\ mm$ and $v = 5.7\ m\ s^{-1}$	Bridge, 100 mm × 3 mm × 0.25 mm	P_{avg} 12.5 mW	N/A	[101, 102]
2010	PVDF	Droplet with $D_{drop} = 3.57\ mm$ and $v = 2.96\ m\ s^{-1}$	Solid film, 35 mm × 80 mm × 52 μm	V_{pp} 0.1 V	N/A	[117]
2011	PVDF	Droplet with $m = 50\ mg$ and $h = 1\ m$	Cantilever, 16 mm × 4 mm × 0.2 mm	V_{peak} 12 V	N/A	[118]
2012	PZT	Droplet with $m = 0.23\ g$ and $v = 0.22\ m\ s^{-1}$	Cantilever, 8 mm × 20 mm × 0.58 mm	V_{pp} 0.8 V	10 $k\Omega$	[119]
2012	PZT	Droplet with $m = 0.23\ g$ and $v = 0.22\ m\ s^{-1}$	Cantilever, 8 mm × 20 mm × 0.58 mm	P_{peak} 12 µW	10 $k\Omega$	[120]
2013	PMMA	Droplet with $m = 5\ \mu g$ and $h = 0.2\ m$	-	P_{avg} 6 nW	N/A	[121]
2013	PVDF	Droplet with $D_{drop} = 5\ mm$	Cantilever, 20 mm × 20 mm × 0.58 mm	P_{avg} 4.5 µW	47 $k\Omega$	[122]
2015	PVDF	Droplet with $D_{drop} = 2\ mm$ and $v = 2.13\ m\ s^{-1}$	Cantilever, 25 mm × 13 mm × 0.25 mm	P_{avg} 2.5 µW	2.2 $M\Omega$	[123]
2017	PVDF	Droplet with $D_{drop} = 2\ mm$ and $v = 2.13\ m\ s^{-1}$	Cantilever, 25 mm × 13 mm × 0.25 mm	P_{avg} 3.6 µW	1 $M\Omega$	[124]
2020	PVDF	Droplet with $D_{drop} = 2\ mm$ and $v = 2.13\ m\ s^{-1}$	Cantilever array, 0.003 m^2	P_{avg} 0.005 µW	1 $M\Omega$	*

D_{drop} is the droplet diameter, v is the fall velocity, m is the mass of droplet and h is the release height.

* Article will be submitted in 2020 for publication

2.6 Summary

PEH is one of the most promising technique that can harvest ambient vibration or motion. PEH devices are well suited to isolated applications where there are sufficient vibrations but lack of access to power supplies. Literature has shown that piezoelectric generators have a very high theoretical and practical energy density in comparison to electromagnetic and electrostatic generators.

Based on the information gathered from literature, it can be concluded that there are four key factors that influence the output of a harvester based on raindrop impact, fluid impact dynamics, surface interaction, impact velocity and behaviour of rain. Equations for the impact velocity and impact force have been established, along with characterisation of different rainstorms. Rain droplets are spherical in nature but with an increase in the diameter of the droplet, it has been shown that the shape can change depending on wind speed and air resistance [67], however that exploration is beyond the scope of this study. Splashing is the most common phenomenon that is observed when droplets impact a solid surface and rain distribution is modelled as a multi-fractal system, behaviour around any point is described by a power law.

A review of existing raindrop impact harvesters demonstrates values of harvested power in the μW region. The energy conversion efficiency compared to the kinetic available energy available is generally below 1% which highlights there are significant losses during this process due to inelastic collisions. There are approaches that could potentially improve the output by using CEH using thermoelectric generators, pyroelectric generator and piezoelectric generators [125] but is out of scope for this research.

There is clear scope for the following key developments to be made in the field which this research will hope to address:

- In-depth study of the droplet impact with a PEH device.
- Investigation into energy output and better understanding of the energy conversion efficiency.
- Experimentally validating an array of harvesters and proposing a design for a REH system as a protype.

CHAPTER 3

3 Piezoelectricity & Transducers

This chapter gives a background in piezoelectricity, materials used for fabricating PEH devices, explores equivalent circuit of the harvester system, and introduces various approaches to rectification.

3.1 Piezoelectric Fundamentals

The idea of electromechanical effect whereby there is a proportional relationship between mechanical stress and electric charges has floated around since the 18th century whilst scientists discovered the pyroelectric effect [126], piezoelectricity was later discovered by bothers Pierre and Jacques Currie in 1880. The Greek word 'piezos' means pressure which simply defines the application of mechanical stress to a piezoelectric material such as quartz which produces electric potential [127, 128].

When force is applied to the piezoelectric material or it is compressed or stretched, this develops a voltage. Conversion of mechanical to electrical signals is known as direct piezoelectric effect. Before subjecting an external force, the molecule is in an electrically neutral state as illustrated in Figure 3.1a. When an external force is exerted the material is deformed generating dipoles (pair of equal and oppositely charged poles) as illustrated in Figure 3.1b. This results in cancellation of opposing poles and fixed charges appear in the material as illustrated in Figure 3.1c. This means the material is polarised and therefore will generate an electric field. The voltage developed by compressing and stretching will have opposite polarity.

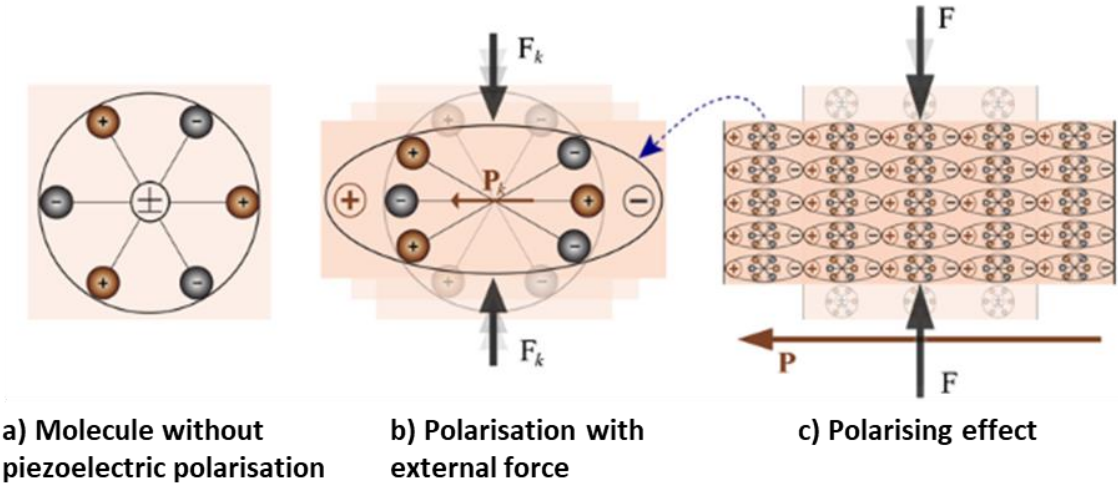

Figure 3.1: Simple molecular model to explain piezoelectric effect [129]

Piezoelectric response by a material can only be demonstrated if the following requirements are met:

- The atomic structure of the material is non-centrosymmetric which ensures a net polarisation is developed under stress due to dipole moments.
- A poling process undertakes to align the dipoles into a uniform direction.

Conversely, if we apply voltage across the piezoelectric material, we will see a deformation in the material either in the form of expansion (with the same polarity) or compression (with reverse polarity). This effect is known as the converse piezoelectric; electrical solicitation into mechanical energy mostly used as actuators.

Material properties depend on the direction of applied electric field, displacement, stress and strain. There are various coefficients that can be described using cartesian coordinate system as shown in Figure 3.2. The axes are represented as 1 (X-axis), 2 (Y-axis) and 3 (Z-axis). The shear about these axes are represented by 4, 5 and 6, respectively. Axis 1 refers to stretching direction, axis 2 refers to transverse planar direction and axis 3 to the poling axis which is perpendicular to material surface.

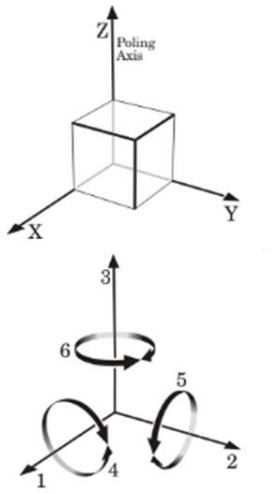

Number	Axis
1	X
2	Y
3	Z
4	Shear around X
5	Shear around Y
6	Shear around Z

Figure 3.2: Piezoelectric material in relation to direction of polarization [130]

Table 3.1 shows some of the important constants related to piezoelectricity where superscripts and subscripts are used to indicate direction.

Table 3.1 : Piezoelectric constants

Constant	**Units**	**Description**
d	C/N	Charge constant
g	V-m/N	Voltage constant
ε	F/m	Permittivity or dielectric constant

d is the piezoelectric charge constant; induced polarization usually takes place in z-axis (direction 3) we will often refer it to d_{3n} , where n represents the direction in which stress or strain is applied.

g is the piezoelectric voltage constant; induced electric field usually takes place in z-axis (direction 3) we will often refer to it as g_{3n} , where n represents the direction in which stress or strain is applied.

ε is the permittivity constant for a piezoelectric material and it is often noted with superscripts; ε^T which is related to stress or ε^S which is related to strain. Additional subscripts are used to denote dielectric displacement and electric field direction.

When a piezoelectric material is excited by an external force, it generates charge density which is shown in Equation 3.1 [131], where D is the surface charge density, Q is the

charge developed, A is the conductive electrode area, d_{3n} is the piezoelectric co-efficient for the axis on which stress/strain is applied and F_n is the force applied dependant on the direction.

$$D = \frac{Q}{A} = d_{3n}F_n\,, \qquad where\ n = 1, n = 2, n = 3 \tag{3.1}$$

The emf can then be defined as Equation 3.2, where g_{3n} is the appropriate voltage piezoelectric coefficient for the axis where stress was applied, F_n is the force applied, and h is the thickness of the film [132].

$$emf = g_{3n}F_n h\,, \qquad where\ \ n = 1, n = 2, n = 3 \tag{3.2}$$

The piezoelectric material generates a charge, which is collected by two electrode plates. The amount of energy stored in a piezoelectric element is the same as the energy stored in a capacitor [133].

In order to understand the piezoelectric effect mathematically, piezoelectric constitutive equations are proposed [134] [135] which can be used to describe both the mechanical and electrical properties. These equations are derived using Hooke's law of elasticity and dielectric equation. Equation 3.3 describes the converse piezoelectric effect and Equation 3.4 describes the direct piezoelectric effect, where S is the mechanical strain, s^E is the mechanical compliance under constant electric field, T is the mechanical stress, $d^t$is the matrix for inverse piezoelectric effect, E is the electric field, D is the charge density, d is the matrix for direct piezoelectric effect and $\varepsilon^T$is dielectric permittivity under constant stress.

$$S = s^E T + d^t E \tag{3.3}$$

$$D = dT + \varepsilon^T E \tag{3.4}$$

Cantilever beams with piezoelectric layers on both sides of the insulator or a unimorph arrangement with protective layers on the outer side is mostly used in application for harvesting energy. These beams can be subjected to two modes; 33 and 31. In 33 mode, voltage and stress act in the same direction whereas in 31 mode, voltage appears along Z-

axis whilst stress acts along the X-axis. A simple representation of this can be seen in Figure 3.3.

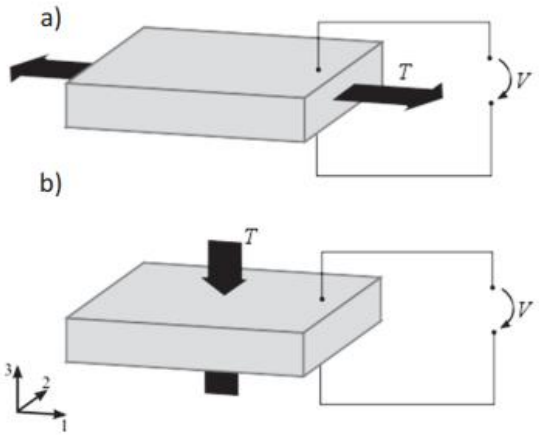

Figure 3.3: Representation of piezoelectric material in (a) 31 mode and (b) 33 mode [136]

The constants in a piezoelectric material referred as d, ε^T and E depend upon direction of electrical field, displacement, stress and strain. Two coefficients, d_{33} and d_{31} are the most significant piezoelectric coefficients used in PEH.

3.2 Piezoelectric Material Classification

As illustrated before, piezoelectric materials can be used to harvest energy by simple conversion of oscillatory energy into electrical energy. Combining this technology with mechanical coupling designs we can harvest energy from mechanical stress and strain. Piezoelectric materials can be divided into 5 types: natural, organic, ceramics, polymers and composites as shown in Figure 3.4.

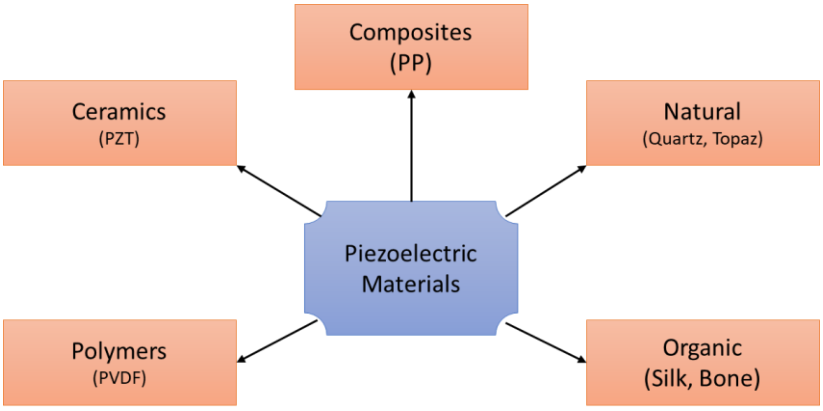

Figure 3.4: Classification of piezoelectric materials

Natural Piezoelectric Materials

There are many materials such as quartz and tourmaline crystals that naturally exist and exhibit piezoelectric effect. These crystals have non-centrosymmetric crystal lattice. These materials have in the past been actively used as electromechanical transducers [137] but as they exhibit relatively small piezoelectric effect their use in the natural formation is not as widespread as the other types of piezoelectric materials.

Ferroelectric Ceramics

Ferroelectric ceramics are an important group that exhibit ferroelectric properties. They can be used as capacitors [138], resonators [139] and surface acoustic wave sensors [140]. Ceramics such as PZT [141] and barium titanate ($BaTiO_3$) [142] have also been widely used in energy harvesting due to its favourable properties.

Piezoelectric Polymers

Polymers are formed when monomers combine with other monomers forming a repeating chain molecule through the chemical process of polymerisation (bonding together identical units). Polymers have favourable properties for actuators (if exhibiting small d constant) and sensors (if exhibiting large g constant). Such an example is PVDF [143] or Parylene-C [144] that exhibit a semi-crystalline structure.

Piezoelectric Composites

Composites can be fabricated using piezoelectric polymers or ferroelectric ceramics. They usually exhibit high coupling factor which makes them suitable as transducers. Such an example is a cellular film made of polypropylene (PP) [145].

Organic Piezoelectric Materials

Certain organic materials already exist such as bone, silk that exhibit some piezoelectric properties, but these materials have limitations. The way forward is for flexible, transparent, and stretchable characteristics. A new organic material developed by Murata Manufacturing Co Ltd, Kansai University and Mitsui Chemicals Inc [146, 147] is undergoing testing for a grip remote controller and a touch pressure pad fulfilling the demand for new human-machine interface applications.

3.2.1 PZT & PVDF

PZT and PVDF are the two promising materials used in most PEH devices [148] due to their favourable properties. This sub-section will explore characteristics and examples of both materials and apply a selection criterion to choose the piezoelectric transducer for this research.

PZT was considered to be a prospective replacement for batteries due to high piezoelectricity and energy density. PZT is often used in a specific composition to achieve a particular crystal structure and the desired piezoelectric effect. PZT is an oxide alloy of lead, zirconium and titanium and is one of the most researched and viable inorganic piezoelectric ceramic to achieve the desired effect [149]. PZT has a rigid lattice which allows the positive ions to move within the structure. With increase in temperature the dielectric constant of PZT starts to increase as seen in [150].

There are many factors that affect the power consumption and life of a piezoelectric device. In conditions of high humidity, leakage current increases the power consumption of devices. This can lead to the device failing but studies have shown no change in piezoelectric properties [151].

PZT has many applications in harvesting energy. One of the applications was developed by Howells, Heel Strike System for military and commercial use [152]. The system consisted of two pieces, the Heel Strike Generator and power electronics circuit. The purpose was to convert the unusable power from the Heel Strike Generator to something more useful. Mechanical energy would be transferred into electrical energy. The system was then tested at various compressions to evaluate the output energy. On average, it was noted that 0.0903 W per compression was produced. Although the desired outcome of power was much less than anticipated as several issues were found during the development of this project. If the issues highlighted in the study are addressed the Heel Strike Generator should be able to produce more energy. Figure 3.5 illustrates the schematic design of the generator and the operating mechanism.

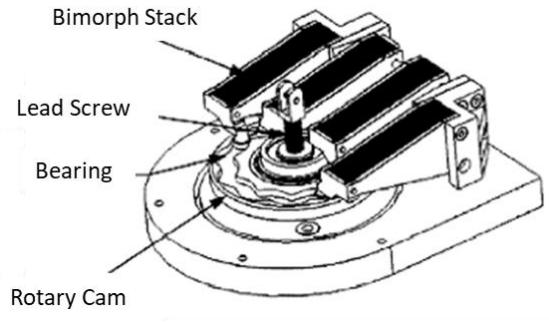

Figure 3.5: Schematic of Heel Strike generator [152]

A harvester [153] was fabricated by sandwiching PZT between two steel strips. The material was then compressed by applying mass in the range between 0 to 1500 g. Two significant tests were carried out for open-circuit and resistive load. The maximum voltage harvested at open circuit was 14 V. At resistive load, the maximum voltage harvested was between 6 – 9 V for 2.2 MΩ and 3.3 MΩ.

No load was connected across the PZT arrangement for linear compressions and the voltage output was measured. The range of test facility was only between 0 – 1500 g which affected the maximum voltage harvested. The voltage is seen to drop just after the 1500 g as the test facility is unable to apply anymore force. Even though the voltage was seen to rise but the force sensor was unable to collect any good data hence any voltage harvested beyond 1500 g was ignored in this study. Figure 3.6 shows the voltage versus mass at no load during the experimental stage.

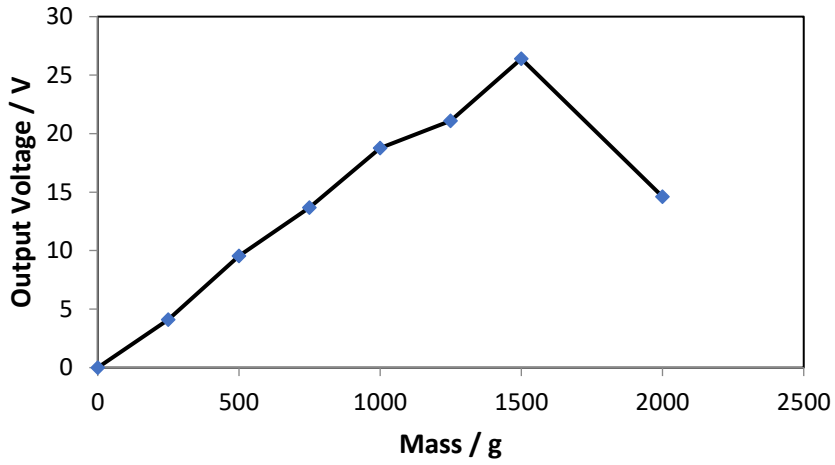

Figure 3.6: Output voltage at no load over mass for PZT arrangement [153]

Figure 3.7 represents the data collected when harvested voltage was measured with resistive loads of 1 MΩ, 2.2 MΩ and 3.3 MΩ, respectively. It was observed that the output voltage was higher during compression rather than de-compression. It was also observed that a maximum value of voltage at output were seen at 1500 g, which was the maximum mass or force applied onto the PZT material through the test facility. Using the trend, we can assume that the output voltage would increase further until the maximum power point was reached.

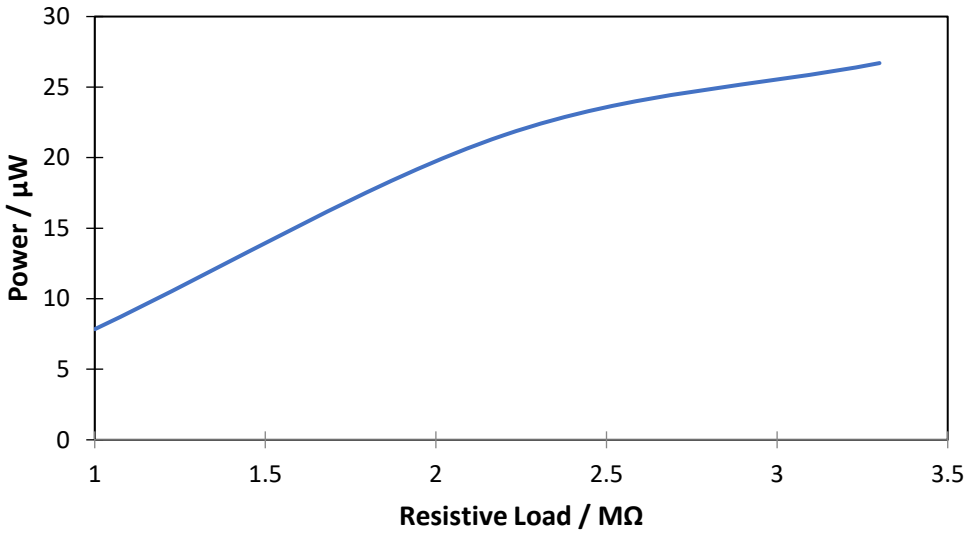

Figure 3.7: Output power against resistive load [153]

PVDF is a solid piezoelectric polymer with a semi-crystalline structure suitable for various applications. PVDF is made from polymerisation of difluoro ethylene ($CH_2 = CF_2$) monomers which can be illustrated in Figure 3.8. PVDF can be fabricated by injection or compression moulding which opens various applications in the form of a thin film, membrane or paste.

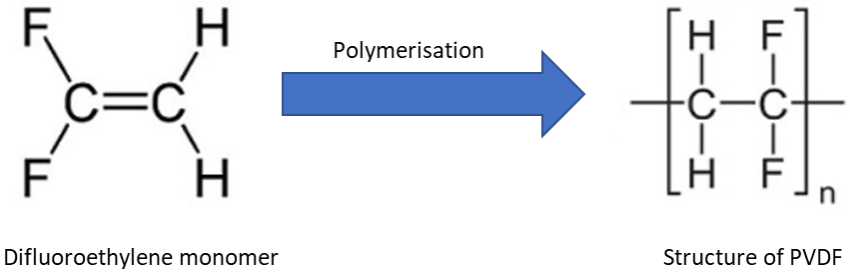

Figure 3.8: Polymerisation and structure of PVDF [84]

One of the application of a PVDF film was in measurement of cardiorespiratory signals [154]. The study showed a comparison of measurement systems using PVDF and electromechanical film (EMFi) using PP. The study concluded both materials were suitable with main advantage of EMFi was its flexibility and for PVDF it was its senstivity. Figure 3.9 shows the structure of sensors for measurement of cardiorespiratory signals made from commercially available PVDF and PP film.

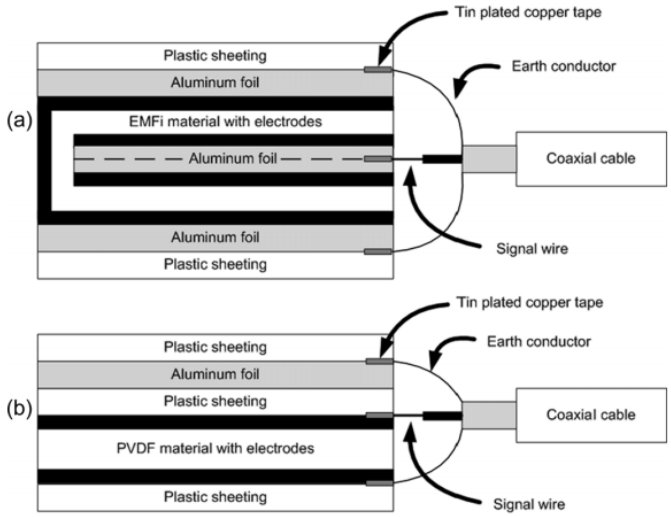

Figure 3.9: (a) EMFi and (b) PVDF sensor structures [154]

3.2.2 Material Selection and Structural Configurations

Selection criterion for the piezoelectric material must evaluate material properties for both PZT and PVDF. Firstly, Table 3.2 shows the piezoelectric parameters for PZT and PVDF which may indicate that PZT has higher piezoelectric properties in comparison to PVDF, but the other disadvantages outweigh this higher piezoelectric property.

Table 3.2 : Piezoelectric parameters for PZT and PVDF [155, 156]

Properties	**PZT**	**PVDF**
Density (10^3 kg m^{-3})	7.534	1.783
$\boldsymbol{d_{31}}$ (10^{-12} C N^{-1})	110	23
$\boldsymbol{d_{33}}$ (10^{-12} C N^{-1})	225 – 590	-33
$\boldsymbol{g_{31}}$ (10^{-3} V m N^{-1})	10	216
$\boldsymbol{g_{33}}$ (10^{-3} V m N^{-1})	26	-330
$\boldsymbol{k_{31}}$	30	12

Secondly, Table 3.3 demonstrates the main difference between PZT and PVDF as identified by other researchers [157-159]. PVDF has low permittivity, wide frequency response, easy fabrication and good choice for power generation. As PVDF is a polymer it is more flexible than PZT which on the other hand is brittle. One of the biggest advantages of PVDF is it is non-toxicity.

Table 3.3 : Comparison of PZT and PVDF

PZT	PVDF
High dielectric and piezoelectric constants	High voltage coefficient
High material density	Low material density
Extremely toxic due to the lead content	Not toxic
Brittle and inflexible	Flexible allowing various applications

Based on the experimental work conducted previously with PZT and information gathered from literature, a fair conclusion is drawn for the use of PVDF given its favourable lightness, flexibility and environmentally friendly properties in comparison to PZT. PZT harvesters are more brittle and not used favourably in cantilever arrangement [160]. PVDF based harvesters have been one of the most popular materials for implementation in harvesting systems and due to its flexibility, has the potential to produce a higher output in a REH system.

3.3 Single Degree of Freedom System

REH system based on a piezoelectric transducer is a simple vibratory system defined as SDOF which is a mass connected to the spring, and the mass travels along the spring elongation direction. This section will explore the free vibrations of the beam under impulse which is reduced to free vibrations with non-zero volicty.

3.3.1 Free Vibrations of SDOF System under Impulse

Most piezoelectric energy harvesting systems are based on a cantilever arrangement as shown in Figure 3.10 and the focus of this research is on such an arrangement with a piezoelectric transducer. The beam has a rectangular cross-section which can be subjected to bending vibration

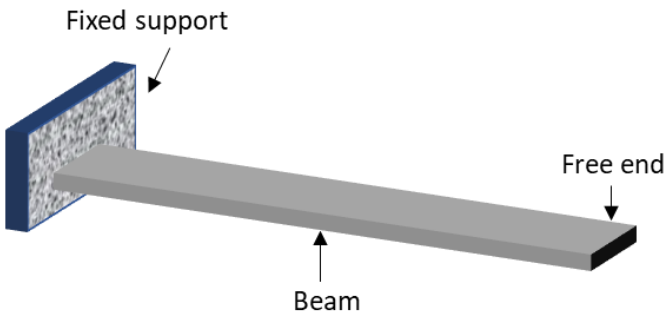

Figure 3.10: Cantilever beam under free vibrations

The natural frequency, f_n is expressed as Equation 3.5 [161] :

$$f_n = \frac{K_n}{2\pi}\sqrt{\frac{EI}{m_l l^4}} \tag{3.5}$$

where K_n is a constant for different modes of vibration, E is the modulus of rigidity of beam material, I is the moment of inertia of the beam cross-section, m_l is the mass per unit length and l is the beam length.

For a rectangular cross-section we can define the moment of inertia, I as Equation 3.6 where l is the length of the beam and w is the width of the beam [161]:

$$I = \frac{lw^3}{12} \tag{3.6}$$

In a SDOF system under impulse, there is going to be an additional mass at the free end which will need to be taken into consideration. The total mass at the free end can be modelled as the sum of discrete effective mass, with stiffness k and the mass of impulse, m. Cantilever beam under impulse can be represented by Figure 3.11, where m_c represents the mass of cantilever and m represents the mass of impulse.

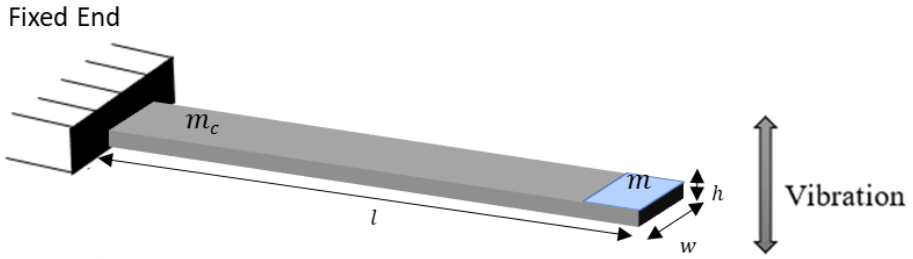

Figure 3.11: Cantilever beam under impulse

The resonant frequency of a spring-mass structure can be determined, where k is the spring constant and m is the inertial mass:

$$f_r = \frac{1}{2\pi}\sqrt{\frac{k}{m}} \tag{3.7}$$

For Figure 3.11 the resonant frequency with a mass at free end can be determined by Equation 3.8 [162]:

$$f_r = \frac{1}{2\pi}\sqrt{\frac{Ywh^3}{4l^3(m + 0.24m_c)}} \tag{3.8}$$

where Y is the Young's modulus, l is the length of the cantilever, w is the width of the cantilever, h is the thickness of the cantilever, m_c is the mass of the cantilever, and m is the mass at the free end.

There are various modes of vibrations for a unimorph cantilever beam under bending motion where mode 0 is when the beam is rigid. Natural frequencies can be calculated using boundary equations for each mode. A table of natural frequencies of a piezoelectric cantilever beam has been presented in Table 3.4.

Table 3.4 : Model frequency of piezoelectric unimorph cantilever [163]

Parameter	**Bending Motion**
f_{n1}	485 Hz
f_{n2}	3 kHz
f_{n3}	4.85 kHz
f_{n4}	8.6 kHz
f_{n5}	14.12 kHz
f_{n6}	17.12 kHz

3.3.2 Mechanical and Electrical Behaviour

Piezoelectric beams are generally a bimorph structure where a substrate layer is sandwiched between two piezoelectric layers. In an equivalent circuit of PEH device, the voltage source is connected in series with RLC (resistor, inductor and capacitor) and builds up a resonant circuit. The mechanical characteristic of a simple harmonic motion

is given as L_m, C_m and R_m, where L_m and C_m components model the behaviour of the transfer of energy in the harvester due to vibrations and R_m models the mechanical losses. The electrical equivalent components for electrical storage and losses are given as C_e, R_{e1} and R_{e2}, where C_e is the capacitance of the transducer as it consists of two parallel plates across the piezoelectric material and R_{e1} and R_{e2} are the electrical losses in the harvester. Figure 3.12 shows an equivalent circuit of the harvester mechanism developed using a piezoelectric transducer.

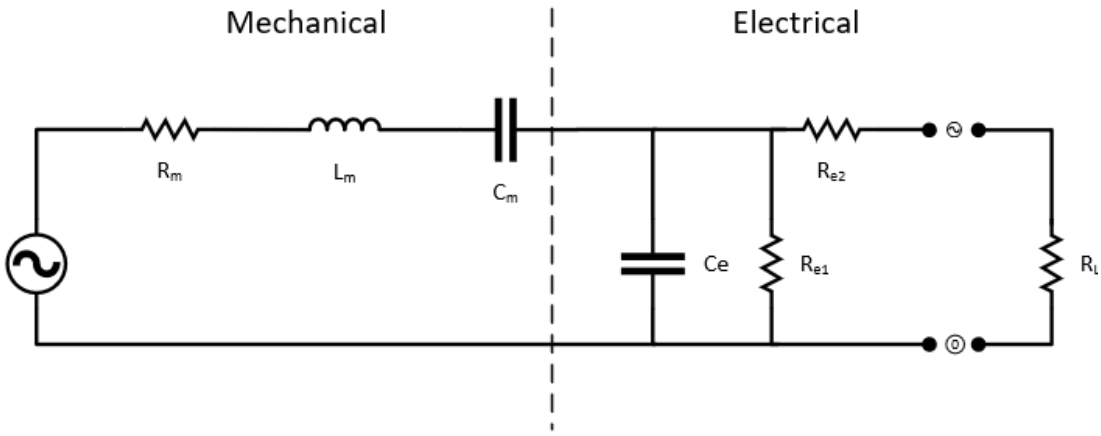

Figure 3.12: Equivalent circuit model for harvester

Most harvesting systems utilise the bending strain of cantilever beams at resonance condition to generate electrical power using piezoelectric materials. However, one of the challenges is that we gain smaller power output than the theoretical power predicted. Moreover, the resonance frequency of conventional piezoelectric energy harvesters is very high and the bandwidth too narrow, which prevents the application of such devices where diverse range of frequencies is substantial. Water layer formed on a piezoelectric transducer will decrease natural frequency of the structure and the rms voltage produced by the system [164] but the cantilever arrangement has been proposed as a better arrangement for PEH devices [165].

3.4 Interface Circuit to Harvester

Piezoelectric material produces alternating voltage and current. In order to harvest energy from a piezoelectric material we need to rectify the alternating output to direct output. This can be achieved in various ways, but 2 commonly used strategies are reviewed in this section and the selection of rectifier circuit for this study.

3.4.1 Full Bridge Rectifier

In vibrational energy harvesting a full bridge rectifier is a common solution to the problem of alternating output due to low internal resistance of such a system. To create a full bridge rectifier, 4 diodes are connected in a Wheatstone bridge formation (in series), smoothing the output. During the positive half-cycle, diodes D_1 and D_2 conduct in series whilst D_3 and D_4 switch off due to being reverse biased and hence the current flows through the resistive load. During the negative half-cycle, diodes D_3 and D_4 now conduct in series and D_1 and D_2 switch off, ensuring current flows through the resistive load. This formation ensures the current flows in the same direction through the resistive load and by adding a capacitor it will smooth out the alternating output to direct output. The bridge rectifier circuit is shown in Figure 3.13.

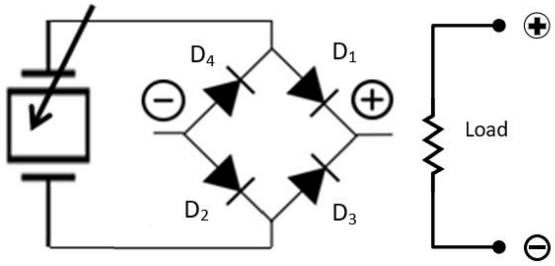

Figure 3.13: Circuit diagram of full bridge rectifier

3.4.2 Voltage Doubler

Voltage Doubler produces twice the amount of voltage at output in comparison to the input voltage as the name suggests. It takes an alternating voltage and converts it to a double direct voltage by using two diodes. The operation of such a circuit can be explained in two steps; on the negative half-cycle C_2 is charged to voltage V_{IN} and on the positive half cycle C_1 is charged to a voltage of V_{IN} too. Capacitors are connected in series to give an output of $2V_{IN}$. This arrangement can be seen in Figure 3.14.

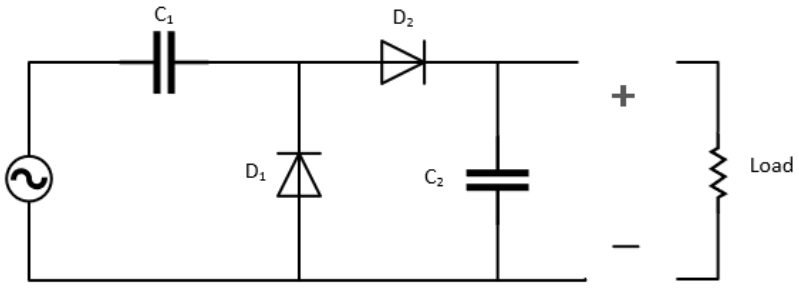

Figure 3.14: Circuit diagram of voltage doubler

Voltage doubler may increase the output voltage but reduces the current and the output has undesired fluctuations which is not ideal for many applications. There are alternative approaches such as a self-biased active voltage doubler [166] but uses parts of the harvested energy to bias the op-amp.

3.4.3 Circuit Selection

Experimental work conducted in the field of PEH has showcased systems either using a full-bridge rectifier or voltage doubler set up as a rectifier to convert alternating voltages to direct voltages. Although work has been carried out at exploring alternative approaches such as using active rectifier [167] but have frequency limitations associated with them.

A trigger circuit rectifier design [168] is proposed to be ideal for low output voltage from the microgenerator mainly consisting of a diode connected MOSFET with an additional parallel synchronous rectifier. Initially the voltage at the buffer capacitance is too small for the additional synchronous rectifier to operate, but once the voltage level starts to increase this provides additional charge at the output which could potentially enhance the output. The trigger circuit performs the operation of a comparator-like hysteresis action for various switching voltages but does consume some power in the region of nW which could be detrimental to the output of harvesters which already rely on low power output. Such an approach may seem ideal but due to the constraints of this research this cannot be used but does highlight an opportunity to be explored in the future. The proposed rectifier and trigger circuits are shown in Figure 3.15.

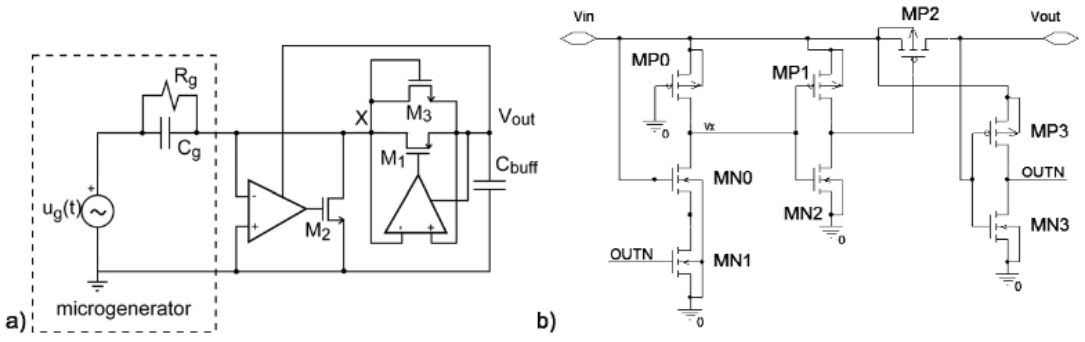

Figure 3.15: Schematic for (a) Rectifier circuit and (b) Trigger circuit for microgenerator [168]

It is proposed for this research a full bridge rectifier arrangement will be used to convert the alternating output of the piezoelectric transducer. An experimental validation [106] using PEH device with water droplet impact compared various rectifying circuits, and established full bridge rectifier as an optimum interface circuit to the harvester. The study compared full bridge, voltage doubler, Cockcroft Walton cascade voltage doubler (CWCVD) and Karthaus Fisher cascade voltage doubler (KFCVD) rectifier circuits. Figure 3.16 shows the voltage output of the harvester with a 100 kΩ load and the best performance is given by the full bridge rectifier.

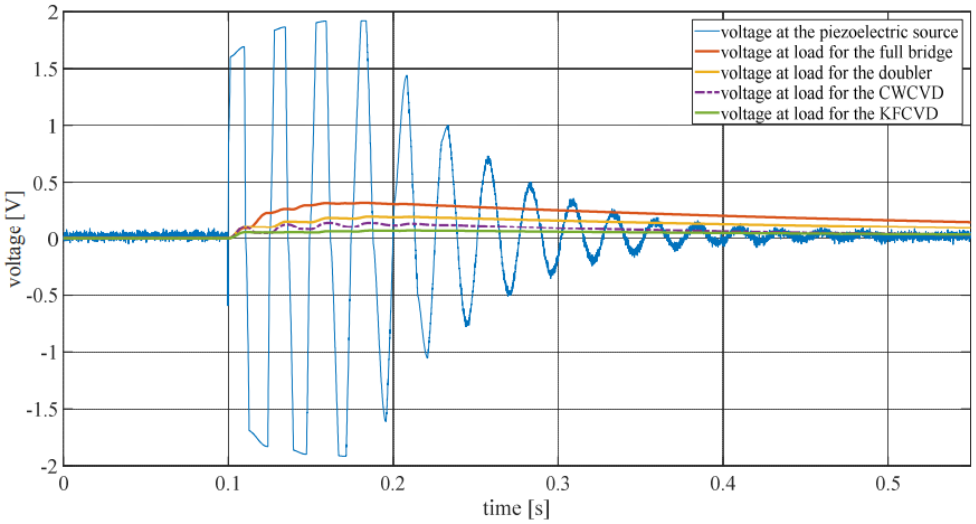

Figure 3.16: Voltages on the load for single droplet using different rectifying circuits [106]

An ideal diode will conduct when applied voltage is forward biased and act like an insulator with applied voltage being reverse biased. These would be ideal circumstances and diodes in fact do not act like this and therefore there is a voltage drop associated with them which has an impact on the rectified output of the harvester. Ideal diodes are impossible to fabricate therefore it is important to establish how standard diodes would behave. One of the studies [169] presented simulation results of a PEH output comparing an ideal and standard diode using both configurations of full bridge rectifier and voltage doubler. Results indicate the same maximum power output but different operating bandwidth. Results comparing these arrangements are shown in Figure 3.17.

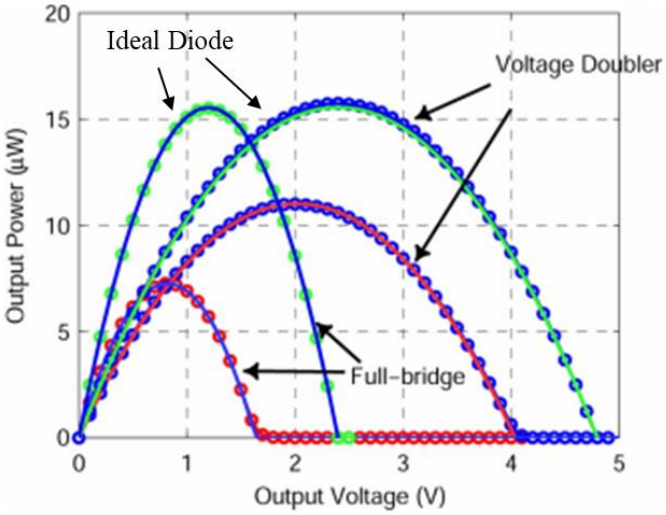

Figure 3.17: Output of full-bridge rectifier and voltage doubler with and without ideal diodes [169]

Circuit selection is an important factor for this study as rectification is needed to convert the alternating output of the harvester. Due to the limitations of budget and the stable output required from the raindrop energy harvester, a full-bridge rectifier circuit will be used. For such a circuit to be developed standard diodes are used which will have a small impact on the output of the device due to voltage drop which is generally between 0.6 to 0.7 V.

3.5 Device Specification

An off-the-shelf piezoelectric sensor by Pro-Wave (FS-2513P) was chosen to be used in this research for experimental data. This piezoelectric transducer based on the active film of PVDF was chosen for its favourable conditions which has been identified as an ideal piezoelectric material for the water droplet impact. The piezo film is further protected by a transparent non-conductive coating. Silver (Ag) electrodes are plated on the top and bottom of the piezo film. The device has low mechanical and acoustic impedance and has a high resistance to moisture. Connecting wires are soldered onto the end terminals to connect the load and measure the voltage output.

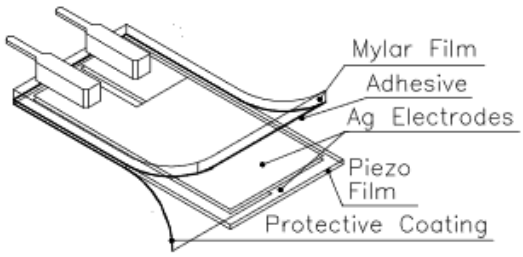

Figure 3.18: Schematic of Pro-Wave FS-2513P

The specification of the transducer with its dimension and operating parameters are presented in Table 3.5.

Table 3.5 : Piezo transducer specification

Parameter	**Units**	**Value**
Length	mm	25
Width	mm	13
Thickness	mm	0.25
Thickness of PVDF film	mm	0.02
Mass of transducer	g	0.1725
Capacitance	nF	1.5 ± 30% @ 1KHz
Voltage sensitivity at	mV/ms^{-2}	70
Operation temperature	°C	-20 to +60

The water droplet can vary depending on the type of rain shower and the air resistance. Most experiments conducted under laboratory conditions, as reported in the literature, using a standard burette or pipette arrangement will typically have the diameter ranging between 1 mm and 5 mm, for which the droplet remains in a spherical shape. With an increase in the diameter as established in the literature, it has been shown that the shape can change depending on wind speed and air resistance [67] The schematic of the cantilever beam is illustrated in Figure 3.19 where the transducer is fixed at one end using the clamping mechanism and the other end is free to oscillate as the water droplet impacts the beam.

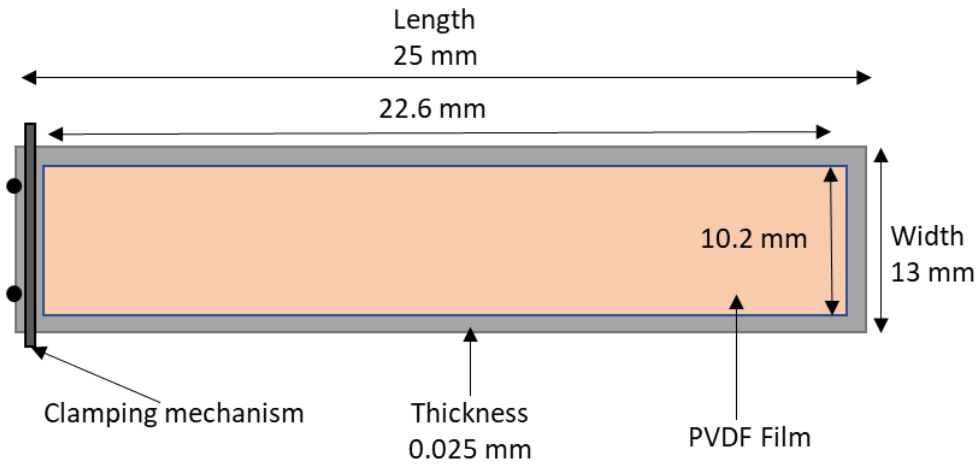

Figure 3.19: Schematic of cantilever beam

The output of the harvester will be measured using a digital oscilloscope (Tektronix – TDS3032B) with differential probe (Testec – TTS19001). Probes are generally designed with high impedance at the point of contact in the hope of reducing the current (energy) drawn from the circuit, thus, reducing the loading. For all the experimental work carried out, same equipment was used. The probes are classed as high impedance proves with an input impedance of 1 MΩ. A minority of the current is used for detection/measurement with a typical experimental load ranging between 1 - 5 MΩ. Droplet impact process is a low frequency event and the sampling frequency is also generally low; therefore has negligible impact on the measurements.

3.6 Summary

This chapter presented the fundamentals of piezoelectricity and gave an in-depth comparison between two competing materials: PZT and PVDF. PVDF has a wide frequency response which would be a good option for REH. Impact of water droplets will produce varying frequency, therefore the PEH device must be able to cope with such a system. PVDF is non-toxic and does not harm the environment and relatively safer to handle and has been chosen for this research.

A simple model of energy harvester is discussed in the configuration of cantilever arrangement where the impact of water droplet will act as a mass for SDOF system. Equivalent circuit parameters with respect to mechanical and electrical behaviour has

been represented, which will be explored in the later chapters to develop an energy harvesting model. This chapter also introduced various approaches to rectifying circuits, which will be crucial in interconnecting several PEH devices to observe the impact of the output of the PEH device and a selection is made for such an arrangement.

A theoretical review [165] uses data collected on annual quantity of water in a region, to propose the ideation of some key patterns for a piezoelectric energy harvesting system from rainy precipitations and proposed cantilever as the best arrangement, which further validates the selection process in this Chapter. An off-the-shelf piezoelectric transducer will be used as a PEH device for experimental work.

CHAPTER 4

4 Impact of Water Droplet on a Piezoelectric Transducer

This chapter analyses the impact of water droplet on a piezoelectric transducer after having been released from various heights to replicate a rain shower. The chapter also presents a model to characterise the output power for one-unit device, which can then be applied to an array of rain impact harvesters. These results have been published in Elsevier Energy Journal in 2015 [123].

4.1 Experimental Arrangement

Raindrops were artificially replicated in the laboratory using a burette and set to produce drops at a constant size of diameter. The diameter of the droplet at the instant before it is released from the burette was measured to be 4.0 ± 0.2 mm. As discussed in Chapter 2, it is assumed the water droplet is spherical just before impact with the harvester device. The water droplet is aimed at the centre of impact zone on the piezoelectric transducer as shown in Figure 4.1 due to limitations of the experimental setup**.** The distance covered by the water droplet from the position it was released from the burette to the surface will be referred to as the impact height, h, for the purpose of this research. The transducer was clamped at one end and the clamping position for all measurements remained constant for all the experiments conducted for single droplet test.

The output from the piezoelectric transducer was measured using an oscilloscope with differential probes. Resistive loads of 1 MΩ (±5 %), 1.8 MΩ (± 5%), 2.2 MΩ (± 5%), 2.7 MΩ (±5 %), 3.3 MΩ (±5 %) and 4.7 MΩ (±5 %) were connected appropriately. The output voltage was measured under impact of water droplets for each of the resistive loads. Each test was repeated several times for reproducibility of data.

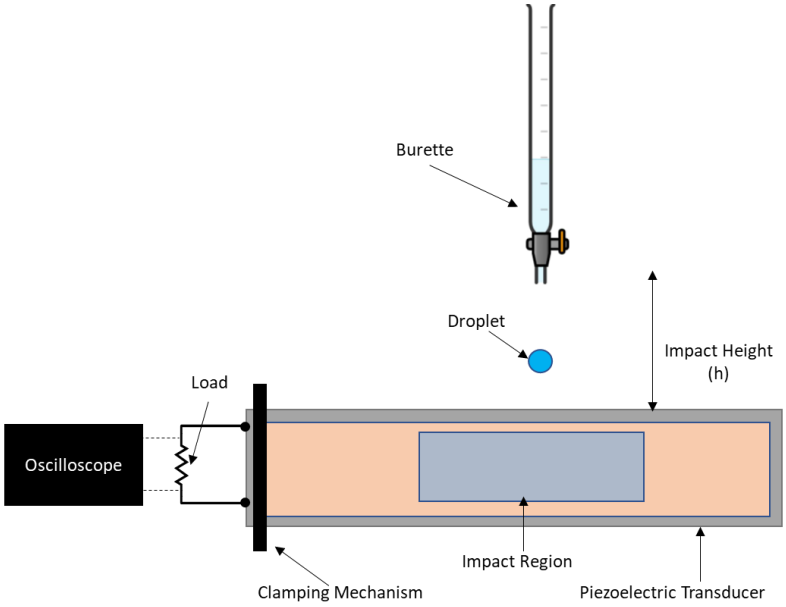

Figure 4.1: Experimental setup to measure impact of single droplet

4.2 Experimental Results

The results are presented in three sub-sections. The first sub-section gives an example of the type of raw data acquired by the investigation. The subsequent two sub-sections are analysis of the two main features observed in the data of any one single event, single droplet impact.

4.2.1 Initial Impact

Before the water droplet impacts the PEH device, the sensor is at a horizontal position close to the zero position. As the water droplet falls onto the sensor, it interacts with the device and starts to push the sensor downwards from position 1 the “Droplet impact start sequence” to position 2 the “Maximum negative velocity of device sensor”. The sensor accelerates during this time and reaches maximum negative velocity at position 2 resulting in a maximum negative voltage. The sensor then decelerates and reaches its full deflection at position 3 the “Full deflection of device sensor” resulting in a zero voltage. The device sensor then starts to rebound and accelerates back in the opposite direction and reaches its maximum positive velocity at position 4 the “Maximum positive velocity of device sensor”. This results in a maximum positive voltage output which is the maximum voltage magnitude of the whole event. After this point in the whole event, the voltage output oscillations and deflection oscillations of the sensor decay away.

As was expected, the first deflection of the sensor in the negative position when pushed down by the droplet impact was the largest maxima of all subsequent maxima of the oscillations. It should be noted that the droplet does not deliver all its energy at the first instant of the impact but takes a finite time as the droplet interacts with the transducer.

The impact mechanism is complete and available energy fully delivered when the full deflection of the device sensor is reached at position 3. All these features are illustrated in Figure 4.2.

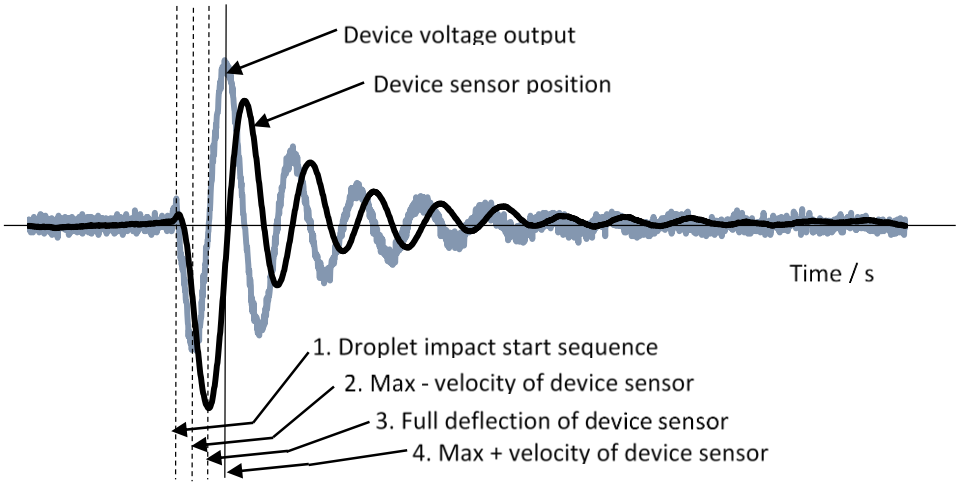

Figure 4.2: Voltage output and sensor position profiles of the device

The frequency of oscillation remains constant throughout the experimental setup for single transducer and single event, which is around 125 Hz. Figure 4.3 depicts the voltage output profile of a single energy harvesting unit of a water droplet impact event. An oscillating profile is shown which consists of two stages as the event evolves with time. These stages are shown as the “log growth” stage as the voltage grows to a maximum followed by the “exponential decay” stage as the voltage decreases to zero.

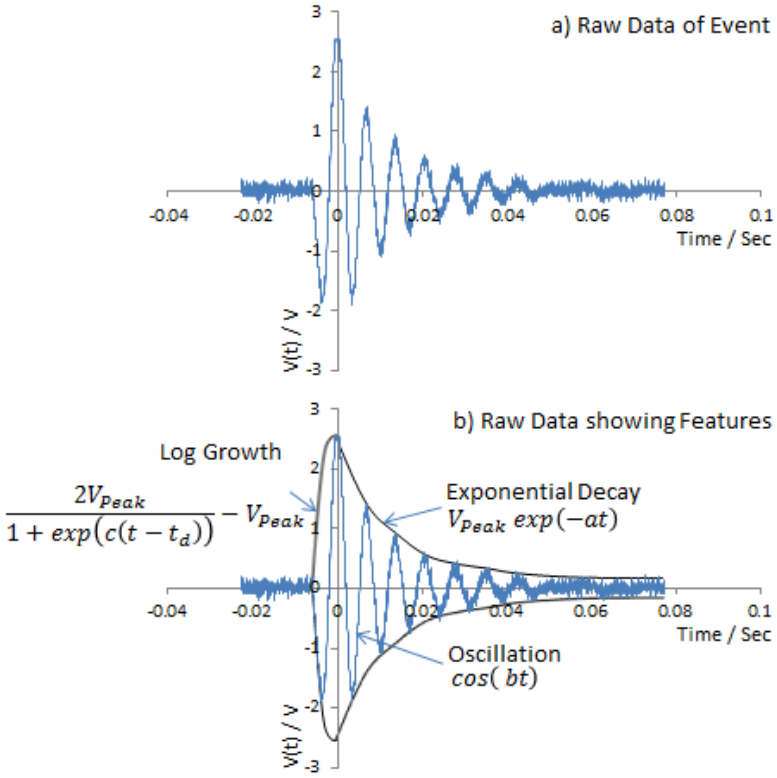

Figure 4.3: Voltage output of harvester for one event (Raw data)

The oscillating profile is of a cosine form which is seen in the two stages of a log growth and exponential decay function. A best fit envelope was developed based on exponential and logarithmic models as it appears to be a best fit for the growth and decay functions. The log growth stage in the voltage consists of a growth term and the cosine term as shown in Equation 4.1, where V_{peak} is the highest voltage attained, t_d, c and e are constants.

$$V(t) = \left(\frac{2V_{Peak}}{1+exp(c(t-t_d))} - V_{Peak}\right) cos(\ et) \qquad 4.1$$

The exponential decay stage of the voltage consists of a decay term and the cosine term as shown in Equation 4.2, where a is the decay constant which relates to the half-life of decay ($t_{1/2}$) and b is the time constant which relates to oscillation frequency (f).

$$V(t) = V_{Peak}\ exp(-at) cos(\ bt) \qquad 4.2$$

where $a = \frac{\ln(2)}{t_{1/2}}$ and $b = 2\pi f$

The equation can be rewritten by substituting the values of a and b in Equation 4.2 which gives us Equation 4.3:

$$V(t) = V_{Peak}\, exp\left(-\frac{In(2)}{t_{1/2}}t\right) cos(\,2\pi f t) \qquad 4.3$$

4.2.2 Growth Stage

During the log growth stage of the harvesting event, the voltage grows to a peak (V_{peak}). A plot of this peak voltage against load for different impact heights is shown in Figure 4.4. By increasing the impact height from 17 cm to 47 cm, we see a trend in the peak voltage output which increases. It can also be seen that as the load is increased the peak voltage also increases, which means the current remains constant. A best fit linear regression is found for each profile with a correlation coefficient (the R-Squared parameter) between 0.43-0.90.

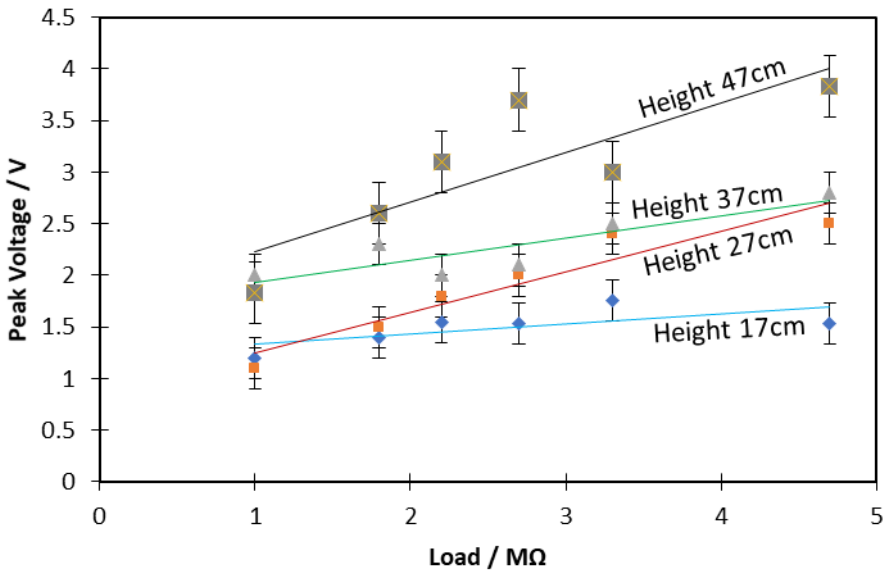

Figure 4.4: Peak voltage from harvester

Mean power has been determined using Equation 4.4 and energy using 4.5 for the data collected, which is then presented later.

$$Power = V^2/R_{load} \quad 4.4$$

$$Energy = Power \times time\ duration \quad 4.5$$

Figure 4.5 depicts the power and energy output of the log growth stage of one event for different impact heights at different loads. Average power of data gathered against load is also plotted as shown in Figure 4.5a, which is consistent with the expectation of higher power with an increase in the impact height. At different loads, the mean power for 17 cm and 27 cm droplet heights is reasonably consistent between 0.2 and 0.6 µW. There is an outlier in the data captured for 37 cm which shows a decrease in the mean power when the load is 1.8 MΩ. However, the rest of the data on 37 cm is reasonably consistent. Impact height of 47 cm shows an increase in mean power with increasing load up to 2.2 MΩ but the mean power decreases with a further increase in load over 2.8 MΩ.

The duration of the log growth stage for the events is shown in Figure 4.5b. No trend is observed in this data in relation to droplet height or loading. The duration for this stage of the event, t_{d1}, is approximately 6 ms. Figure 4.5c shows the energy harvested during the growth stage of the event (product of data in power and duration).

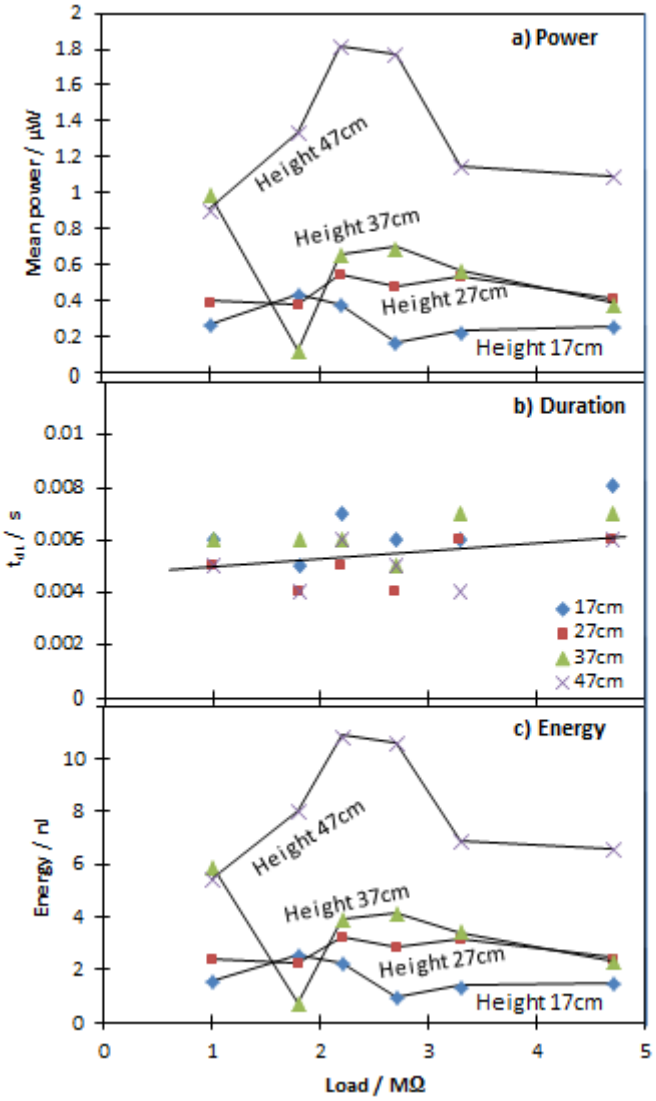

Figure 4.5: (a) Power, (b) Duration and (c) Energy output of the log growth stage of one event

4.2.3 Decay Stage

During the exponential decay stage of the harvesting event, the voltage oscillations decay away. The decay constant (a) and time constant (b), for Equation 4.2 are found and plotted in Figure 4.6. As can be seen, the influence of the impact height and the load, R, have on these coefficients shows no clear trend within the resolution of the experiments. Trend lines have been fitted to all collected data points.

Figure 4.6a shows that the decay constant, a, across all loads, is approximately 60 s^{-1} which is a half-life, $t_{1/2}$, of 0.0115 s. Figure 4.6b shows that the time constant, b, across

all loads is approximately 900 s^{-1} which is the frequency of decaying oscillations with a frequency of 143 Hz.

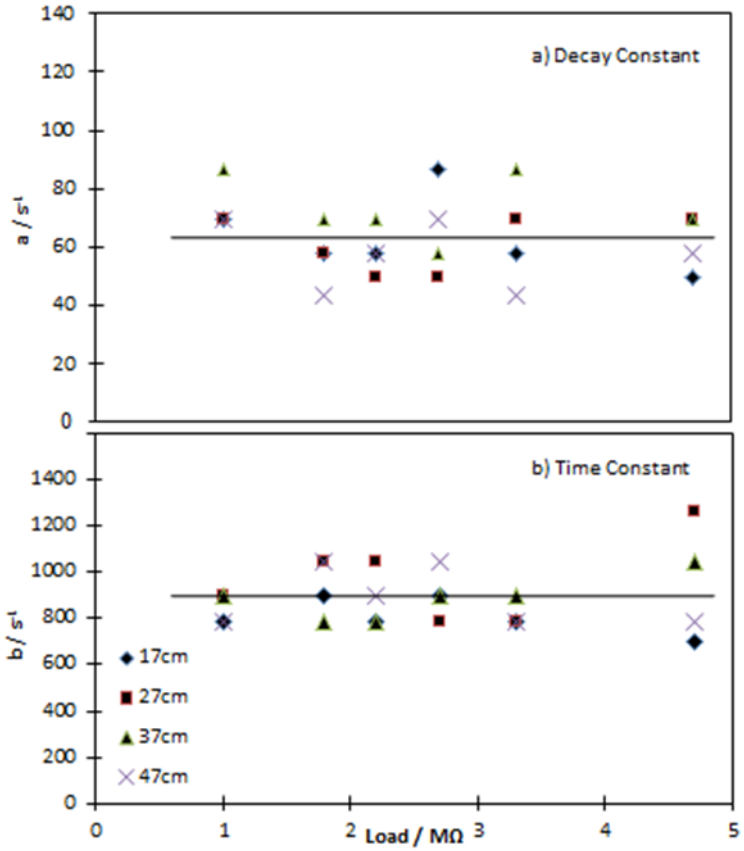

Figure 4.6: (a) Decay constant and (b) Time constant for one event

Figure 4.7 shows the power and energy output of the exponential decay stage of one event for different impact heights at different loads. The plot of mean power against load is once again reasonably consistent with the trend of a higher power with an increase in the impact height as shown in Figure 4.7a. Impact height of 47 cm shows an increase in power with an increase in load from 1 MΩ to 2.2 MΩ. However, the power output starts to decrease if the load is increased over 2.2 MΩ possibly because of the issue of impedance matching. There is an outlier in 37 cm impact height, which shows the maximum power at 1 MΩ and then decreases as the load increases. It is speculated this could be because of damping at a particular height and load connection. Power values for 17 cm and 27 cm are reasonably consistent.

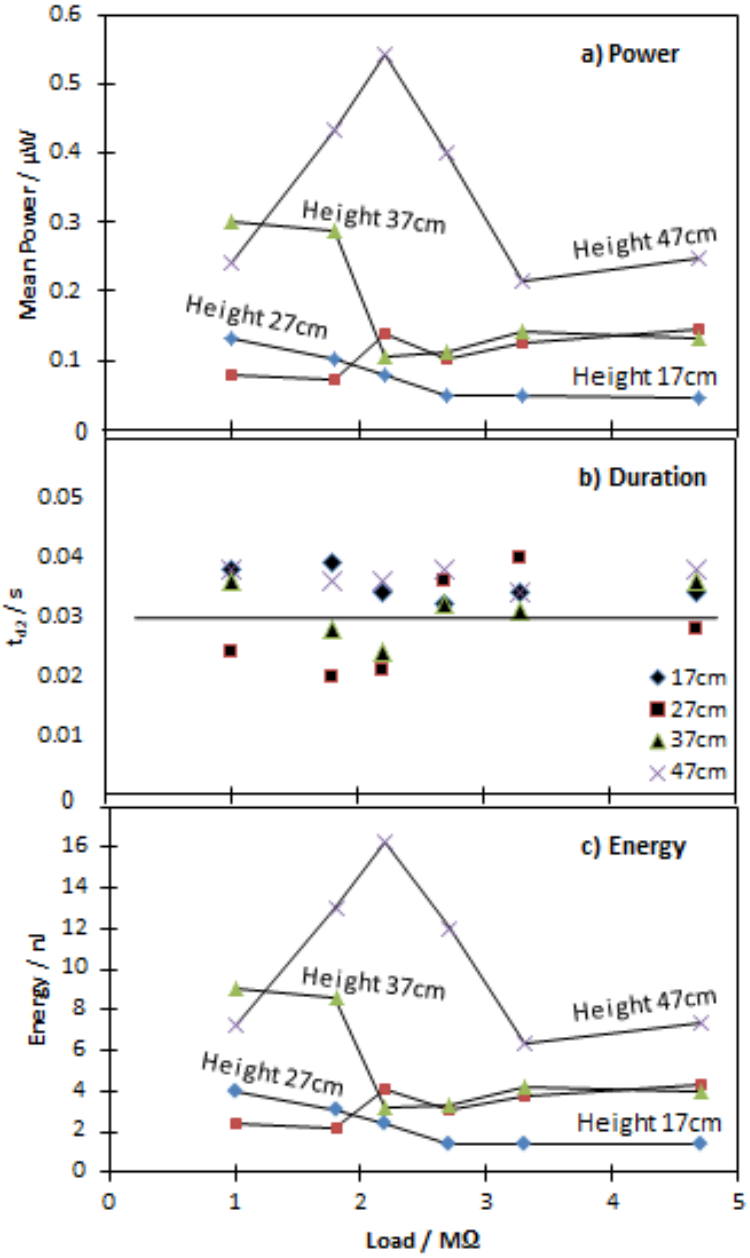

Figure 4.7: (a) Power, (b) Duration & (c) Energy output of the exponential decay stage of one event

Figure 4.7b shows the duration of the exponential decay for different impact heights and loads. Trend line has been fitted to all collected data points. The duration of this stage of the event, t_{d2}, is approximately 30 ms. Figure 4.7c shows the energy harvested during the decay stage of the event (product of power and duration)

The mean power during second stage, the decay stage, is around 30% smaller than the growth stage. The average time duration of 0.006 s for the growth stage is 20% that of

the decay stage. The energy of the growth stage is around 69% that of the decay stage. All this shows that in the growth stage of the event, the impact process of the droplet, has a significant contribution to the overall output of the device.

4.3 Discussion of Implementation

The discussion starts by dealing with data collected from the single harvesting unit as a complete system. A calculation of the droplet velocity is made to relate the voltage output to the droplet velocity under different electrical load conditions. It is also examined how the experimental data evolves with time giving rise to the mean power and energy from one unit during one event. The third sub-section proposes a multi-harvester array by using the data from the single unit and examines the expected output from multi-events of raindrops with time.

4.3.1 Harvesting System Model

A full understanding of an EH system requires a description of a) the input to the harvester, b) the harvester's converter processes and c) the output to a load or consumer.

The energy input to the harvester from a droplet impact is related to the kinetic energy of the droplet and the impact mechanism giving rise to an energy transfer function/coefficient. The kinetic energy, as described by Equation 2.8, is a function of the density of the droplet, its diameter and the square of its impact velocity.

A numerical method based on Equation 2.9 and 2.10, was employed to relate the height, h, of the droplet to its expected velocity, v, on impact with the device. The density of air and water are taken to be 1.2041 kg/m^3 & 999.97 kg/m^3 respectively. The droplet is considered to be a sphere of diameter 4 mm, and the drag coefficient is considered for a sphere to be 0.47. Velocity profiles are illustrated as it can be seen in Figure 4.8a that a terminal velocity of 9.62 ms^{-1} is attained if the droplet is allowed to fall for more than 3 seconds. In the experiments conducted, at a maximum height of 47 cm is expected to achieve a velocity of 2.13 ms^{-1}, as shown in Figure 4.8b.

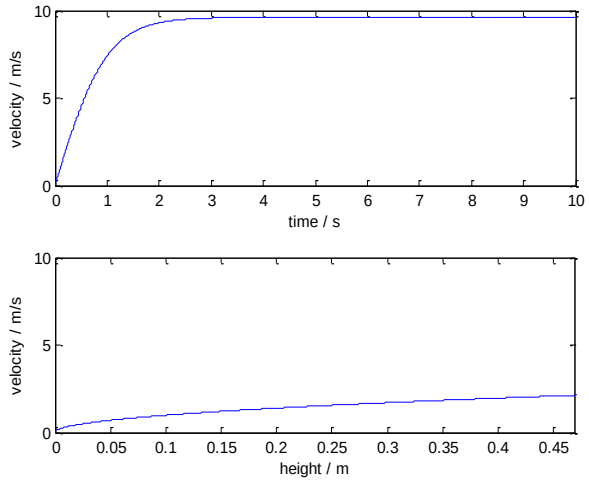

Figure 4.8: Relating droplet fall height to velocity

Table 4.1 presents the kinetic energy values from a raindrop based on the impact height for this study using Equation 2.8.

Table 4.1 : Kinetic energy of water droplets

Height (m)	**Velocity (m/s)**	**Kinetic Energy (µJ)**
0.17	1.28	27.43
0.27	1.62	43.95
0.37	1.89	59.81
0.47	2.13	75.97

Figure 4.9a shows the relationship between the peak voltage produced by the device and the expected velocities of the droplets on impact from the experiments conducted under different electrical loads. Clear trends are seen, and gradients of best fit lines are found with coefficient of correlation ranging from 0.63 – 0.94. These gradients of peak voltages per impact velocity from Figure 4.9 are plotted against the electrical loads in Figure 4.9b, to give a volt per impact characteristic of the harvester.

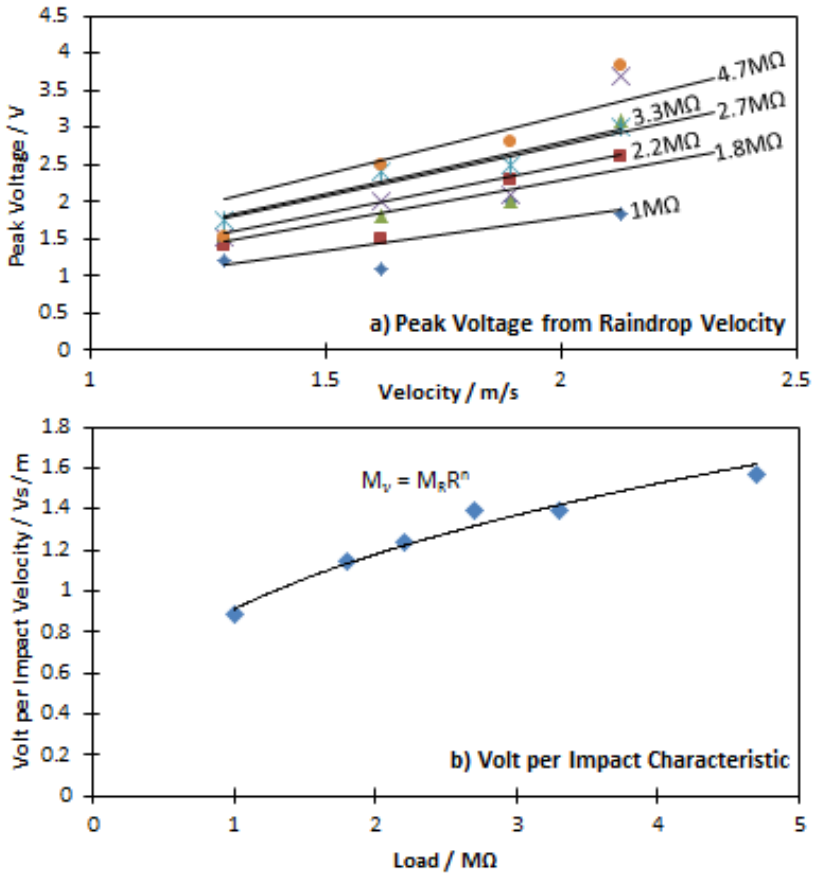

Figure 4.9: (a) Peak voltage from raindrop velocity and (b) Volt per impact characteristic of the harvester

A power law fit is used in Figure 4.9b as this had the best fit with a coefficient of correlation of 0.97. From the experimental data in Figure 4.9b, an empirical relationship between the peak voltage and raindrop impact velocity is given in equation 4.6

$$V_{peak} = M_R \frac{R^n}{R_0} v \qquad 4.6$$

where v, the velocity, which is dependent on the impact height, R is the external electrical load, R_0 is a constant to conserve units of value 1 Ω^n and M_R is the volt-impact coefficient. From the analysis of the data in Figure 4.9, the following parameters are found: where M_R = 0.0054 Vsm^{-1} & n = 0.3714. These values are used to calculate the peak voltage to model the voltage profile over an event. This is discussed hereafter.

4.3.2 One Unit Harvester

The experimental data acquired is from a single unit harvester and the analysis focuses on the profile of an event (repeated many times) which typically lasts for a total 0.036 s. The mean power of an event caused by different impact velocities is calculated from the log growth stage and the decay stage data. This total mean power is plotted in Figure 4.10a which is found to be generally below 2.5 µW. Energy is plotted in Figure 4.10b which is found to be generally below 90 nJ.

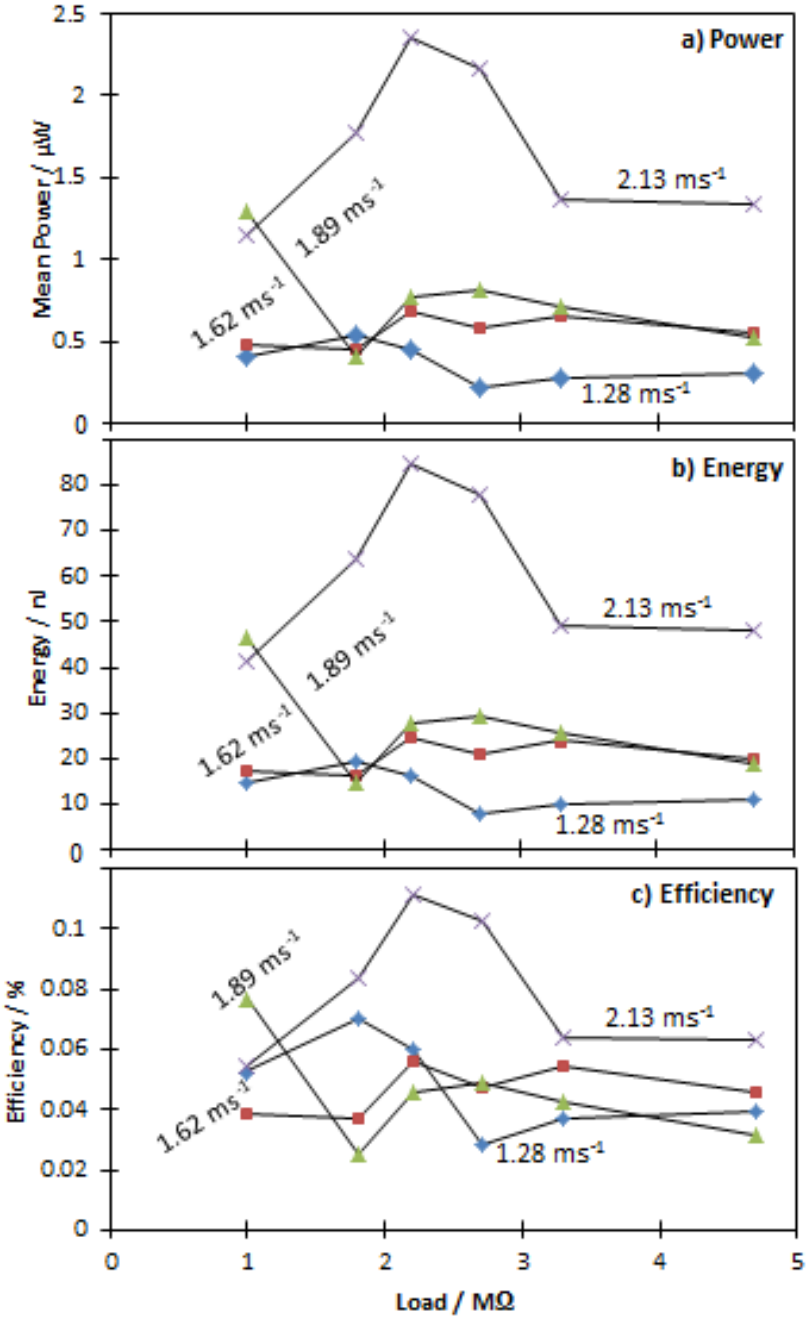

Figure 4.10: Output of the device

The energy conversion efficiency is calculated based on the theoretical value of kinetic energy available through the droplet as shown in Table 4.1. The energy conversion efficiency of the harvester is found to generally less than 0.12% which is in line with literature. However, there is opportunity to understand all the factors that influence this conversion and efficiency and present a more detailed way of defining this efficiency and explore mechanism where this efficiency could be improved by using the idea of an array of harvesters.

4.3.3 An Array of Harvesters

Having multiple harvester units, given appropriate design constraints, will enable more power to be delivered. Once a model of a single harvester unit is available, this can be used to scale up to an array of units. In this chapter, the mean power from one event has also been empirically modelled to observe trends in the data which is used for building a harvester array model (HAM).

The calculation of the instantaneous power output from single harvester from one event is modelled in Equation 4.7 by combining Equations 4.1 and 4.3. Values for this instantaneous power can be found by using data from the results acquired in this research.

$$P_{inst} = \left| \frac{1}{R_{load}} \left(\frac{2V_{Peak}}{1 + exp\big(c(t - t_{d1})\big)} - V_{Peak} \right)^2 cos^2(\,2\pi f t) \right|_{t<0} + \left| \frac{V_{peak}^2}{R_{load}} exp^2 \left(-\frac{In(2)}{t_{1/2}} t \right) cos^2(2\pi f t) \right|_{t\geq 0} \quad 4.7$$

Equation 4.7 can be combined with Equation 4.6, and integrated over the event duration shown in 4.9 to give us the equation for P_{mean}.

$$P_{mean} = M_R^2 \, R^{-0.2572} \, v^2 \, \tau \quad 4.8$$

$$\tau = \int_{t_{d1}}^{0} \left(\frac{2}{1 + exp\big(c(t - t_{d1})\big)} - 1 \right)^2 cos^2(\,et) \frac{dt}{-t_{d1}} + \int_{0}^{t_{d2}} exp^2(-at) cos^2(bt) \frac{dt}{t_{d2}} \quad 4.9$$

Where τ is the integration parameter, resulting in τ = 0.5169, and the other parameters are taken from the experimental results of a = 60, b = 900, c = -1200, e = $2\pi\ 3/(4t_{d1})$, t_{d1} = 0.006 s and t_{d2} = 0.03 s.

By using Equation 4.8, a graph of simulated mean power against the load is presented in Figure 4.11

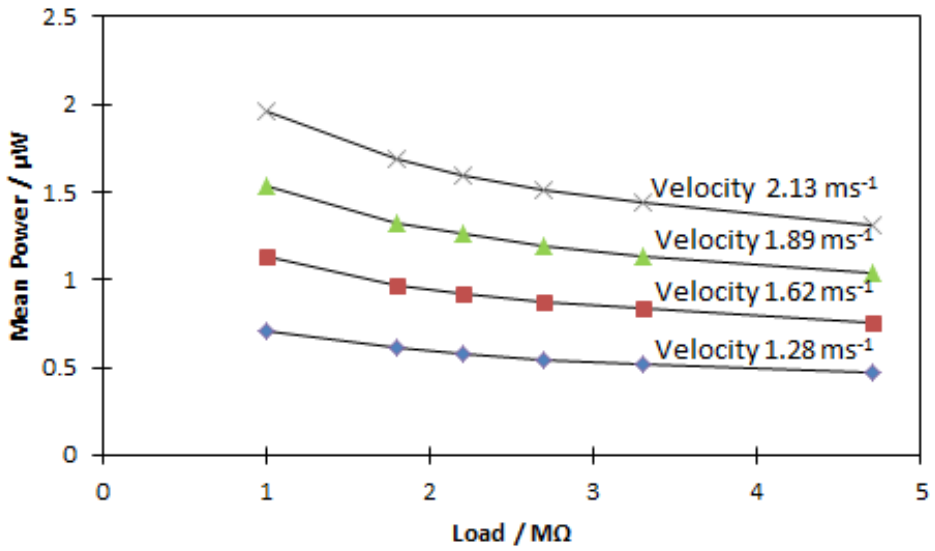

Figure 4.11: Mean power found from model

This modelling approach loses the fine detail of the expected behaviour within the range of loads studied but does show a general trend of decreasing power with load. Also, it can be seen that the influence of impact velocities is appropriately modelled by comparing Figure 4.10a with Figure 4.11. This approach is used in modelling the output from an array of these harvester units.

Equation 4.8 is used to model the behaviour of a unit harvester, based on the empirical data acquired and implemented in an algorithm to model a harvester array in MATLAB. A numerical approach is used for multiple units in an array of defined size for a rainstorm of duration 300 s and quantity of 32 mm.

Figure 4.12 represents the mean power output for a load of 1 MΩ, with rainfall of 32 mm (quantity of 32 litres per cubic metre) and a duration of 300 s. Figure 4.12a shows the power output for a 1 m^2 harvester array to a resolution of 0.036s (the duration of one event). It should be noted that the whole area of the array is not considered as actively

harvesting but only a proportion of it. In this study the relevant proportion is taken to be 80%. It can be seen that the power output for 1 m^2 HAM is noisy due to the random nature of rainfall. However, the probability of the power output dropping below 100 µW is remote.

Figure 4.12b shows the distribution of expected power output (a frequency plot of the number of units of power within 0.036 s resolution) with a mean of 150 µW for a 1 m^2 HAM. Figure 4.12c shows the power output for a 10 m^2 HAM with its respective distribution plot in Figure 4.12d. It can be seen that the deviation from the mean is lower with large arrays.

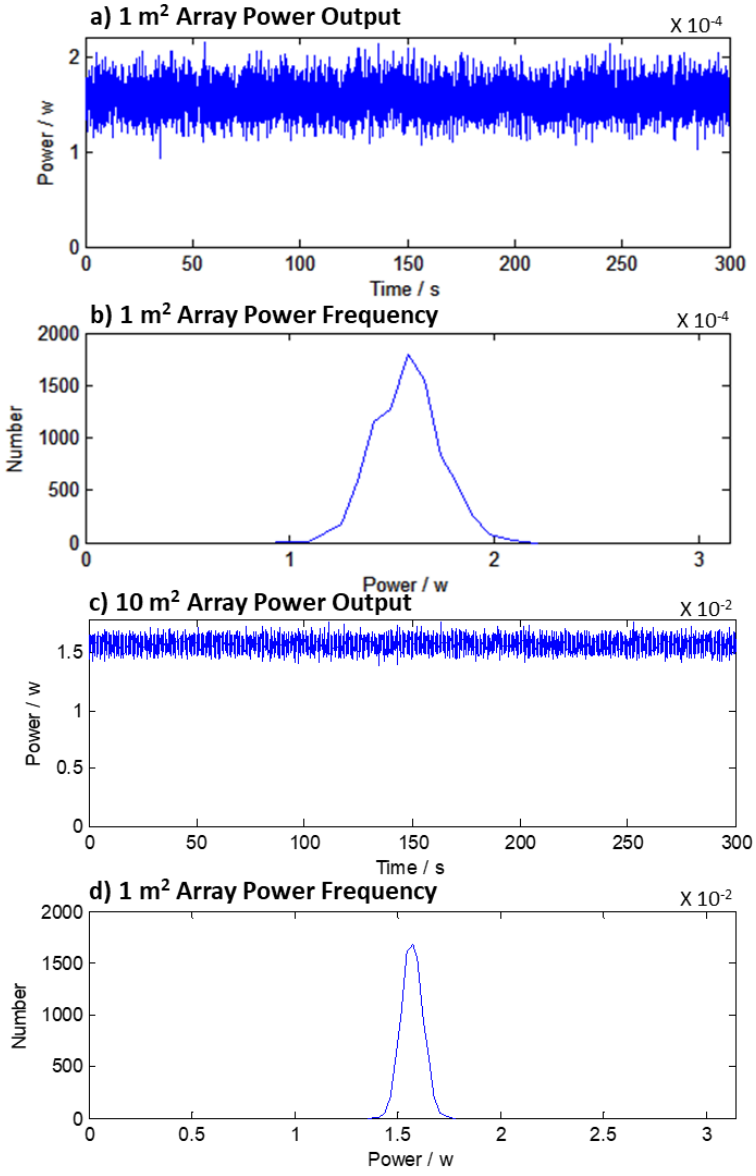

Figure 4.12: Power output for HAM at (a) 1m^2 and (b) 10m^2

As the size of the array is increased, power output is increased as a result, with the highest power of 160 mW and 3.5 W for different velocities attained at 100 m^2 as shown in Figure 4.13a and c. With an increase in the size of the array, deviations are reduced significantly with a change of size from 1 m^2 to 1000 m^2 as shown in Figure 4.13b and Figure 4.13d.

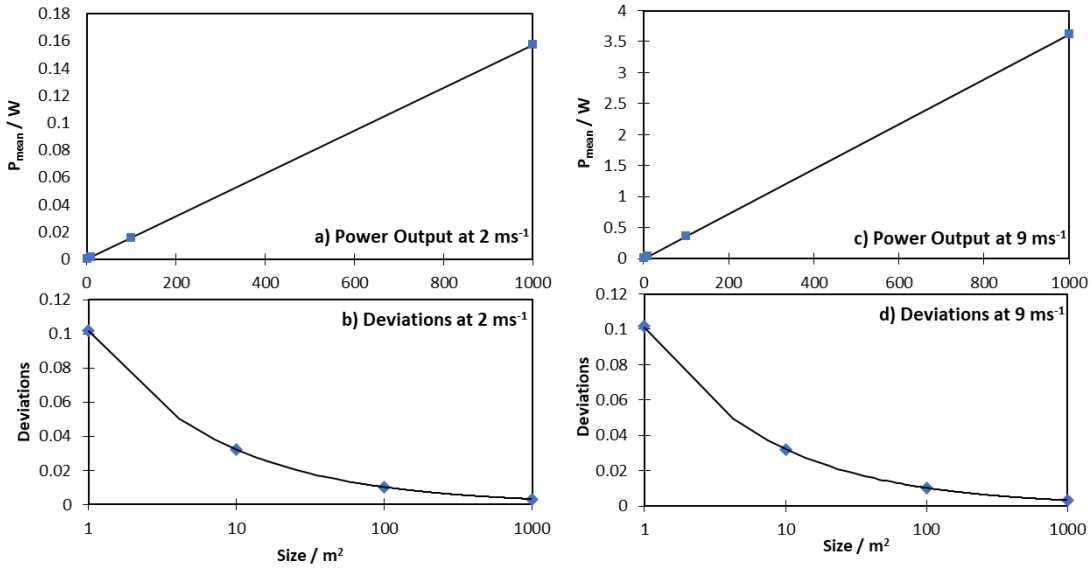

Figure 4.13: Power output from an array for different droplet impact velocity

4.3.4 Experimental Limitations and Assumptions

One of the assumptions made is that the raindrop fell from a low altitude and therefore the changes in temperature, air pressure, air density and gravity are ignored. Another assumption is that the raindrop maintains its spherical shape just prior to impact. The raindrop is also assumed not to be affected by any extraneous force such as wind. Since all experiments are conducted based on a single impact which lasts around 0.036s, the model is limited to single impact and does not take into account multiple impacts occurring simultaneously. All raindrops behave similarly upon impact based on the model presented here. It is an empirical model based on the data acquired and is dependent on the impact behaviour. However, it was found from running the multiple array simulation with appropriate levels of rainfall that, multiple impacts within the 0.036 s time window are a rare occurrence.

Given these assumptions the main forces acting on the raindrop are, air resistance and gravity as discussed in Chapter 2.2.3. The main factor which may influence the velocity under these conditions is the shape of the raindrop but for the purpose of these

experiments it has been assumed that the raindrop maintains a spherical shape during freefall. In fluid mechanics, Re and We are dependent on the velocity at which the raindrop is travelling. When the diameter of the raindrop increases, the drag coefficient decreases, respectively. The drag coefficient is also dependant on the Reynolds number [170].

Tap water is used in this study which has many nutrients and minerals [171, 172]. However, rainwater generally contains fewer minerals in comparison to tap water. The surface tension of tap water at room temperature (20 °C) is 0.072 N/m [173] and dynamic viscosity at room temperature (20 °C) is measured as 0.982 cP [174]. There is no easily accessible published data available as regards to raindrop surface tension and viscosity.

Given these assumptions and approach, it is thought that the experimental study presented in this chapter would give a good, if conservative, estimate of possible power output from rain droplet energy harvesting using an unmodified off-the-shelf commercially available PVDF device.

4.4 Summary

This chapter has demonstrated the detailed behaviour of a harvesting system scavenging energy from raindrop impacts. Three main findings in particular have been highlighted in this work:

- The detailed voltage output profile from PEH device shows an impact stage during droplet impact process, followed by a decay stage as stored energy in the harvester is dissipated, with an oscillatory character to the harvesting event of a single impact.
- The impact stage lasts for a significant time period when compared to the duration of the entire harvesting event and has a significant amount of energy associated with it.
- The power output is very small and is consistent with the findings of other researchers.

The focus of this study has been to show the behaviour of a harvesting system scavenging energy from raindrops. To this end the design of the experimental conditions has been carried out with the aim of replicating a typical raindrop. The size of the rain droplet varies between 0.5 mm to 5 mm depending on the type of rain as discussed in the earlier

section. The droplet size used in the experiments is chosen within this range at a radius of 2 mm. The droplet velocity is calculated to be as much as 2.13 ms^{-1} depending on the height from which the droplet is released. This allows for a conservative estimate of a raindrop velocity and thus less than under optimistic expected power output. The terminal velocity of 9.62 ms^{-1} is calculated in this study in comparison to 6.49 ms^{-1} for stratiform rain of similar droplet size as shown in Table 2.3.

This chapter investigates experimental results with distinct features highlighting the log growth and exponential decay of the harvesting process of a droplet impact. It has been shown that the droplet impact stage has a significant contribution to the overall power output of the device. The energy output of the device is found to be less than 90 nJ with the mean power below 2.5 µW for a single unit harvester during one impact event under different conditions of height and load. The efficiency is found to be low, generally registering less than 0.12%. However, with the opportunity to improve the efficiency of the system, raindrop energy harvesters have many possible applications. The results in this chapter showcase that we were able to harvest power in the µW region.

A model has been developed which takes the empirical data for the single unit harvester during a single event and uses this for an array of harvesters with particular areas. Calculations for arrays of $1m^2$ and more are presented. The smaller arrays show larger noise to mean power ratios which demonstrates the random nature of rainfall.

CHAPTER 5

5 Single and Multiple Unit Module

In this chapter an energy harvesting module is developed consisting of multiple piezoelectric devices which uses impacts of water droplet to generate electrical power. The effect on the efficiency of the module with non-rectified and rectified outputs is investigated. Additionally, the voltage, power and energy were found for different surface angles, surface conditions and impact regions for single devices with a view to maximise module efficiency. These results have been published in Elsevier Energy Journal in 2017 [124].

5.1 Experimental Arrangement

5.1.1 Test Facility

Water droplets are made to fall onto the piezoelectric transducer under laboratory conditions. The PEH device is mechanically fixed at one end so that it is free to move at the other end, oscillating in a bending motion in the vertical direction. Figure 5.1 represents a device beam fixed at the left-hand side which has a water droplet impacting the surface allowing it to oscillate along the length of the device (also known as a pitching motion). This causes compressions and extensions in the piezoelectric material resulting in the charge displacements and energy conversion mechanism. Additionally, there are further possible vibrational modes, for example allowing it to oscillate along the width of the device (also known a rolling motion). Most droplet impacts will cause a pitching motion due to the limitations of the experimental setup, but some droplets might be able to cause a rolling motion when the device is tested under replicated rain shower in the laboratory.

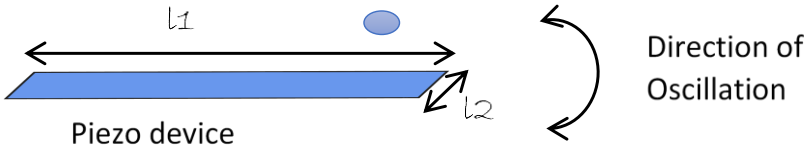

Figure 5.1: Impact of water droplets on PEH device

The PEH device is integrated in a test facility made of Perspex and is anchored on a stainless-steel plate with a rotary protractor to measure the angle of incline of the setup. Figure 5.2 shows the CAD drawing for the test facility before it was fabricated. The PEH device is clamped into a single position on the test bench. The voltage output of the device is measured using a Digital Oscilloscope with differential probes. Each test was repeated several times (usually at least 4 times) to show the reproducibility of the data.

The test facility allows consistency of clamping the device into position and flexibility of connecting various devices to form a module. Piezoelectric transducer is slotted into the clamping mechanism area which is made of rubber to provide firm support for the transducers.

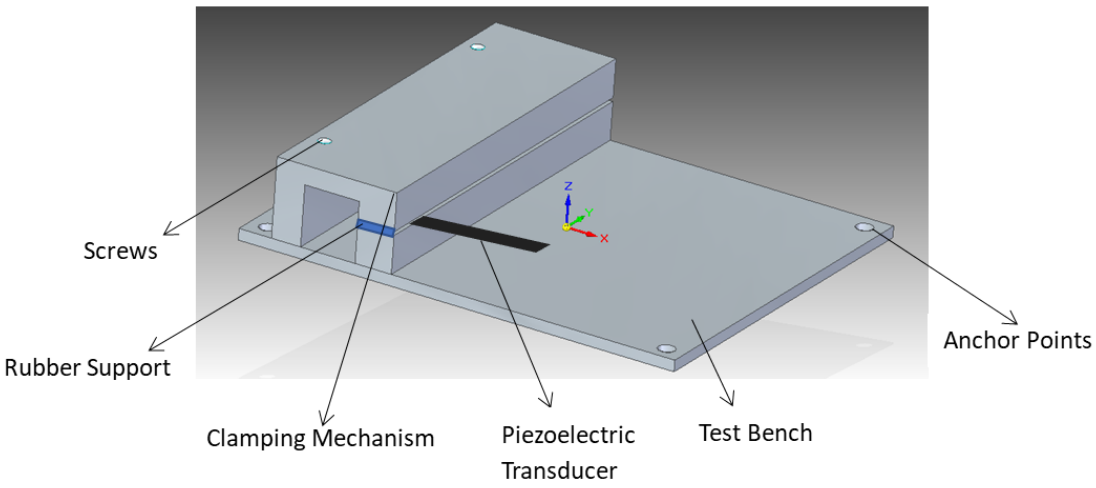

Figure 5.2: Schematic of test facility

Three impact regions are identified on the transducer surface as illustrated in Figure 5.3 for targeting of the droplet. The transducer is clamped towards the left-hand side as illustrated allowing the right-hand side of the device to move up/down freely with the

impact of water droplet. Change of voltage overtime is measured as part of this experimental study.

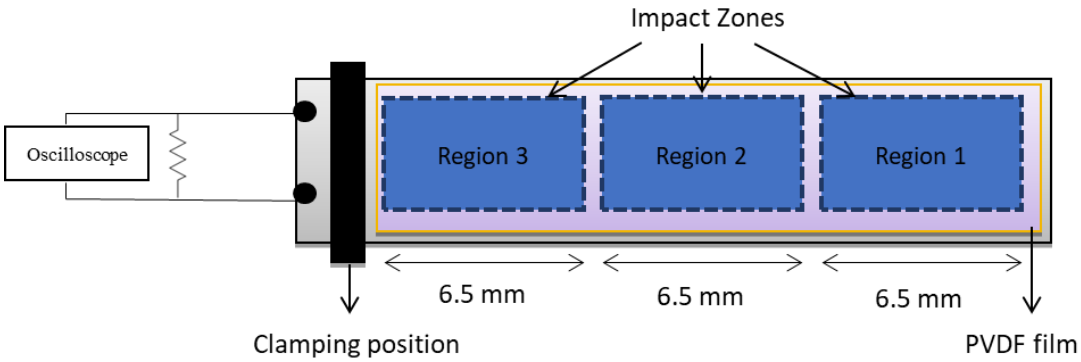

Figure 5.3: Impact region on the PEH device

5.1.2 Experimental Set-up

In this Chapter, two main experimental tests were carried out which included single unit test and module test with several transducers connected in parallel. For the single unit test, a single piezoelectric transducer is connected to the 1 MΩ resistive load and the voltage across the load is captured on a digital oscilloscope.

A module with multiple units is formed where transducers are connected in parallel arrangement. The first series of tests on the module is conducted with 1 MΩ resistive load and no rectifying circuit was integrated. The general configuration of this non-rectified arrangement of the module is illustrated in Figure 5.4a. The change of voltage output overtime is measured. The second series of tests on the module with multiple units is conducted with each transducer having its own rectifying circuit. The units are also connected in parallel with a 1 MΩ resistive load. The general configuration is shown in Figure 5.4b. During both these tests on non-rectified and rectified module, only one transducer (Unit 1) is excited by the impact of water droplet which is represented by the blue arrow in Figure 5.4. Tests are repeated at least 4 times for both configurations for repeatability.

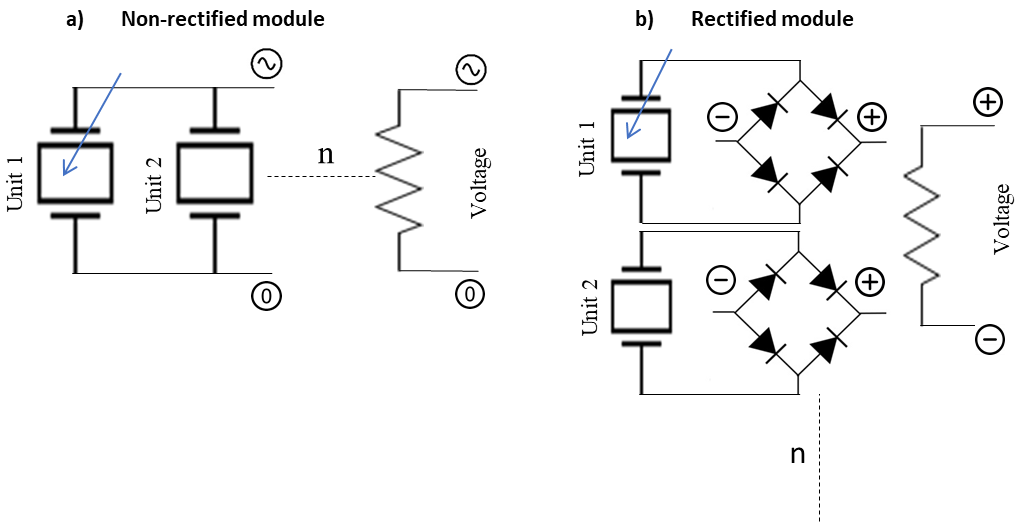

Figure 5.4: Circuit diagram of parallel connection with n number of units (a) non-rectified module and (b) rectified module

5.2 Single Unit

5.2.1 Voltage Measurements

Peak voltage over the three regions was measured with changing the surface angle at which the device is declined (angle is reduced). As discussed in Chapter 2, the impact mechanism plays an important role in the overall output of the device. The results in Figure 5.5 demonstrate that Region 1 gives out maximum voltage when the device is anchored at horizontal position (surface angle set as 0°).

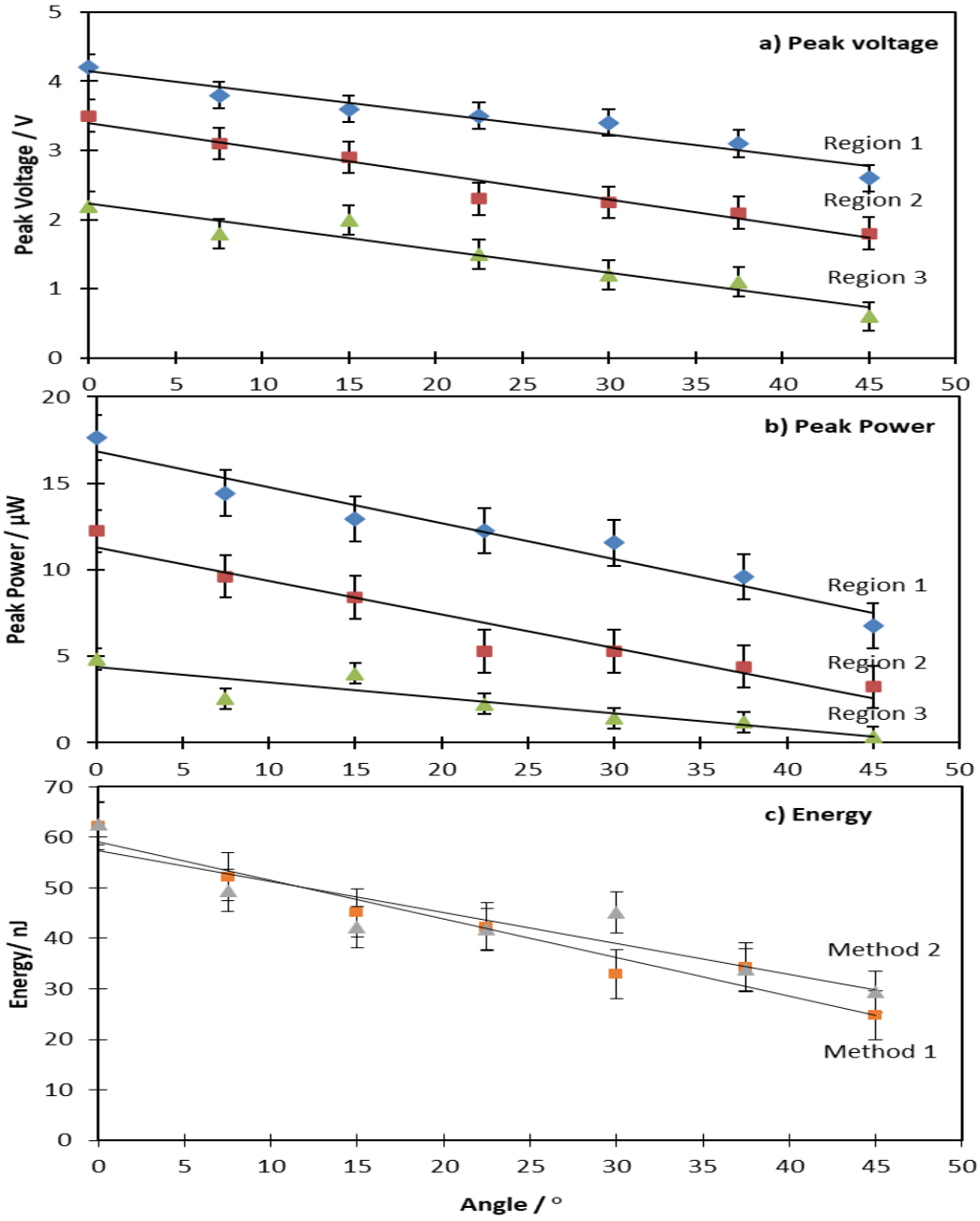

Figure 5.5: Parameters of single PEH device (a) peak voltage, (b) power output from harvester, (c) energy output

Experiments were conducted with different angles to see how the output would decrease to quantify any degradation. It was expected that Region 1 would be give the maximum output, but these experimental results give some real values of how this off-the-shelf transducer behaves when droplet falls on it. As the angle of the device is increased from 0° to 45° it was observed that the peak voltage generally decreases. This is mainly due to

the change in impact position of the droplet. When the device is at 0° the droplet normally splashes on the transducer and most of it is retained on the surface, hence giving a higher output. When the droplet impacts the transducer at an angle, most of it disperses and bounces off the transducer hence a lower output is observed. The peak power attained was in the region of 4 to 18 μW which is in line with data presented in Chapter 4.

Additional experimental work was carried out to ascertain the effect of different surface conditions. Peak voltage measurements were recorded with change in surface conditions using different materials on the active surface of PEH; cellulose based tape and vinyl-based tape. The results do not show any significant change in the peak output voltage of the device as all these materials would be classed as hydrophilic, due to the limitations of the off-the-shelf transducer, the surface could not have been modified to see the impact of hydrophobic surface. The results are shown in Table 5.1 with a resistive load of 1MΩ and at horizontal position (0°) at Region 1.

Table 5.1 : Peak voltage at various surface conditions

Surface	**Peak Voltage (V) (±0.2V)**
Dry surface on sensor	2.9
Wet surface on sensor	3.0
Transparent Tape (Cellulose based)	2.9
Transparent Tape (Cellulose based) with holes	2.8
Insulation Tape (Vinyl based)	3.0
Insulation Tape (Vinyl based) with holes	2.9

A series of results were captured for the ramp-up (initial impact) of water droplet to impacting on a dry and wet device. For consistency and repeatability, the resistive load was 1MΩ, with 0° angle, impacting at Region 1 with a frequency of oscillation of 250 Hz.

For the dry condition, the PEH device was wiped clean before each measurement was taken. Any water droplets that may have been deposited on the surface of the device were wiped dry before each set of results were analysed. This shows an 'edgy' initial impact with the surface of the device. The wet device replicates real rain conditions where the water droplets may already be deposited on the surface of the device. The results show a smoothing of initial impact as the water droplet impacts the surface of the device. The two different waveforms are shown in Figure 5.6.

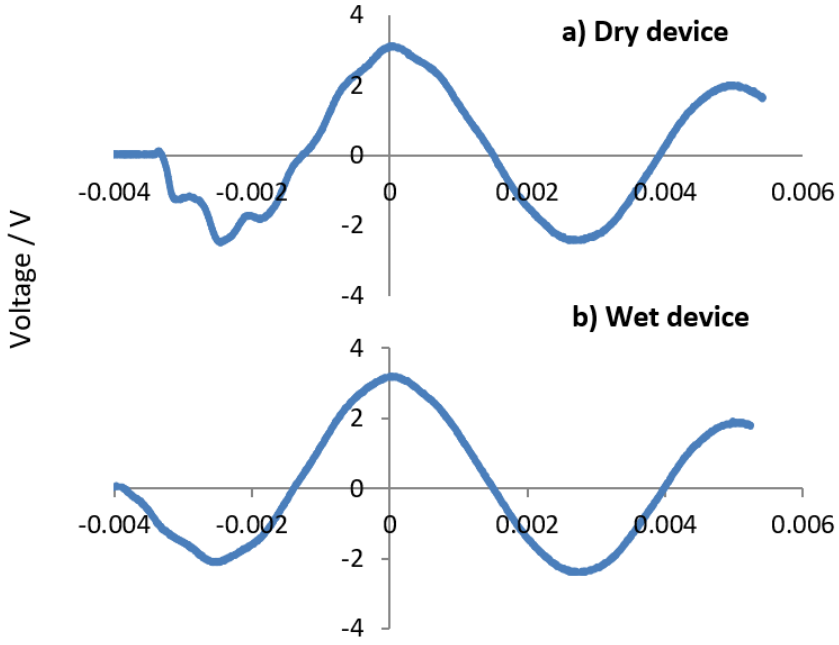

Figure 5.6: Device output in different conditions (a) Dry device and (b) Wet device with frequency of oscillation of 250 Hz

As explained earlier there may be multiple modes of oscillation; vertical oscillations and width-ways oscillations. The dry transducer in Figure 5.6a shows the initial impact as a 'high-frequency wobble'. When the water droplet interacts with the surface of the transducer it can possibly be oscillating the device sideways thus giving us an edgy curve. Figure 5.6b shows a 'low-frequency wobble' as the curve is smoothed out indicating that the transducer has only oscillated in vertical direction. The difference between the peak voltage of wet and dry device is negligible. However, it is determined that the surface interaction and the way the device oscillates is of importance but due to the resolution of

the scope and measuring system the difference in output was seen negligible., However the importance of this has been highlighted in Chapter 2.2. The dominant fact regardless of whether the device is dry or wet the peak voltage remains roughly the same. The difference in the waveform can be explained by assuming the material is homogenous in every direction.

5.2.2 Power and Energy Calculations

The instantaneous peak power, P, has been determined using Equation 4.4 for the data collected. The resistive load was set as 1 MΩ (±5%) and peak instantaneous power was calculated as shown in Figure 5.5b. As detailed in Chapter 4, the impact of water droplet on the piezoelectric transducer was broken into two stages: log growth and exponential decay. The energy delivered to the load is calculated from the voltage data collected by two different methods:

Method 1

The energy graph of the harvester is plotted in Figure 5.5c. The energy output of the impact was found by these steps:

- Instantaneous power was calculated for each data point where P_g represents data points for growth stage and P_d represents data points for decay stage. The average of these power values was found.
- The duration of log growth (t_1) and exponential decay (t_2) were determined.
- The energy was calculated using Equation 5.1.

$$E = \left(< P_g > \times t_1\right) + \left(< P_d > \times t_2\right) \qquad 5.1$$

Method 2

The energy output of the impact was found by these steps:

- Instantaneous power was calculated for each data point where the limits 0 to x represent time duration for growth stage and limits x to x' represent time duration for decay stage.

- The time step for each data point, t_s, is calculated to be 0.04 $\times 10^{-3}$ seconds.
- The energy was calculated using Equation 5.2.

$$E = \sum_{0}^{x} (P_g \times t_s) + \sum_{x}^{x'} (P_d \times t_s) \quad 5.2$$

5.3 Multiple Unit Module

5.3.1 Voltage Measurements

Generally, raindrops will not be able to impact all units simultaneously within a defined time period which will be dependent on the size of the array and rainstorm type. Therefore, it is important to measure the coupling between individual piezoelectric transducers with single droplet impact. Unit 1 is excited by water droplet initially, then more units are added in the arrangement. Voltage output across Unit 1 is measured, and as more units are added in parallel, there is a decline in peak voltage as the arrangement that is not rectified. With single unit we can see the peak voltage output was approximately 2.9 V. With the addition of Unit 2, voltage output at Unit 1 drops to 2.1 V and then keeps decreasing until the peak voltage is at 0.9 V with a sixth unit, Unit 7 added in the configuration. Adding additional units seems to have a negative impact in the non-rectified arrangement which can be seen in the results. This is possibly caused by the oscillating pulses with opposing phases of these additional transducers, resulting in a reduction of voltage at the terminals. As additional units are coupled in, the voltage drops, and this gives us data of how much energy is being lost during coupling. The data gathered can then be extrapolated back to find out the loss in the piezoelectric transducer that was excited (Unit 1) by the impact of water droplet. Figure 5.7 shows the different voltage waveforms obtained at Unit 1, when up to 6 additional units are connected in parallel for the non-rectified arrangement where only one device was excited.

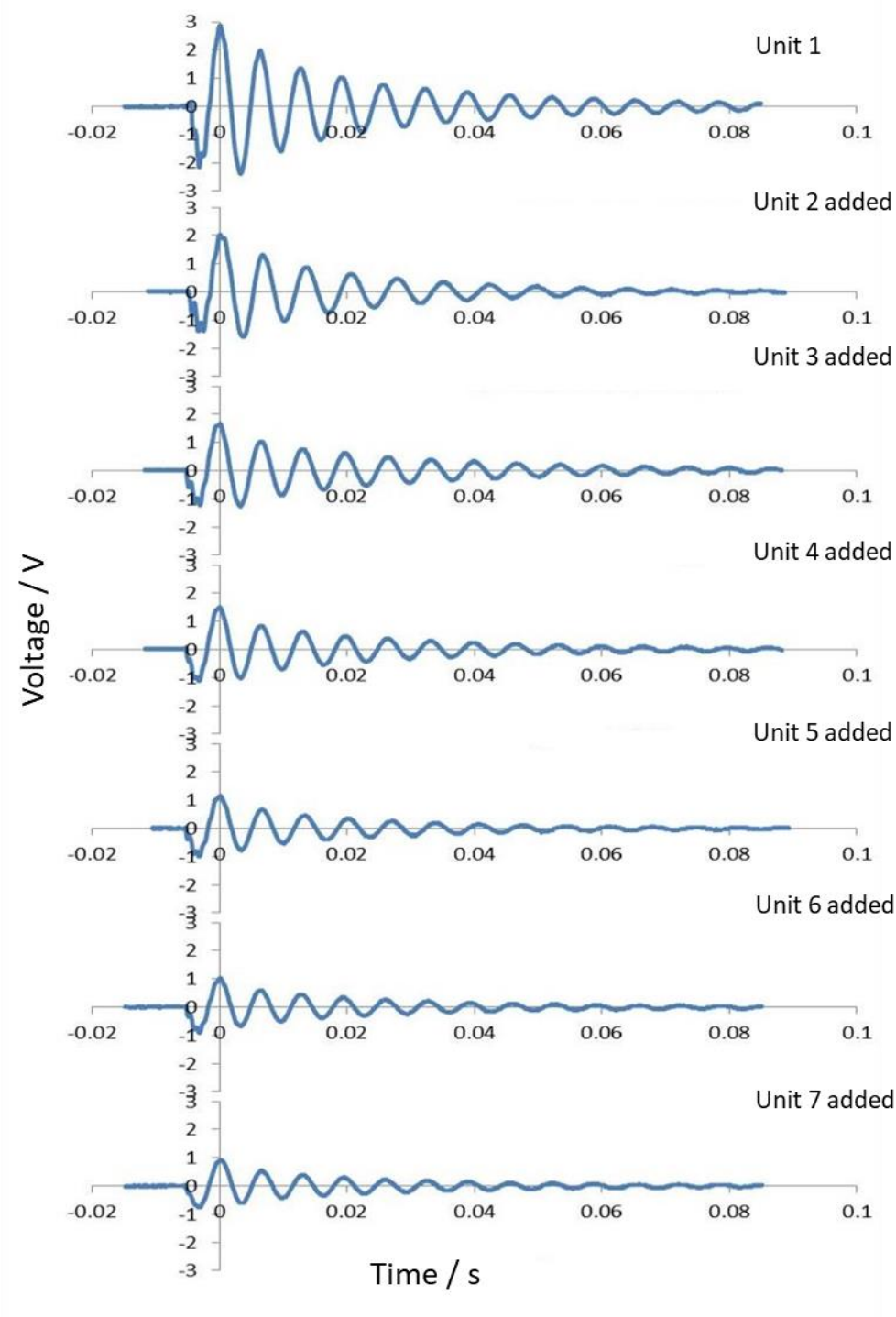

Figure 5.7: Non-rectified voltage output of Unit 1 with six additional units added in parallel

Figure 5.8 shows the voltage waveform obtained at Unit 1, when up to 6 additional units are connected in parallel for the rectified arrangement with only one device being excited (Unit 1). The rectified arrangement decouples the transducers and shows there is no

negative impact of adding additional devices apart from the voltage drop associated with the diodes used in rectifying circuit. This voltage drop due to the use of diodes can be seen in the voltage output of Unit 1 in when compared to the peak voltage of the non-rectified arrangement.

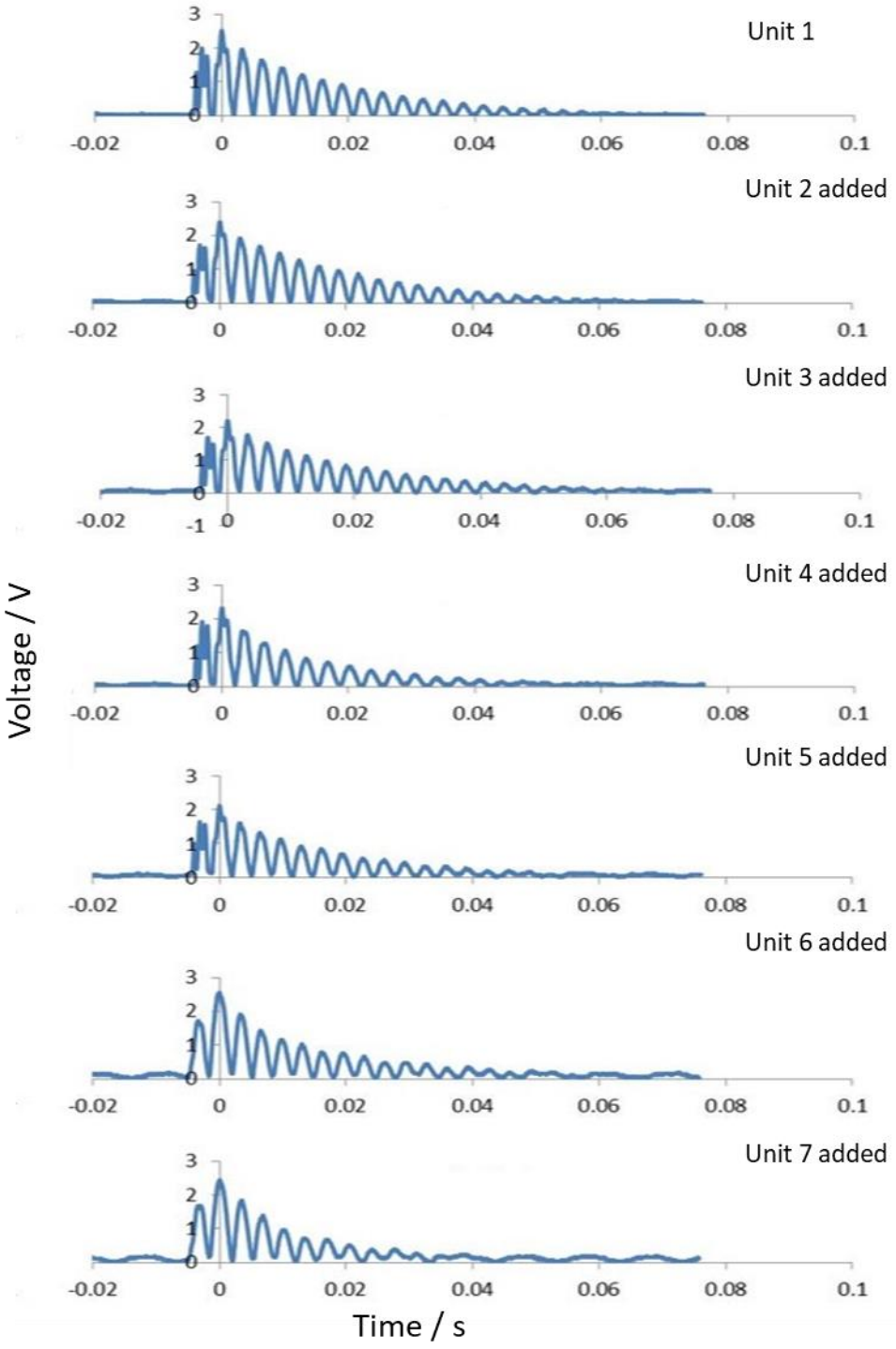

Figure 5.8: Rectified voltage output of Unit 1 with six additional units added in parallel

5.3.2 Power and Energy Calculations

The peak power of the module is calculated for devices connected in parallel. Figure 5.9a shows the peak power of the non- rectified devices and rectified devices in the module. The root mean square (RMS) voltage of the non-rectified transducers is plotted in Figure 5.9b. This output voltage is defined as a function of n unit and is empirically modelled by Equation 5.3.

$$V_{em}(n) = 0.9117n^{-0.629} \qquad 5.3$$

The energy output of the module is shown in Figure 5.9c. The non-rectified module shows a significant decline in energy output as more devices are added in parallel in the module as the electrical output or power is being lost when additional devices are connected. Therefore, rectification is needed to decouple devices and stop this loss of power.

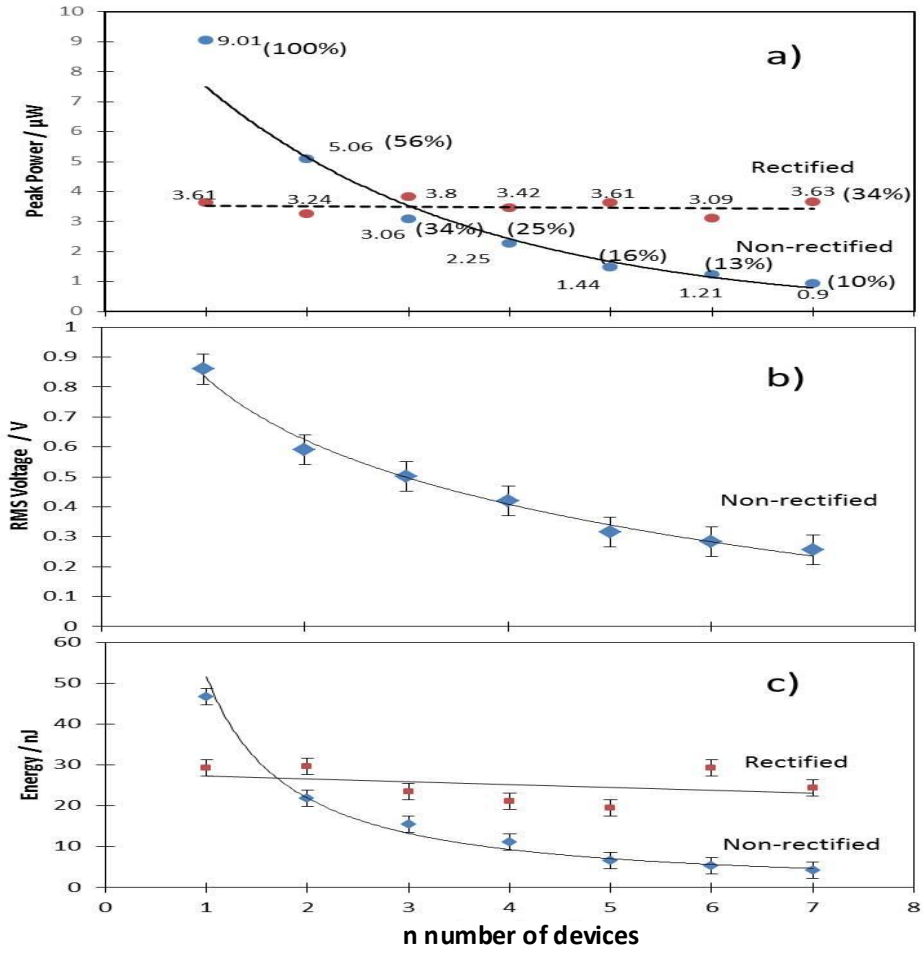

Figure 5.9: Parameters of the module (a) peak power, (b) RMS voltage, (c) energy delivered

5.4 Analysis of Module Experiments

The analysis of non-rectified devices is discussed in detail first before considering the effect of rectification. Figure 5.10a illustrates the equivalent circuit for this harvesting device which has an impact event of a droplet where the transducer is connected to n number of units with no droplet impacts. The electrical power sources in Figure 5.10a indicates the power which has been captured from the droplet that is, the power available after the impact mechanism. The droplet falls with a particular kinetic energy and inelastically impacts the harvesting device. If we take this kinetic energy as 75.97 μJ for the maximum height achieved in this experimental study, the droplet undergoes its impact mechanism with the water bouncing back and spreading across the surface taking a portion of the initial kinetic energy with it. Also, a proportion of this initial kinetic energy is captured, E_0, by the transducer and mechanically sets the device in damped simple harmonic motion. The mechanical characteristic of this simple harmonic motion is modelled with the equivalent circuit previously presented in Figure 3.12, where L_m , C_m and R_m represent the mechanical components, and the full model for the module is shown in Figure 5.10a. The L_m and C_m components model the behaviour of the transfer of kinetic and potential energy in the transducer as it vibrates, and R_m models the mechanical losses. Also, in Figure 5.10a for the module also represents the equivalent components for electrical storage and losses, where C_e is the capacitance of the transducer as it consists of two parallel plates across the piezoelectric material, and R_{e1} and R_{e2} are the electrical losses in the transducers, for example, current leakage across the piezoelectric material.

When additional units are connected to the active transducer, Unit 1, which undergoes an impact event, these additional units do not have a power source at the start as they are not excited due to no water droplet impact events on them. However, as n units are electrically connected, these connected units will be excited by the electrical power produced from Unit 1. This is shown in Figure 5.10a consisting of mechanical and electrical behaviour modelled with the equivalent circuit.

Figure 5.10b is a simplified theoretical equivalent circuit of the n connected devices used to model the energy flow when Device 1 undergoes an impact event over the whole duration t_d of the event and damping of the vibration of the device, with duration of for example 0.06 s. The voltage drop across the source and load resistor R_{load} is given by Equation 5.4, the voltage of the simplified theoretical model (STM):

$$V_{stm}(n) = \left(\frac{E_0}{t_d}\right)^{0.5} \left(\frac{1}{R_{load}} + \frac{n}{R_0}\right)^{-0.5} \quad 5.4$$

It is assumed that the losses within each transducer are the same, such that $R_1 = R_2 = R_0$. We can define R_0 as the component which lumps together all mechanical and electrical losses in a single transducer. It is also assumed that the energy captured from the droplet impacted is not a function of n units connected as no energy is returned back to the remains of the droplet water from the energy that was captured (the energy is not being given back to the droplet for it to catapult off the unit).

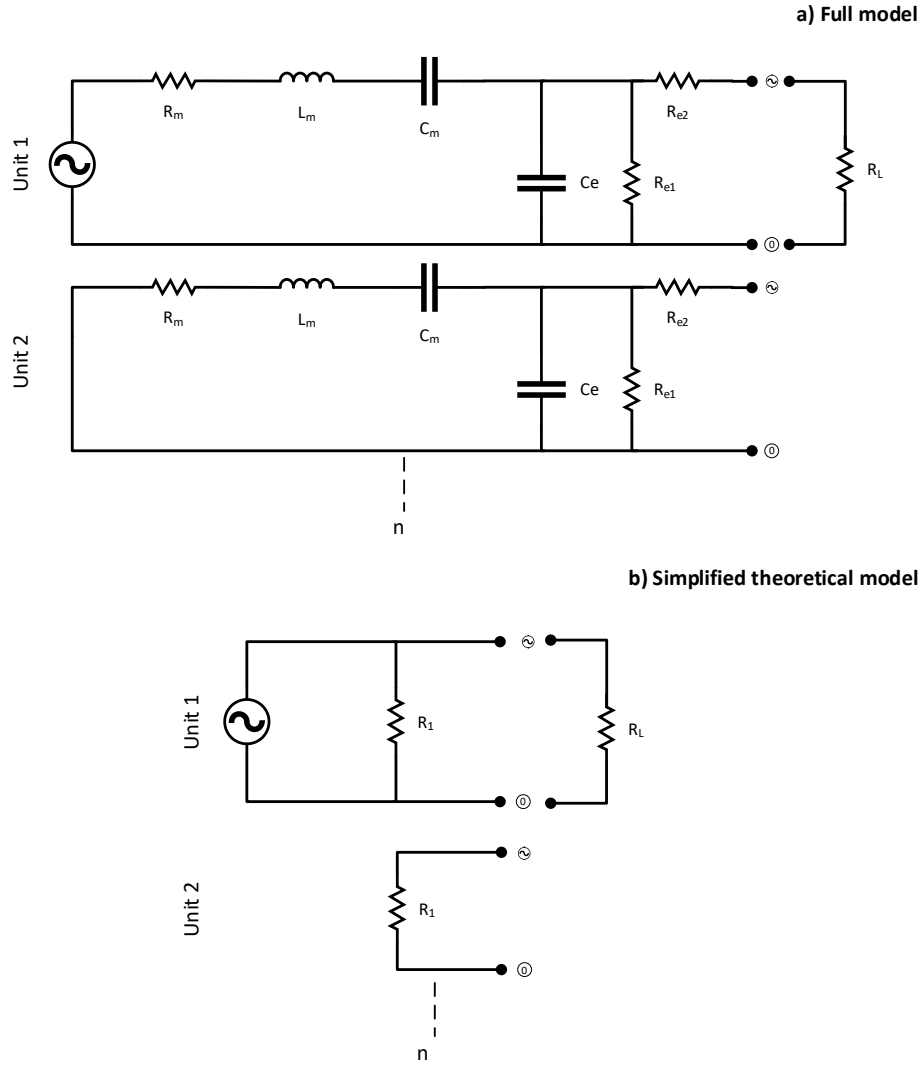

Figure 5.10: Equivalent circuit model of the module with multiple units

5.5 Energy Conversion Efficiency

In Chapter 4, the energy conversion efficiency calculations were based on the peak mean power achieved by the transducer compared to the kinetic energy of the droplet impacting the transducer. This approach can be further explored as the overall efficiency of a REH device will depend on 3 key factors: impact conversion, mechano-electric conversion and losses through rectification. This section will present a value for the two stages that contribute significantly to these losses; impact mechanism and mechano-electric conversion.

5.5.1 Impact Mechanism

Using the STM from Figure 5.10b and Equation 5.4 with the experimental data empirically modelled in Equation 5.3, the energy captured from the impact mechanism, E_0, can be found. This is the energy transferred from the droplet to the harvester as the droplet impacts the surface.

A simple procedure is presented which uses the voltage profile with n number of units to extrapolate to give $V_{stm}(0)$, the excitation voltage of the transducer with no internal losses to find E_0:

a) Plot experimental data (circle data points in Figure 5.11) and fit a trend line to acquired empirical model $V_{em}(n)$. The best fit is a power function which is valid between the limit of $(7 \geq n \geq 1)$ and thus $V_{em}(0)$ cannot be found.

b) Find the change in V_{em} with the change in the number of units n for each n, $\Delta V_{em}/\Delta n$, from the empirical model $V_{em}(n)$ data. These data points are plotted as triangle on Figure 5.11.

c) Plot a best fit line for $\Delta V_{em}/\Delta n$ data to give $dV_{em}(n)/dn$ and extrapolate back to $n = 1$. The data point for $n = 1$ is plotted as a square in Figure 5.11.

d) Therefore, the change is V_{em} from $n = 0$ to $n = 1$ can be found and thus $V_{stm}(0)$ is estimated. This value is plotted as a diamond data point in Figure 5.11. $V_{stm}(n)$ can be plotted once R_0 is found, plotted as a dotted line.

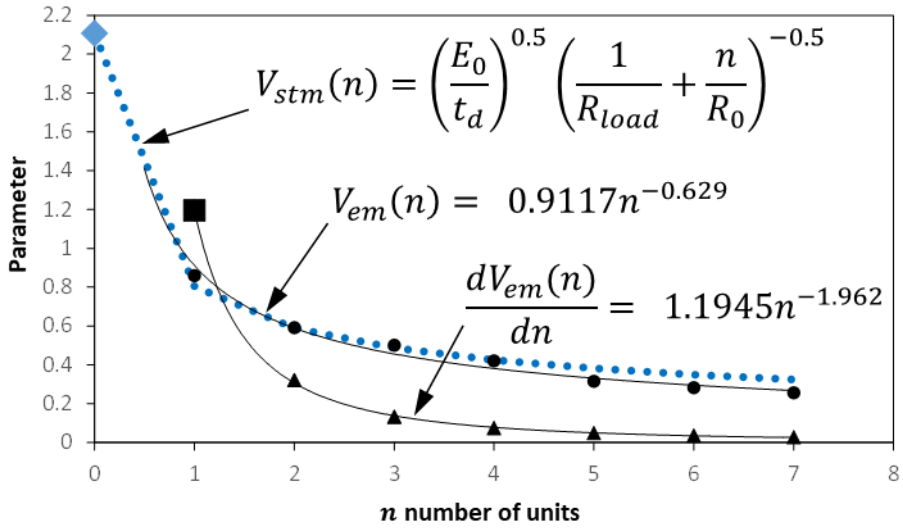

Figure 5.11: Finding the excitation voltage $V_{stm}(0)$

One active transducer (excited by the impact of water droplet) is used and then n units are added to the module which takes away energy from it. The graph is then extrapolated to an ideal harvester which is $n = 0$ to find the energy that goes to the load. Using the data from the experiments for the velocity of droplet at 2.13 m/s, $V_{stm}(0)$ is found to be 2.106 ± 0.11 V. Given that the whole harvesting process duration is t_0, estimated at 0.06 s, E_0 is found to be 266.2 ± 29 nJ. Comparing this value of impact mechanism with the value of kinetic energy of a single droplet at 47 cm, the energy conversion efficiency of the impact mechanism can be estimated and is found to be 0.35 %.

5.5.2 Mechano-Electric Mechanism

Again, using the STM from Figure 5.10b and Equation 5.4 with the experimental data empirically modelled in Equation 5.3, and also knowing the energy captured from the impact mechanism E_0, the losses within a harvester R_0 can be found. This is realised by using a numerical method by inputting trial values of R_0 in Equation 5.4 to find best fit to the experimental data empirically modelled by equation 5.3. This analysis is shown in Figure 5.12 with 3 trial values of R_0. Giving an estimate of R_0 = 170 ± 30 kΩ.

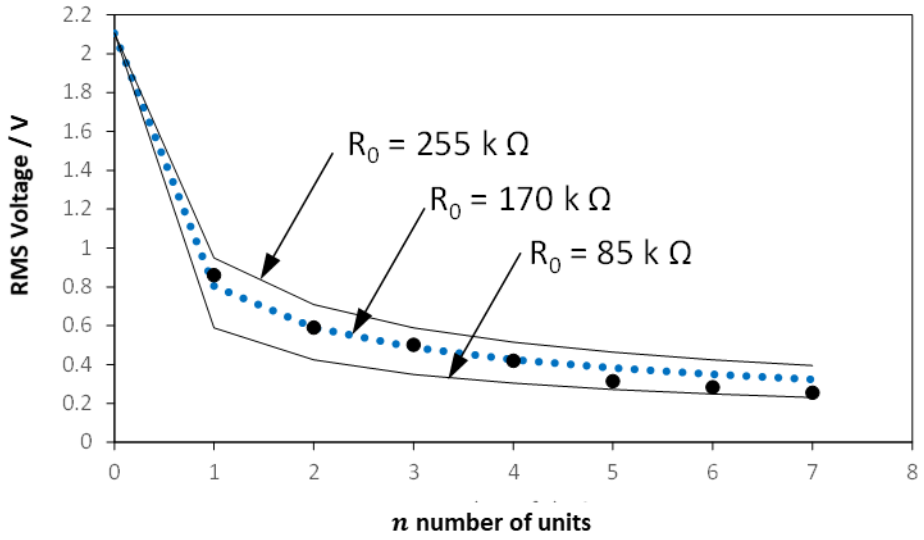

Figure 5.12: Finding the internal resistance (losses) R_0 of a harvester

The energy delivered by a single transducer is experimentally found to be 51 ± 12 nJ as seen in Figure 5.5c and Figure 5.9c. This energy comes from the energy delivered by the impact mechanism which is 266.2 ± 29 nJ giving an efficiency for the mechano-electric conversion mechanism as 0.3 %

5.5.3 Overall Device and Module

The overall efficiency of a single device without rectification is found to be 0.671 %. It was observed that by adding further devices in parallel in a harvesting module (without rectification) reduces the efficiency of the output during a single droplet impact. With 7 devices, the efficiency is reduced to 10% of the case with a single device producing power. This is due to the additional devices being excited by the one device which has the droplet impact and not being in phase would cancel each other. A way to overcome this is to prevent the additional devices from being excited. One means is to use semiconductor diode rectification.

The rectified devices were connected in parallel to build a module of up to 7 devices. A disadvantage with using the silicon diode technology is that there is a voltage drop of the silicon diode of around 0.7 V. The effect of this can be seen in the results. For the single device case, there is a drop of power output from the non-rectified device to the rectified device. Figure 5.9c illustrates the rectified case maintains a consistent power out as a

function of n device which is around 34% of the single device non-rectified case. Using rectification ensures that the efficiency to not fall with increasing number of device n as in the non-rectified case.

5.6 Summary

This chapter presents the voltage output of a piezoelectric transducer connected to a resistive load and voltage measurements were taken to calculate the power output of the device. The effect on the efficiency of the module with and without rectification is investigated to understand the effect of coupling these devices in a parallel arrangement. Additionally, the voltage, power and energy were found for different surface angles, surface conditions and impact regions for single devices with a view to maximise module efficiency before a prototype is built and tested under a replicated rainstorm. One of the main contributions of this Chapter was to find a technique to identify the losses within the harvester; impact mechanism and mechano-electric conversion to be able to quantify it.

The energy delivered from the impact mechanism E_0 is found to be 266.2 ± 29 nJ. Given 75.97 µJ of kinetic energy in the falling droplet, the efficiency of the impact mechanism is estimated to be 0.35 %. The energy delivered from the device is found to be 51 ± 12 nJ. Given 266.2 ± 29 nJ of energy from the impact mechanisms, the efficiency of the mechano-electric conversion mechanism is estimated to be 0.3 %. The overall efficiency of a single device is found to be 0.67 %. Adding further devices to make a multi-device module without rectification reduces the efficiency as other devices are a source of power loss for any one device that is impacted by a droplet. Rectification on the output of each device ensure there isn't a substantial negative impact of an array of harvesters which does improve the performance for a multi-device module where only one unit in the array is excited by the impact of water droplets.

CHAPTER 6

6 Prototype Device & Final Discussion

This chapter explores the performance of a prototype device with multiple piezoelectric transducers and investigates the output with varying time period over a replicated rain shower with multiple impact events. The empirical results lead to a mathematical estimation of the maximum power output of the harvester system under different rainstorms.

6.1 Experimental Arrangement

Piezoelectric transducers were used to build a prototype device that consisted of several units to perform as an array of harvesters. Prototype device specification data is gathered in Table 6.1.

Table 6.1 : Prototype device specification

Parameter	**Units**	**Value**
Prototype dimensions	mm	130 × 95
Transducer dimensions	mm	25 × 13 × 0.25
Active area of prototype	m^2	2.925×10^{-3}
Diameter of droplet	mm	4.0

The design of the prototype consisted of a total 9 piezoelectric transducers connected in parallel, across a 1 MΩ resistive load. The voltage output of the prototype device is measured using a Digital Oscilloscope with differential probes. The overall active area covered by the prototype device was approximately 0.003 m^2. The prototype design is shown in Figure 6.1a and the full bridge rectifying circuit is shown in Figure 6.1b.

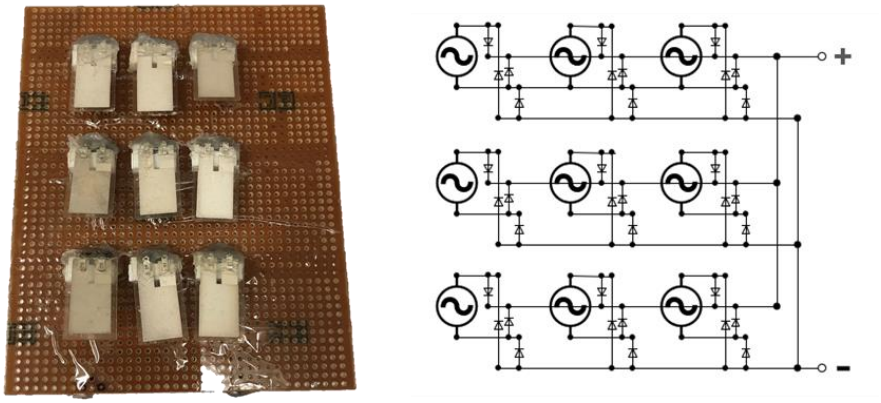

a) Prototype device b) Rectifying circuit

Figure 6.1: Prototype device (a) and (b) Rectifying circuit

Prototype device consisting of 9 piezoelectric transducers was fabricated on a stripboard using connectors for each unit to hold them in position. The connectors also acted as a fixed point for the transducer to be connected in the form of a cantilever beam. The electrodes of the piezoelectric transducers were protected using petroleum jelly to avoid any exposed elements resulting in a short-circuit. At the back of the striboard, the rectifying circuit was integrated which was sealed and insulated using a hot melt adhesive (Ethylene-vinyl acetate) to protect the rectifying circuit. This also protected the entire prototype module to avoid any short-circuits caused by water droplets. Figure 6.2 shows the prototype device with adjustable shower head in the test chamber.

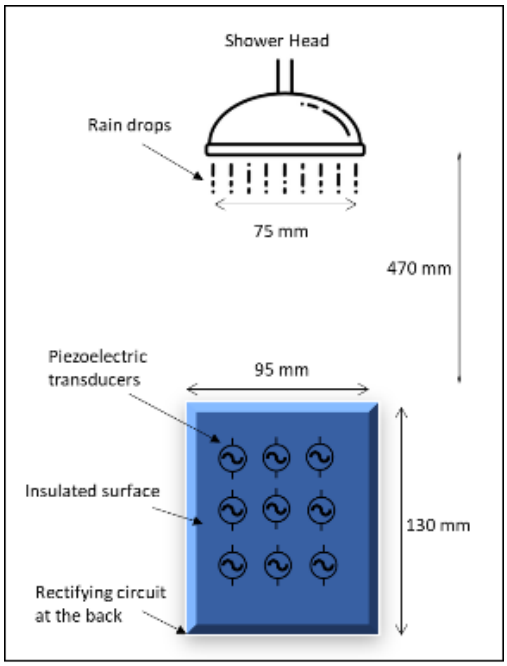

Figure 6.2: Experimental equipment and set-up

6.2 Empirical Results

In this section voltage profile is shown that was measured on the oscilloscope along with power calculations using the voltage data. The prototype module consisting of 9 devices was connected across a load of 1MΩ.

6.2.1 Voltage Measurements

Rain was replicated using a standard shower head connected to a water pipe. Lab conditions were monitored to ensure there was no change in temperature or pressure. The rain rate was measured as approximated 4 mm/hr with the velocity of droplets at 2.13 m/s. The droplet diameter size of 4 mm was consistent with previous experimental work carried out. One of the limitations of this experimental work is the random nature of water droplets (unknowns such as impact position of droplets and number of droplets impacting a transducer), which is also true for a natural rain shower.

Voltage measurements were taken over three time periods; 0.5, 1 and 2.5 seconds. Each experiment was repeated several times (at least six sample data was collected) to get consistent results. Figure 6.3a shows one experimental run with a time period of 0.5 second resulting in the peak voltage range between 1 and 2.5 V, with an average of all the experimental runs of 0.32 V. Figure 6.3b shows one experimental run with a time period of 1 second resulting in the peak voltage range between 0.8 V and 2.2 V, with an average of all the experimental runs as 0.26 V. Figure 6.3c shows one experimental run with a time period of 2.5 seconds resulting in the peak voltage range between 0.8 V and 2.5 V, with an average of all experimental runs as 0.28 V. As the time duration was increased it was observed that there was a small loss of voltage, this is due to the inconsistency of controlling the water droplet hits from the shower head.

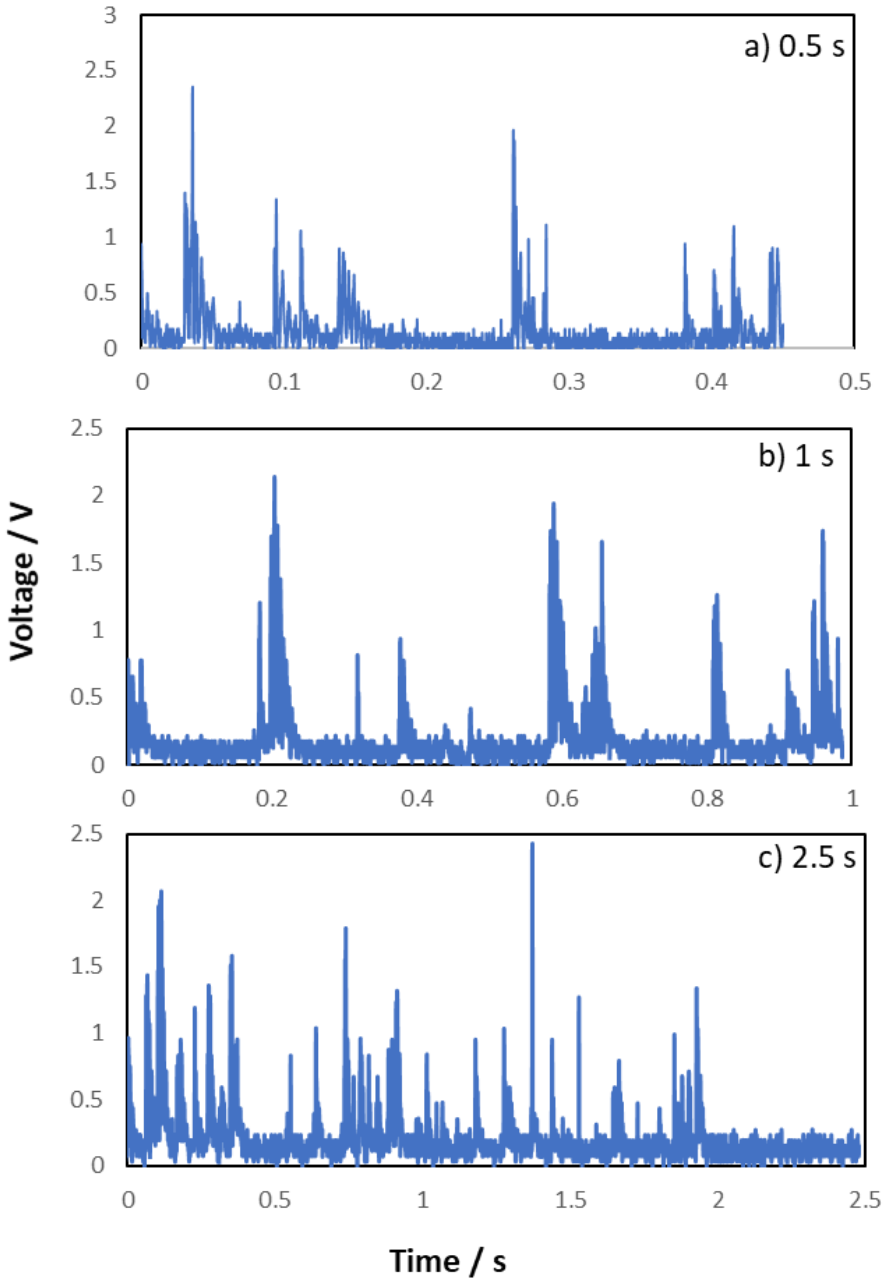

Figure 6.3: One experimental run voltage profiles for (a) 0.5 second, (b) 1 second and (c) 2.5 seconds

6.2.2 Power Calculations

The instantaneous peak power (P) has been determined using Equation 4.4 for the voltage data collected. The resistive load (R_{load}) in this experiment was set as 1 MΩ.

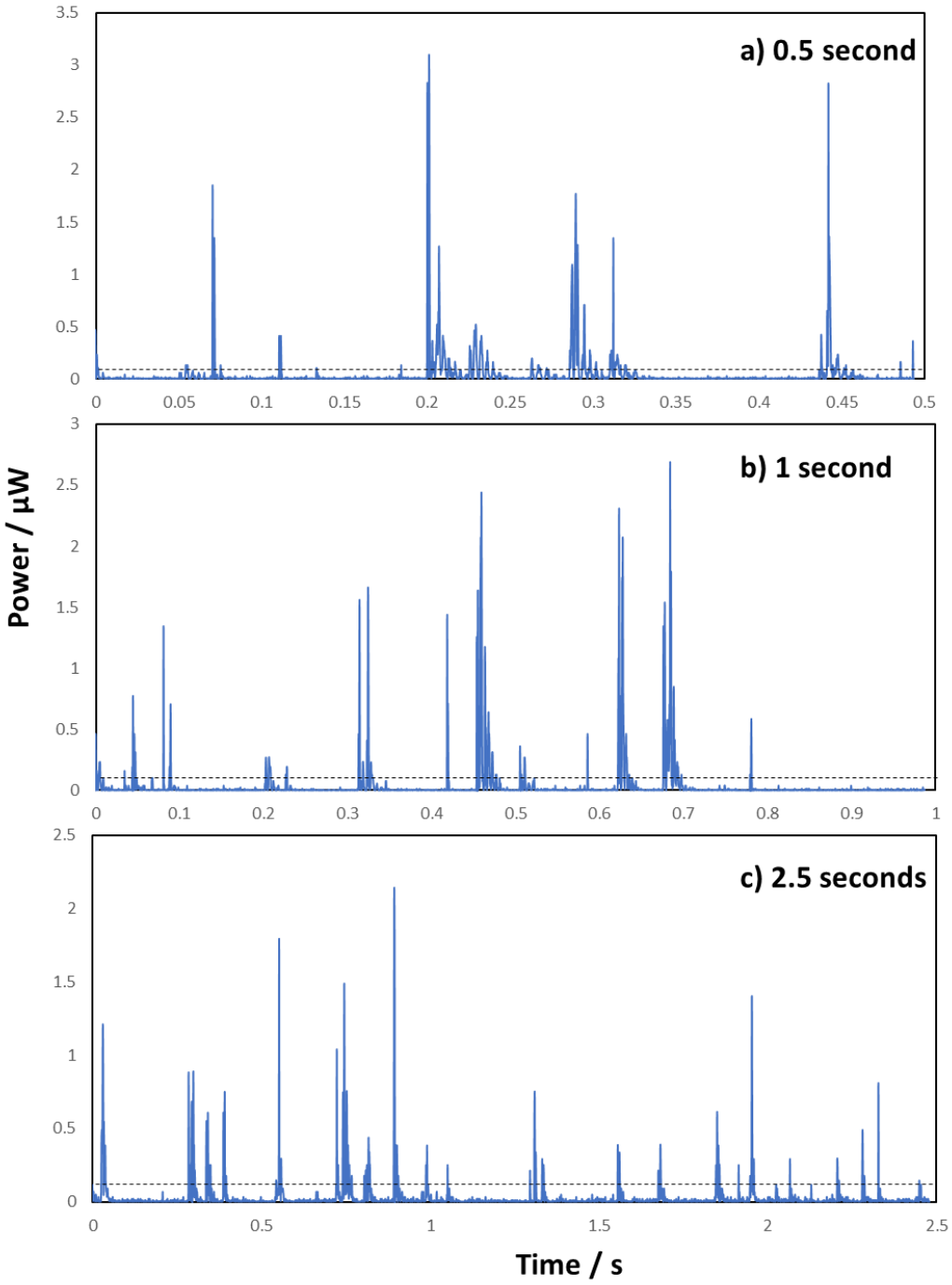

Figure 6.4: One experimental run peak power profiles for (a) 0.5 second, (b) 1 second and (c) 2.5 seconds

Figure 6.4 shows the power calculations of the prototype device over different time periods. The sampling frequency of the different time periods was 5 kHz, 2.5 kHz and 1 kHz respectively. The maximum peak attained was with a 0.5 second time period which resulted in 3 µW for one of the impact events. It can be seen that the prototype was only able to capture very few impact events which resulted in these high instantaneous power

peaks but due to the inconsistency of controlling the impacts (hits on the transducer) using the shower head, the overall average was calculated at around 0.04 µW. Due to the random nature of rain, water droplets can impact any region of the transducer sometimes not producing hight impact event and at times several water droplets can impact a particular transducer simultaneously resulting in a high impact event. Therefore, it is difficult to predict at what region the droplet will impact the piezoelectric transducer and the voltage profile can be seen to be inconsistent and the output can vary slightly due to these factors.

6.3 Comparison of Empirical Results with HAM

This section looks at comparing the prototype device data with HAM developed in Chapter 4. Analysis of the data generated from the prototype device is presented followed by a comparison with the simulated result of average power.

6.3.1 Empirical Data Analysis

The area covered by the prototype was calculated precisely as 2.925×10^{-3} m^2 which is much smaller than the original simulations in Chapter 4. Precipitation rate was measured using a standard 203 mm rain gauge which was roughly 4 mm in volume, which would class this as a light rain shower. MATLAB code was amended to reflect these laboratory conditions replicating a light rain shower with the associated volume and size of the array. The average power was calculated as 0.05 µW and with maximum deviation of around 0.03 µW which as discussed before, is due to the random nature of rainfall with inconsistent impacts on the transducers of the prototype device. As the replicated rain continues for longer, the transducer surfaces get wet and it takes longer for the water droplets to run off the surface, resulting in low frequency impacts. Figure 6.5 shows the power output against experimental runs for the three different time periods: 0.5 second, 1 second and 2.5 seconds.

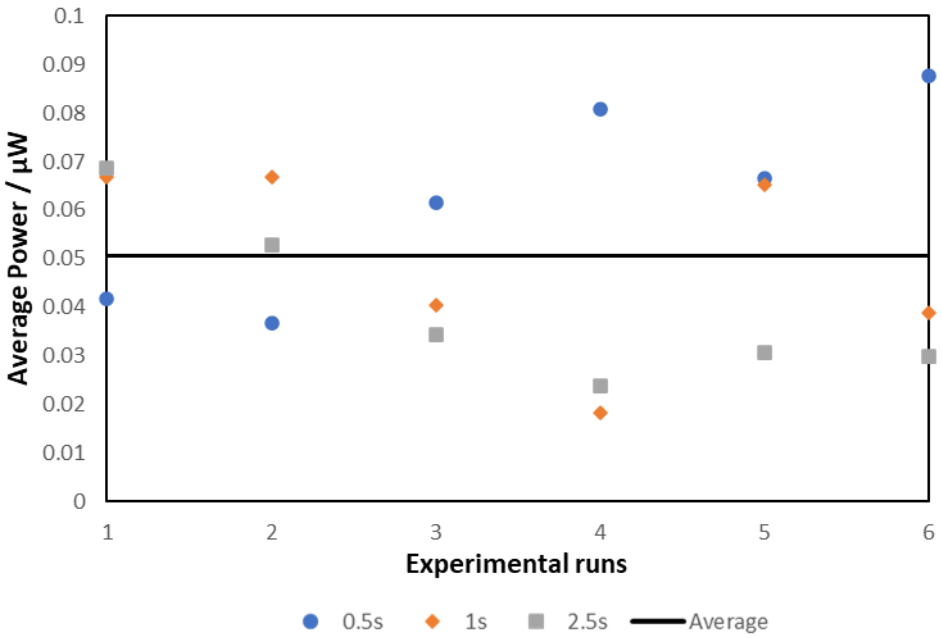

Figure 6.5: Empirical data for prototype device with all experimental runs

6.3.2 Discussion of HAM

HAM was initially developed based on the empirical data gathered using a single piezoelectric transducer with a single impact event. Data presented in this Chapter is for output of multiple events using multiple transducers. The model does not consider the exact number of devices connected but is related through the size of the array (active area coefficient is added to improve the accuracy of the results). The significant parameters include rainfall, rainfall duration, the diameter of the droplet, size of the array and impact velocity (which is related to the height of release of droplet).

Table 6.2 : Storm type characterisation

Storm Type	**Droplet Size (mm)**	**Rainfall (mm/hr)**	**Impact Velocity (m/s)**	**Estimated Impact Force (N)**
Light	2	2.5	6.49	0.13
Moderate	2.6	5	7.57	0.30
Heavy	4	7.6	8.83	0.98
Thunderstorm	5	10	9.09	1.62
Experimental	4	4	2	0.05

Table 6.2 shows a simpler version of characterisation of different types of rainstorm (data has been taken from Chapter 2.3.1, this data will be used in the discussion in subsequent sections of this Chapter as mathematical behaviour of these impacts as events that produced power.

Simulations from HAM are presented in Figure 6.6 based on the characterisation of the storm types. As the size of the array is increased, power output is increased as a result, with the highest power of 245 µW with a 10 m^2 array for the experimental without changing any other parameters. With an increase in the size of the array, the deviations are reduced significantly with a change of size from 0.003 m^2 to 10 m^2.

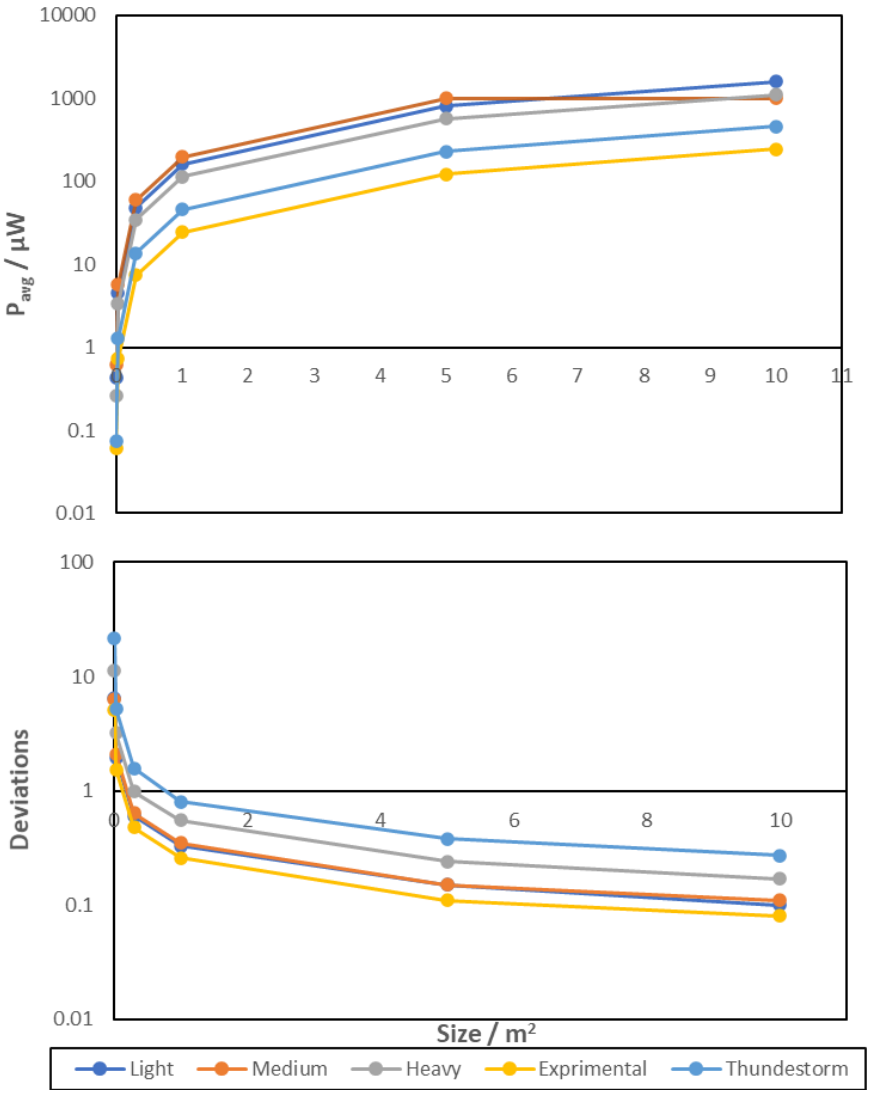

Figure 6.6: Power output from HAM

6.4 Log-Log Investigation

This section looks more closely at the prototype device data and compares the power distribution of the harvester. A mathematical description is sought to model the underlying process.

6.4.1 Empirical Data Analysis

To analyse the data gathered, log-log plot of the bin and distribution was plotted using the power data gathered over three time periods; 0.5 second, 1 second and 2.5 seconds respectively. For one experimental run, the total data points collected were 2500. For each time period, the log-log plot included six experimental runs resulting in total data points of 15000 with a bin of 0.002.

Figure 6.7 shows an example profile of 0.5 second log-log plot of distribution which demonstrates a dual PL. Data plotted is of the number of events of power equal to a reference size (or bin size P_{ref} to P_{ref} + 0.002 µW). Linear trendlines are plotted on the log-log graph of 0.5 second example. These trendlines are power laws as show in Equation 6.1. There are two profiles shown; the main profile and high-power profile. The main profile captures majority of the data points that resulted in a power event, whereas the high power profile captures a few data points that resulted in high power but the number of these events is very small.

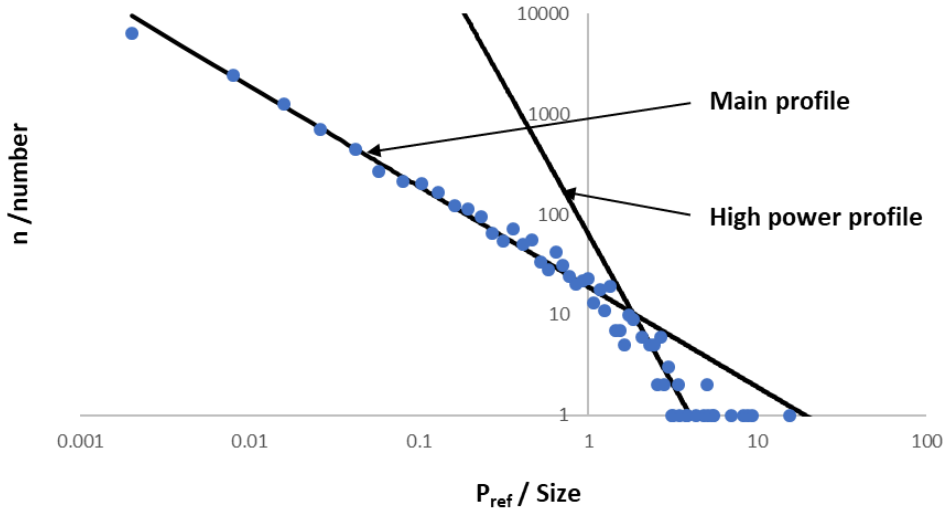

Figure 6.7: Example distributive profile of data gathered in a time period of 0.5 seconds

Equation 6.1 represents this number of events:

$$n\left(P_i = P_{ref}\right) = \left(\frac{P_\lambda}{P_{ref}}\right)^{D'} \quad 6.1$$

where P_λ is maximum predictive power output, D' is the exponent value of rate of change of n with respect to P_{ref}.

Distribution function and trendlines are plotted in Figure 6.8 for all the time periods (0.5, 1 and 2.5 seconds respectively). Table 6.3 shows the parameters of power law behaviour of the experimental work as plotted in Figure 6.8.

Table 6.3 : Power law parameters for distribution function

Time (s)	Main profile	P_λ	D'	High-power profile	P_λ	D'
0.5		19	1		4	3
1		19	1		3.5	3.5
2.5		19	1		2.8	3.5

As can be seen from the linear trendlines, it exhibits fractal behaviour across the scale of measurement of 0.5 second, 1 second and 2.5 seconds, the distribution function exhibits double PL. To verify that the data exhibits fractal behaviour, cumulative distribution function (CDF) must be also of linear form, which will be explored later.

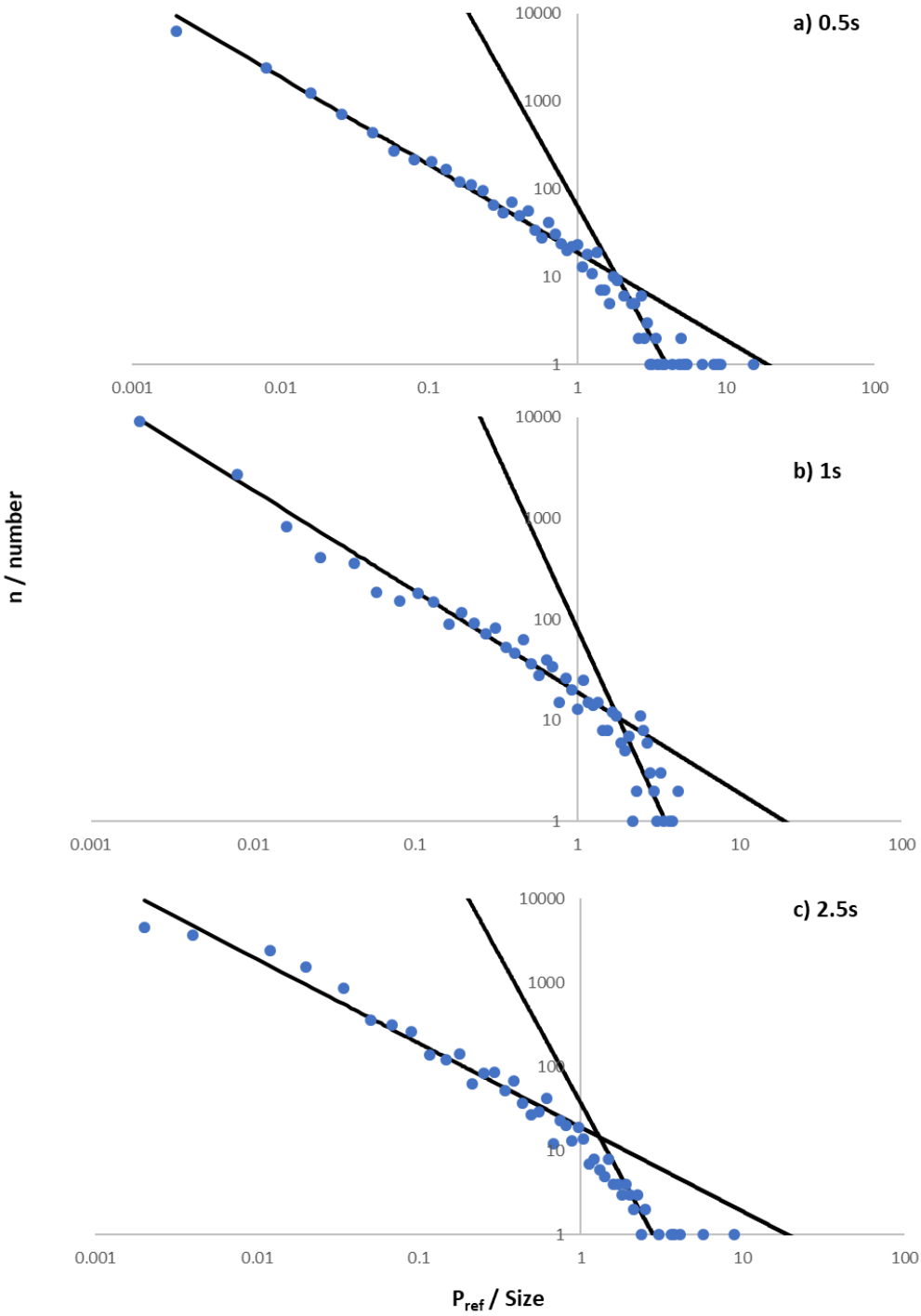

Figure 6.8: Distribution function of empirical data for 0.5 second, 1 second and 2.5 seconds

Figure 6.9 shows the log-log plot of CDF of number of events of power greater than a reference size (or bin size P_{ref} to P_{ref} + 0.002 µW). Trendlines were plotted as the distribution follows exponential PL.

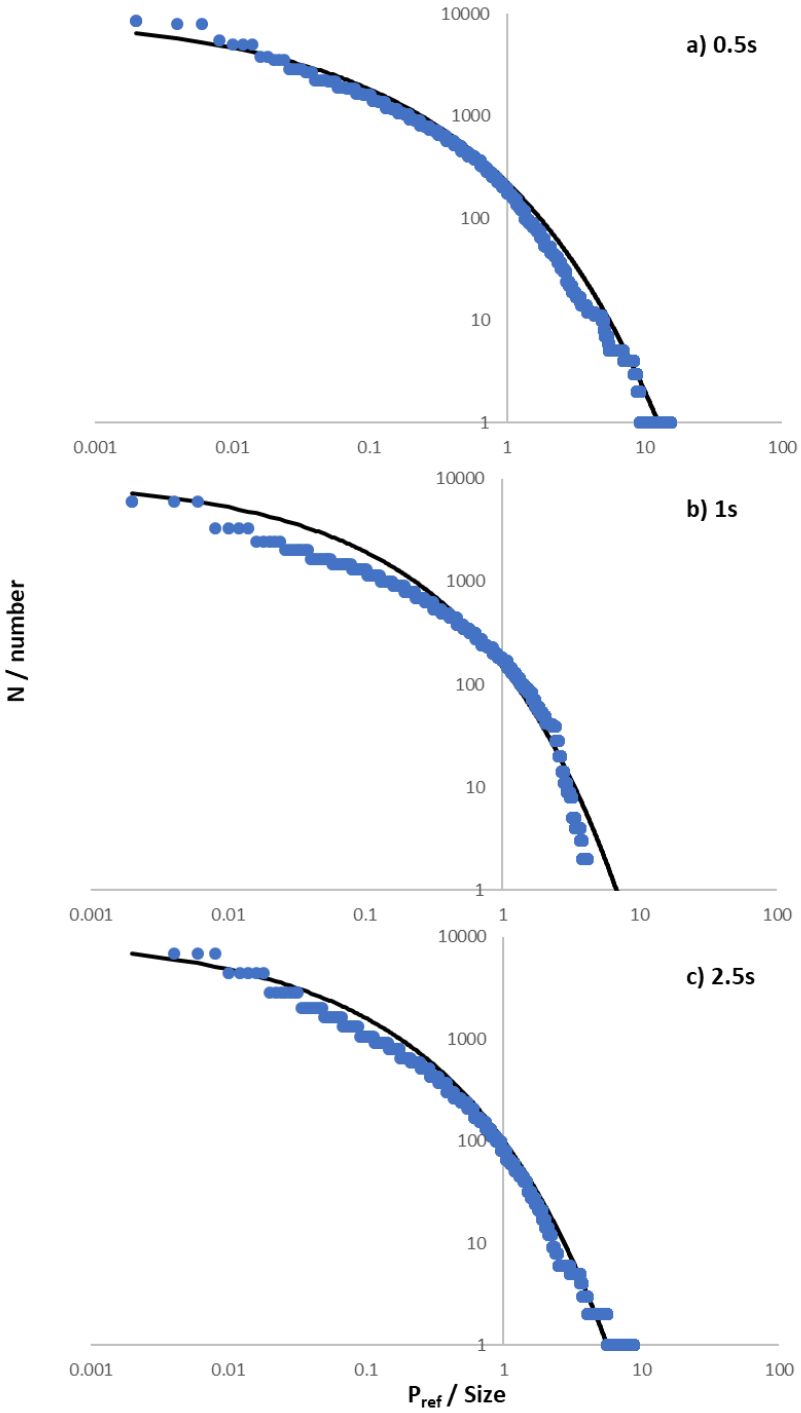

Figure 6.9: CDF of empirical data for 0.5 second, 1 second and 2.5 seconds

Equation 6.2 represents this number of events:

$$N\ (P_i >\ P_{ref}) = A \exp\ (-B.{P_{ref}}^{C}) \qquad 6.2$$

Table 6.4 shows the parameters of the exponential PL behaviour of the CDF for the experimental work as plotted in Figure 6.9.

Table 6.4 : Power law parameters for CDF

Time (s)	A	B	C
0.5	10,000	3.8	0.4
1	10,000	4.3	0.4
2.5	10,000	4.6	0.4

6.4.2 Empirical Data Modelling

Harvester model developed in this paper is based on rain characteristics identified as droplet size (D_{drop}), amount of rainfall (R) and terminal velocity (v) as shown in Table 6.2. With the help of these characteristics we can define the experimental parameters identified in Table 6.4 and develop a mathematical model for the harvester.

Experimental parameter A can be defined as the measurement of data points collected. The overall data points (non-zero data points from CDF) are 10,000 and this value remains consistent for the time durations (t) due to the limitations of the experimental set-up.

Experimental parameter B can be defined as a measurement characteristic in relation to the time duration (t) of the total experimental data collected in that run. Taking the reciprocal of B, β has characteristics of an energy term C_B and power term C_2 related to the measurements, assuming the exponential term is dimensionless. Using the data from Table 6.4 this gives Equation 6.3 with constants $C_B = 0.0289$ and $C_2 = 0.2049$ µW.

$$\beta = \left(\frac{C_B}{t}\right) + C_2 \qquad 6.3$$

Experimental parameter C can be defined as a measurement characteristic, which for simplification, is assumed to be the only parameter related to the storm type. It is fully

recognised that this may not be the case but for simplicity this assumption has been made which is validated by the data collected.

Equation 6.4 proposes the overall rainfall data, assuming a spherical droplet of an average droplet size (D_{drop}) and terminal velocity (v) and constant C_α. Rainfall data is typically measured by meteorologists in units of mm which is a measure of volume or amount of rain that has fallen.

$$R = \frac{4}{3}\pi\left(\frac{D_{drop}}{2}\right)^3 C_\alpha \qquad 6.4$$

Constant C_α includes the total number of average droplets and brings together all the dimensions are compatible with each other.

Equation 6.5 represents simplifying of Equation 6.4 taking into account the volume of droplet (spherical in nature). All the constants are embedded in K_C which relates to the rainfall (R), droplet size (D_{drop}) and terminal velocity (v).

$$K_C = \frac{R}{\left(D_{drop}{}^3\right)} \qquad 6.5$$

By calculating different values for K_C for various storm types, precise value of C can be calculated which shows the modelled rainstorm types. Figure 6.10 shows the modelled plots with varying rainstorm types using Equation 6.5 by which can be used to calculate the various values of K_C and plot trendlines to model them.

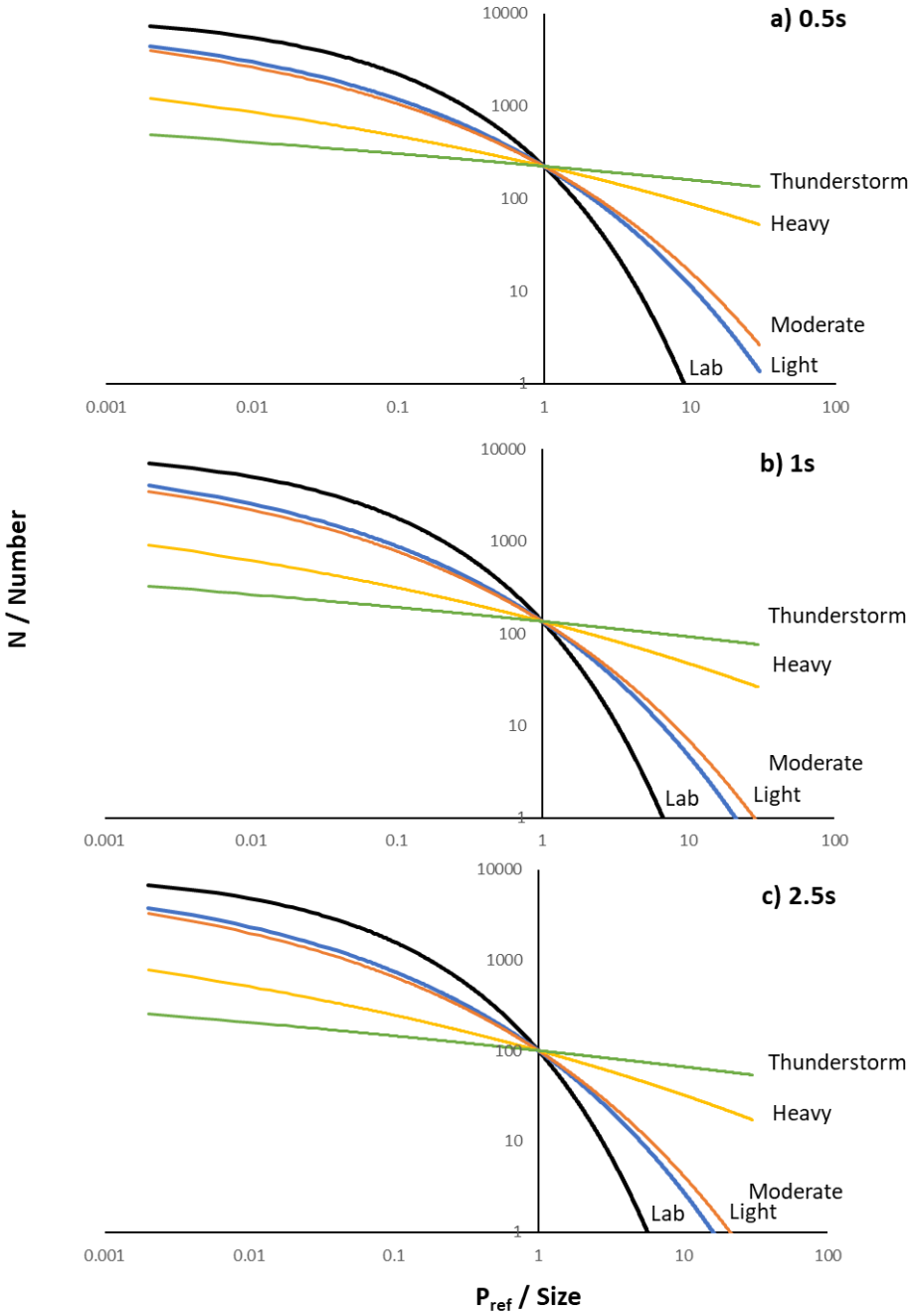

Figure 6.10: Modelled plot of P_{ref}

6.4.3 Log-log Discussion

The distribution exhibits a power-law tail (which can be seen in Appendix B). The dominating factor is usually described when the data is plotted on a logarithmic scale to ascertain whether it exhibits fractal behaviour. The trendlines of data indicate fractal behaviour as double PL is observed for the distribution function of power data calculated

for the prototype device. P_λ is the maximum likelihood estimator which is the maximum predictive power output. This gives a good indication of the predicted maximum power output of the harvester proposed. The main profile is the same across the scale of measurement (0.5 second, 1 second and 2.5 seconds) which is predicting a harvester system design of 19 μW for an upper limit, using an area of array of 0.003 m^2.

The CDF of events (resulting in power output) demonstrates a non-linear trend which exhibits exponential PL. For the CDF, A represents the number of time events that produce power and for the different time periods. The data predicts that we have a consistent value of A, that of 10,000. The harvester measurement system developed in this section has its limitations due to P_{res}(the smallest power resolution that can be measured by the system) which is 0.0016 μW. As the data is used to produce CDF any data point lower that of P_{res} will not be registered, as the analysis only takes in to account $P_i > P_{res}$.

Three time periods (0.5 second, 1 second and 2.5 seconds) used in this empirical study each have a t_{res} (the smallest time resolution that can be measured by the system) which is 0.03×10^{-3} s, 0.06×10^{-3} s and 0.16×10^{-3} s respectively.

6.5 Final Discussion

This section presents a discussion of the empirical work carried out in this thesis which include results of the harvester performance from a single unit-single event, to multiple units-single event, and finally multiple units-multiple events.

6.5.1 Single Event

Detailed empirical work was carried out as part of this research, using a single piezoelectric transducer to explore how a single unit would operate with a single event (single water droplet impact). An oscillating profile is shown which consisted of two stages; log growth as the voltage grows to a maximum and exponential decay as the voltage decreases to zero. This event resulted in total mean power of 2.5 μW which is relatively very small. Based on the information gathered from experimental work, the energy conversion efficiency was calculated as 0.12 % which is in line with what other researchers have published, but gives scope for improvement using non-commercial transducers which was out of scope for this research.

For a valid analysis, further tests were carried out to explore the effect of change in surface interaction, the angle of device relative to the droplet and an array of units connected. The optimum arrangement for the piezoelectric transducer is at 90 ° to the water droplet and the region furthest away from the fixed position of the transducer, but this is challenging from a design point of view as rain droplets could impact at any point on the transducer surface.

Piezoelectric transducer was connected in an array with multiple units, but only one device was excited by the impact of water droplet to measure degradation caused by coupling. A technique is found to separate this energy conversion as efficiency of the impact mechanism as the droplet interacts with the device and the efficiency of the mechano-electric conversion mechanism due to internal losses in the device. Significant amount of energy is also lost in the impact mechanism in comparison to the kinetic energy available in a droplet that impacts the harvester. This has a further impact on the overall efficiency as most of the droplets will break away on impact and hence only exerting a smaller impact force. If somehow these splinter droplets (after impact) could bounce off the surface of the transducer before another droplet impacts, the output can be increased in return increasing the overall efficiency of such a harvester. Such mechanism can probably be developed in lab conditions but, the application of this research is using rainfall which cannot exhibit such a behaviour.

Multiple units were connected to form a module with rectification which resulted in an efficiency of the overall harvester at 0.671 % compared to the kinetic energy available in the droplet. This was a slight improvement on the initial study with single event purely based on where the droplets were impacting on the transducer. Furthermore, based on the empirical data gathered for an array of 0.003 m^2, a mathematical behaviour can be established in the design process of a harvester using water droplet impacts. The data exhibits power law behaviour which can predict the limits of the harvester system. This behaviour is helpful in designing new harvesters using PEH techniques with raindrops. The mathematical expression developed predicts the lower and upper limit of the harvester output. The distribution of power data gathered also gave an indication of number of positive hits (impacts where power was produced in comparison to a reference value). The nature of rainfall is random, which makes it very difficult to accurately predict positive hits and what impact region on the transducer it would impact.

6.5.2 Harvester Array Model

It was proposed in Chapter 4, that by using an array of harvesters we could improve the output of the harvester system. Empirical data gathered to understand the full impact of water droplet on a single piezoelectric transducer led to HAM which outlined favourable output if array was larger arrays than 1 m^2. Empirical data gathered gives similar power output in comparison to the simulated data values, which validates HAM with small deviations. The model shows a small sized prototype device that can produce up approximately 0.06 µW of average power in comparison to the experimental value of 0.05 µW. HAM output loses the finer details of interconnecting units and therefore does not account for losses such as diodes used in the rectifying circuit. As the size of the array is increased the power output can be increased based on the empirical model developed using an off-the-shelf commercial piezoelectric transducer.

Figure 6.11 shows the parameters of HAM developed which takes into account two groups of parameters; rainstorm type and type of harvester used. It is understood the storm type cannot be adapted as this a naturally occurring phenomenon but characterisation of a different type of piezoelectric transducer can be done to model such a harvesting system to give us power characteristics. In this research a model was developed based on a piezoelectric transducer and several rainstorm power output characteristics have been presented that could be used for different applications.

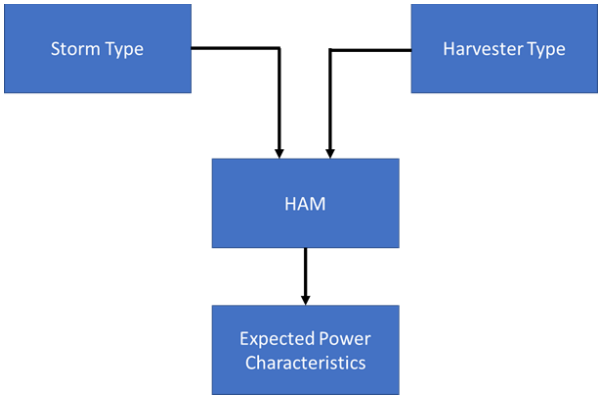

Figure 6.11: Proposed use of HAM

6.5.3 Power Output Comparison

Over the course of this research, various experimental work was carried out to understand the output characteristics of a piezoelectric transducer using a PVDF film. The average power values may have been low, but this has been the result of shorter time periods. The

maximum duration for which data was captured was of 2.5 seconds time period. It is proposed if the measurement capability could have been enhanced, this would have provided opportunities to expand this research and capture data for much longer time periods to fully establish the usefulness of REH devices. Table 6.5 outlines three significant approaches to harvest where the diameter of droplet, impact height and resistive load are kept consistent.

Table 6.5 : Power output of the research study

Impact Mechanism	**Size**	**Mode**	***Power*** **(µW)**
Single piezoelectric transducer with single event	Cantilever, 25 ×13 ×0.25 mm	Non-rectified	P_{avg} = 2.5
Multiple piezoelectric transducers with single event	Cantilever, 25 ×13 ×0.25 mm	Rectified	P_{avg} = 3.6
Multiple piezoelectric transducers with multiple events	Cantilever array, 0.003 m^2	Rectified	P_{avg} = 0.05

$D_{drop} = 4\ mm, v = 2.13\ ms^{-1}\ and\ h = 47\ cm$

It was noted empirically, the maximum mean power output was attained with a set-up that only had one device and one droplet impact at a precise region on the piezoelectric transducer. Such controlled experiments may offer higher outputs but deviate from the real rain experiments. Average power output relatively decreased with new approaches that were expected to give higher output values. The contributing factors towards this decline are due to the following reasons:

- Degradation of the samples used for harvesting system developed.
- There are a lot more water droplets present in this experimental stage for the prototype in this Chapter than previous experiments conducted.
- Rectifying circuit also plays a small part in voltage drop ultimately affecting the power output and performance.

One of the limitations of this study was the use of an off-the-shelf commercially available piezoelectric transducer, which had an active layer of PVDF. Although PVDF has been

one of the most viable options to use as an active material to harvest power, there are other composites being fabricated that have better properties and fabricating such new devices was beyond the scope of this study. Most harvesting systems utilise the bending strain of cantilever beams at resonance condition to generate electrical power using piezoelectric materials, therefore the resonance is high and the bandwidth too narrow. As this research used an off-the-shelf transducer for experimental work, several readings were taken to ensure consistency. All transducers were individually checked by performing single impact experimental tests on region 1 with a 1 MΩ load to ensure the response was similar before they were connected in an array in the prototype.

.

CHAPTER 7

7 Conclusion

This chapter gives an overview of PEH using water droplet impacts and a summary of research outcomes. This section concludes with a way forward for this research to improve the efficiency and performance of water droplet impact harvesters.

7.1 Achievements

Precipitation is a freely available source of mechanical energy, occurring mainly in the form of low-energy water drops. This work investigates the design analysis of a piezoelectric system capable of converting the mechanical energy generated by the impact of water drops into electrical energy. The system is not designed for any specific rain type and responds to the whole range of raindrops.

This study focused on experimental validation using an off-the-shelf commercial piezoelectric transducer to harvest power using water droplets, and the results were published as scientific contribution:

- Journal 1 showcased significant work carried out in the form of features demonstrated by impact and decay stage with oscillatory characters, and an energy harvesting model in MATLAB to simulate single device and an array of harvesters.
- Journal 2 showcased techniques to identify the efficiency of the impact mechanism, mechano-electric conversion mechanism, and presented an optimum arrangement for a single PEH device.
- Journal 3 aims to showcase the performance of a prototype device and mathematical explanations of the measurement system of the harvester to predict optimum parameters for such a device.

The published articles have been regularly cited by various other researchers [60, 89, 106, 175, 176] conducting studies within the field of PEH using water droplet impacts and some included over review of PEH harvesters in a different context [177-181] rather than raindrops. Over the recent years, there has been a handful of studies conducted on scavenging energy from PEH devices by the impact of raindrops or water droplets.

Literature has been reviewed for mechanical to electrical generators, raindrop energy harvesting and provides an overview of current harvesters.

Background in piezoelectricity has been presented, materials used for fabricating PEH devices and a developed a simple model for the harvester which was later revised based on the empirical data collected.

- Material Selection
- Simple model of PEH (mechanical and electrical)
- Rectifying circuit selection

7.1.1 Investigation of a Single PEH Device

Initial analysis has been conducted on the impact of water droplets on a piezoelectric transducer after having been released from various heights to replicate a rain shower. The initial impact showed the deflection of the transducer (active area with piezoelectric material).

The detailed voltage output profile from the piezoelectric transducer shows two distinct stages; log growth and exponential decay. The growth stage during the droplet impact process, followed by a decay stage (as stored energy in the harvester is dissipated), with an oscillatory character to the harvesting event of an impact. The impact stage lasts for a significant time period when compared to the duration of the entire harvesting event (0.0036 s). Peak power found was approximately 16 μW. The mean power of the decay stage is around 30% smaller than the growth stage which has a significant contribution to the overall output of the PEH device. The maximum mean power of 2.5 μW was attained at 2.13 m/s (for a height of 47 cm) for the piezoelectric transducer with an efficiency of approximately 0.12%.

Further experimental work was carried out with varying the angle of piezoelectric transducer and exploring the degradation of coupling multiple units. Region furthest away from the fixed position of the PEH device gave the maximum output as it causes maximum oscillatory movement with the device being at 90° angle (horizontal) to the droplet. The results were consistent with initial experimentation and varied between 4 – 18 µW.

7.1.2 Investigation of a Harvester Module

An energy harvesting module consisting of multiple piezoelectric transducers triggered by impact of water droplet to generate electrical power has been developed. Non-rectified and rectified modules were compared. The module arrangement was tested in such a way that only Unit 1 had a water droplet impact, whilst the other devices added in parallel did not undergo a water droplet impact. With an increase in the number of units, the non-rectified arrangement showed a decrease in peak power from 9 µW to 0.9 µW which showed the impact of coupling. The rectified arrangement resulted in a consistent power output of 3.6 µW.

The effect on the efficiency of the module with non-rectified or rectified outputs of each transducer connected in parallel was also investigated. A technique was found to separate the energy conversion efficiency of the impact mechanism (as the droplet interacts with the device) and the efficiency of the mechano-electric conversion mechanism (due to internal losses in the device). The impact mechanism energy was found to be 266 nJ and energy loss of mechano-electric conversion was found to be 51 nJ. The overall efficiency of non-rectified arrangement was found to be 0.67 %.

7.1.3 Investigation of Prototype Device

A prototype device was developed using several piezoelectric transducers used in previous experimental work. The prototype device was tested in replicated rain shower conditions (depicting a light rain shower) and units were impacted by water droplets. The average power output of the prototype device was measured around 0.05 µW over an array of 0.003 m^2 for a time period of 2.5 seconds.

A mathematical description is presented to predict the maximum power output of the prototype device. The distribution of events (number of events that produce power in comparison to a reference size of power) was plotted which showed a trend that exhibits

fractal behaviour (double PL). It is difficult to predict the number of hits (droplets that produce power) due to the random nature of rain. Therefore, estimate or prediction on the performance of the harvester design can be made based on these mathematical expressions. For an array of 0.003 m^2 it was estimated that the harvester system design of 19 µW for an upper limit.

Work carried out as part of this research only includes parallel connection of transducers, whereas it has been shown [182] that the output can be further enhanced by using mixed arrangement of series and parallel connections of piezoelectric transducer.

7.1.4 Harvester Array Model

A model was developed to characterise the output power for one piezoelectric transducer, which was then modified to simulate the performance of the harvester with an array of units. HAM was based on the empirical data gathered, and a relationship between the peak voltage and water droplet impact velocity was deduced based on a numerical method (relating the height and impact velocity). At a height of 47 cm (max height attained in the experimental setup) with an array of harvesters covering 1 m^2 of the active area, the model predicted up to 160 mW or 3.5 W for an array size of 100 m^2.

HAM simulations were compared to experimental data gathered by testing the prototype device and the results were consistent. For an array area of 0.003 m^2, HAM simulations found the power output value at 0.062 µW which shows a deviation of 0.0012 µW. The empirical results further validate HAM which can be modified for various rain conditions. Power output is small but consistent with the findings of other researchers.

7.2 Objectives Achieved

The following objectives have been met over the course of this research.

- A detailed literature review was conducted on PEH using water droplet impacts which identified various gaps. Limitations were identified and experimental work was carried on that basis to develop a model and working prototype.

- Initial experimental work carried out was focused on understanding the behaviour of piezoelectric transducer using single water droplet and working out the efficiency of such a harvester.
- A harvesting model was developed based on empirical data collected for a single device and single event which could be simulated in MATLAB.
- Trials were conducted on single unit, module and prototype and the results were published in the form of two journal publications and one monograph. The two journals have inspired various researchers to explore the potential of harvesting energy using water droplet impacts.
- A model was presented that can provide small amounts of power based on a modest area size. The recommendation and future should be focused on a much larger array for useful energy

7.3 Future Work

REH is a fascinating field and the full potential of this ambient source is yet to be discovered. PEH devices used to harvest kinetic energy of the water droplets are mostly only able to generate power in the μW region. Due to limited budget for this research an off-the-shelf transducer was used that was good enough for the application of harvesting power through the impact of water droplets and did produce power output in the μW region. If more funding were available for this research, I would have liked to focus on four improvements:

i) Test chamber that was able to reach an impact height between 2 – 4 m to increase the impact velocity of droplets.
ii) Integration of laser precipitation counter to characterise the rainfall pattern and use of disdrometer to accurate measure the droplet diameter.
iii) Fabrication of cantilever beam using several off-the-shelf transducers and develop prototype beam using materials with enhanced characteristics.
iv) Use of novel interface circuits to rectify the output such as an active rectifier with a trigger circuit.

In order to get a better understanding of the energy harvesting behaviour of PEH devices, experiments could be repeated in a more systematic way. The outlined approach on the proposed experimental work is as following:

- Single drop on single device (repeated for different droplet sizes)
- Multiple drops on a single device (repeated for different droplet sizes)
- Single drop on up to two devices when connected in parallel and series
- Single drops on an array of devices when connected in parallel, series and mixed arrangement (series-parallel circuit)
- Multiple drops on an array of devices when connected in parallel, series and mixed arrangement

The following areas also present the future direction of this research:

Design Improvements

It is known that the presence of a tip mass at the end of a PEH device can increases the excitation or vibrations in the system, which could increase the output voltage. A raindrop harvester developed by adding a spoon like structure at the tip of the cantilever beam [183], such a design would ensure the water droplet impact would be as far from the fulcrum or pivot point of the cantilever beam at the end of a cantilever harvester demonstrating improvements in voltage generated. Figure 7.1 shows the prototype and schematic of a harvester system with spoon.

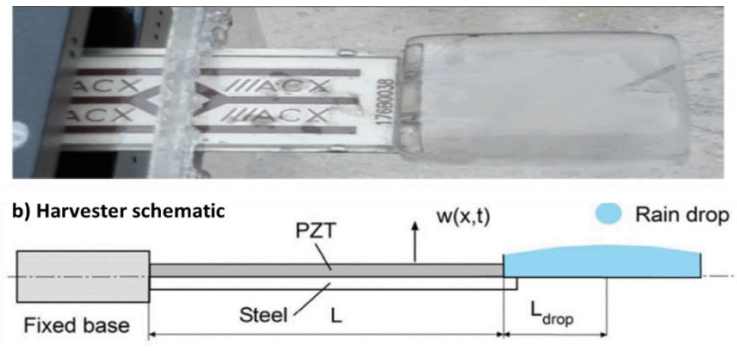

Figure 7.1: Harvester system with a spoon [184]

The design of such a system could include blocking off areas of the cantilever beam so water droplet impacts are aimed at the catchment area. Cantilever beams could be designed to be further away from each other, so that the droplets do not bounce from one harvester to the other as the excitation frequency of such bounced off impacts would be very low. The aim of this design enhancement is to improve the efficiency of the harvester as much as possible. Another design element could include not to use direct impact of

raindrops, instead rain could be collected and passed through a tank/reservoir that has been positioned at least 2 m from the ground. This arrangement could control the precise impacts on a cantilever beam for optimum output.

Further testing on Array of Harvesters

The array model has proven to showcase positive potential as the size of the array is increased. Therefore, the use of organic or lead-free composites would be ideal [185]. Further testing is required to try different arrangements, to improve the output with a focus on robust systems to measure the output. Mechanical design of the array is very important as multiple devices are excited they must be done so in phase otherwise that could have a detrimental impact on the power output as excitations might cancel each other out and therefor won't give the output need. A meshed model with multiple devices where cantilever beams are placed on the outside and central diaphragm in the middle to harvest the impact of water droplets highlight this issue. Figure 7.2 illustrates this design concept of a meshed model where care is taken in the mechanical design to ensure devices are excited in phase.

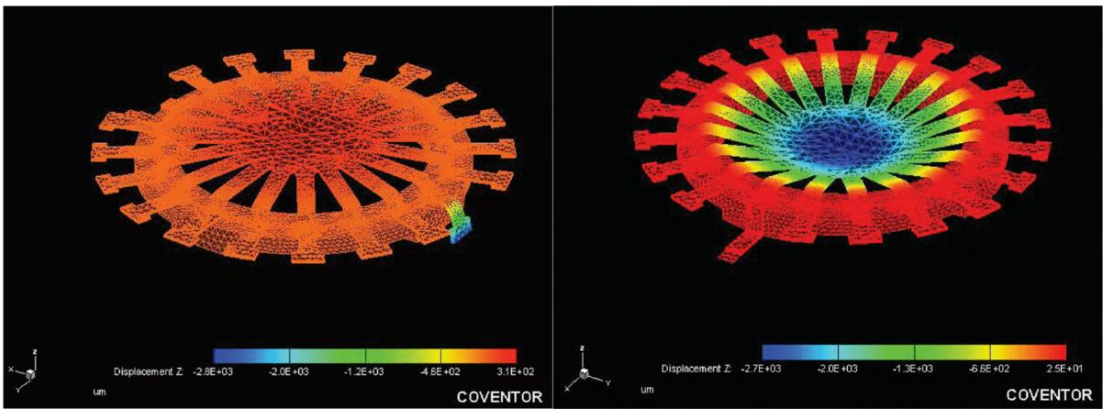

Figure 7.2: Large harvesting system with advanced Arduino-based measuring system [108]

REFERENCES

[1] P. D. Mitcheson, E. M. Yeatman, G. K. Rao, A. S. Holmes, and T. C. Green, "Energy harvesting from human and machine motion for wireless electronic devices," *Proceedings of the IEEE,* vol. 96, no. 9, pp. 1457-1486, 2008.

[2] M. A. Hannan, S. Mutashar, S. A. Samad, and A. Hussain, "Energy harvesting for the implantable biomedical devices: issues and challenges," *Biomedical Engineering Online,* vol. 13, no. 1, p. 79, 2014.

[3] G. Park, T. Rosing, M. D. Todd, C. R. Farrar, and W. Hodgkiss, "Energy harvesting for structural health monitoring sensor networks," *Journal of Infrastructure Systems,* vol. 14, no. 1, pp. 64-79, 2008.

[4] J. Lee and B. Choi, "Development of a piezoelectric energy harvesting system for implementing wireless sensors on the tires," *Energy Conversion and Management,* vol. 78, pp. 32-38, 2014.

[5] B. W. Cook, S. Lanzisera, and K. S. Pister, "SoC issues for RF smart dust," *Proceedings of the IEEE,* vol. 94, no. 6, pp. 1177-1196, 2006.

[6] Y. Chao, "Autonomous underwater vehicles and sensors powered by ocean thermal energy," in *OCEANS* Shanghai, 2016: IEEE, pp. 1-4.

[7] R. Murai *et al.*, "A novel visible light communication system for enhanced control of autonomous delivery robots in a hospital," in *2012 IEEE/SICE International Symposium on System Integration (SII)*, Fukuoka, 2012, pp. 510-516.

[8] F. Hossain *et al.*, "Self sustainable energy harvesting system," in *2018 IEEE Symposium on Computer Applications & Industrial Electronics (ISCAIE)*, 2018, pp. 59-64.

[9] M. Kiziroglou and E. Yeatman, "Materials and techniques for energy harvesting," in *Functional Materials for Sustainable Energy Applications*: Elsevier, 2012, pp. 541-572.

[10] Y. Tian and C.-Y. Zhao, "A review of solar collectors and thermal energy storage in solar thermal applications," *Applied energy,* vol. 104, pp. 538-553, 2013.

[11] A. A. F. Husain, W. Z. W. Hasan, S. Shafie, M. N. Hamidon, and S. S. Pandey, "A review of transparent solar photovoltaic technologies," *Renewable and Sustainable Energy Reviews,* vol. 94, pp. 779-791, 2018.

[12] H. Tang, X.-G. Tang, M.-D. Li, Q.-X. Liu, and Y.-P. Jiang, "Pyroelectric energy harvesting capabilities and electrocaloric effect in lead-free SrxBa1-xNb2O6 ferroelectric ceramics," *Journal of Alloys and Compounds,* vol. 791, pp. 1038-1045, 2019.

[13] M. Gao, C. Su, J. Cong, F. Yang, Y. Wang, and P. Wang, "Harvesting thermoelectric energy from railway track," *Energy,* vol. 180, pp. 315-329, 2019.

[14] K.-T. Park *et al.*, "Lossless hybridization between photovoltaic and thermoelectric devices," *Scientific Reports,* vol. 3, p. 2123, 2013.

[15] N. Wang, L. Han, H. He, N.-H. Park, and K. Koumoto, "A novel high-performance photovoltaic–thermoelectric hybrid device," *Energy & Environmental Science,* vol. 4, no. 9, pp. 3676-3679, 2011.

[16] W. Van Sark, "Feasibility of photovoltaic–thermoelectric hybrid modules," *Applied Energy,* vol. 88, no. 8, pp. 2785-2790, 2011.

[17] L. T. Nyamayoka, L. Zhang, and X. Xia, "Feasibility study of embedded piezoelectric generator system on a highway for street lights electrification," *Energy Procedia,* vol. 152, pp. 1015-1020, 2018.

[18] X. Xu, D. Cao, H. Yang, and M. He, "Application of piezoelectric transducer in energy harvesting in pavement," *International Journal of Pavement Research and Technology*, vol. 11, no. 4, pp. 388-395, 2018.
[19] D. Barkas, C. Psomopoulos, P. Papageorgas, K. Kalkanis, D. Piromalis, and A. Mouratidis, "Sustainable energy harvesting through triboelectric nano–generators: a review of current status and applications," *Energy Procedia*, vol. 157, pp. 999-1010, 2019.
[20] M. Cansiz, D. Altinel, and G. K. Kurt, "Efficiency in RF energy harvesting systems: A comprehensive review," *Energy*, 2019.
[21] T. Tan *et al.*, "Renewable energy harvesting and absorbing via multi-scale metamaterial systems for Internet of things," *Applied Energy*, vol. 254, p. 113717, 2019.
[22] R. Yang, Y. Qin, C. Li, G. Zhu, and Z. L. Wang, "Converting biomechanical energy into electricity by a muscle-movement-driven nanogenerator," *Nano Letters*, vol. 9, no. 3, pp. 1201-1205, 2009.
[23] H. Mutsuda, Y. Tanaka, Y. Doi, and Y. Moriyama, "Application of a flexible device coating with piezoelectric paint for harvesting wave energy," *Ocean Engineering*, vol. 172, pp. 170-182, 2019.
[24] Gov UK. "Climate Change Act 2008." http://www.legislation.gov.uk/ukpga/2008/27/pdfs/ukpga_20080027_en.pdf (accessed 9 May, 2018).
[25] Committee on Climate Change. "UK becomes first major economy to pass net zero emissions law." GOV UK. https://www.gov.uk/government/news/uk-becomes-first-major-economy-to-pass-net-zero-emissions-law (accessed 1 November, 2019).
[26] R. Schmalensee, T. M. Stoker, and R. A. Judson, "World carbon dioxide emissions: 1950–2050," *Review of Economics and Statistics*, vol. 80, no. 1, pp. 15-27, 1998.
[27] Committee on Climate Change. "Reducing UK emissions: 2019 Progress Report to Parliament." https://www.theccc.org.uk/publication/reducing-uk-emissions-2019-progress-report-to-parliament/ (accessed 4 March, 2019).
[28] P. Biswas *et al.*, "Harnessing raindrop energy in Bangladesh," in *Proceedings of the International conference on mechanical engineering*, Dhaka, 2009.
[29] Met Office. "UK temperature, rainfall and sunshine time series." https://www.metoffice.gov.uk/research/climate/maps-and-data/uk-temperature-rainfall-and-sunshine-time-series (accessed 10 July 2019).
[30] The Commonwealth. "Member Countries: United Kingdom." https://thecommonwealth.org/our-member-countries/united-kingdom (accessed 15 July 2019.
[31] Centre for Atmospheric Science. "Cloud Classification." The University of Manchester. http://www.cas.manchester.ac.uk/resactivities/cloudphysics/background/classification/ (accessed 10 July, 2019).
[32] G. Montero-Martínez and F. García-García, "On the behaviour of raindrop fall speed due to wind," *Quarterly Journal of the Royal Meteorological Society*, vol. 142, no. 698, pp. 2013-2020, 2016.
[33] M. Raju and M. Grazier, "ULP meets energy harvesting," 2012. Accessed: 10 June 2017 [Online]. Available: https://www.mouser.cn/pdfDocs/TI-ULP-meets-energy-harvesting-A-game-changing-combination-for-design-engineers.pdf

[34] B. H. Calhoun *et al.*, "Design considerations for ultra-low energy wireless microsensor nodes," *IEEE Transactions on Computers*, vol. 54, no. 6, pp. 727-740, 2005.
[35] A. Hajati and S.-G. Kim, "Ultra-wide bandwidth piezoelectric energy harvesting," *Applied Physics Letters*, vol. 99, no. 8, p. 083105, 2011.
[36] R. Vullers, R. van Schaijk, I. Doms, C. Van Hoof, and R. Mertens, "Micropower energy harvesting," *Solid-State Electronics*, vol. 53, no. 7, pp. 684-693, 2009.
[37] P. Harrop. "Energy harvesting: off-grid microwatt to megawatt 2017-2027." IDTechEx Research. https://www.idtechex.com/en/research-report/energy-harvesting-microwatt-to-megawatt-2019-2029/615 (accessed 10 June, 2018).
[38] Z. L. Wang, "Towards self-powered nanosystems: from nanogenerators to nanopiezotronics," *Advanced Functional Materials*, vol. 18, no. 22, pp. 3553-3567, 2008.
[39] K. H. Kim, F. Cottone, S. Goyal, and J. Punch, "Energy scavenging for energy efficiency in networks and applications," *Bell Labs Technical Journal*, vol. 15, no. 2, pp. 7-29, 2010.
[40] S. Roundy, P. K. Wright, and J. M. Rabaey, "Energy scavenging for wireless sensor networks with special focus on vibrations," Springer, 2003, pp. 45-47.
[41] T. J. Kazmierski and S. Beeby, *Energy harvesting systems*. Springer, 2014.
[42] M. Soliman, E. El-Saadany, and R. Mansour, "Electromagnetic MEMS based micro-power generator," in *2006 IEEE International Symposium on Industrial Electronics*, 2006, vol. 4: IEEE, pp. 2747-2753.
[43] E. K. Reilly, F. Burghardt, R. Fain, and P. Wright, "Powering a wireless sensor node with a vibration-driven piezoelectric energy harvester," *Smart Materials and Structures*, vol. 20, no. 12, p. 125006, 2011.
[44] S. Trolier-McKinstry and P. Muralt, "Thin film piezoelectrics for MEMS," *Journal of Electroceramics*, vol. 12, no. 1-2, pp. 7-17, 2004.
[45] G. Ottman, A. Bhatt, H. Hofmann, and G. Lesieutre, "Adaptive piezoelectric energy harvesting circuit for wireless, remote power supply," in *IEEE Transactions on Power Electronics*, 2002, vol. 17, no. 5, pp. 669-676.
[46] E. Zakar, "MEMS piezo pressure sensor for military applications," Defense Technical Information Center, 2004. Accessed: 1 January 2017. [Online]. Available: https://apps.dtic.mil/dtic/tr/fulltext/u2/a433154.pdf
[47] H. A. Tilmans, "Equivalent circuit representation of electromechanical transducers: I. Lumped-parameter systems," *Journal of Micromechanics and Microengineering*, vol. 6, no. 1, p. 157, 1996.
[48] I. Lipscomb, P. Weaver, J. Swingler, and J. McBride, "The effect of relative humidity, temperature and electrical field on leakage currents in piezo-ceramic actuators under dc bias," *Sensors and Actuators A: Physical*, vol. 151, no. 2, pp. 179-186, 2009.
[49] I. Lipscomb, P. Weaver, J. Swingler, and J. McBride, "Micro-computer tomography—An aid in the investigation of structural changes in lead zirconate titanate ceramics after temperature-humidity bias testing," *Journal of electroceramics*, vol. 23, no. 1, p. 72, 2009.
[50] W. S. Jung *et al.*, "Powerful curved piezoelectric generator for wearable applications," *Nano Energy*, vol. 13, pp. 174-181, 2015.
[51] Y. Xin *et al.*, "Shoes-equipped piezoelectric transducer for energy harvesting: A brief review," *Ferroelectrics*, vol. 493, no. 1, pp. 12-24, 2016.

[52] N. J. Ramer, T. Marrone, and K. A. Stiso, "Structure and vibrational frequency determination for α-poly (vinylidene fluoride) using density-functional theory," *Polymer,* vol. 47, no. 20, pp. 7160-7165, 2006.
[53] S. Roundy and P. K. Wright, "A piezoelectric vibration based generator for wireless electronics," *Smart Materials and Structures,* vol. 13, no. 5, p. 1131, 2004.
[54] D. F. Berdy, P. Srisungsitthisunti, X. Xu, J. Rhoads, B. Jung, and D. Peroulis, "Compact low frequency meandered piezoelectric energy harvester," *Proc. PowerMEMS,* pp. 71-74, 2009.
[55] S. Suraprapapich, S. Thainoi, S. Kanjanachuchai, and S. Panyakeow, "Quantum dot integration in heterostructure solar cells," *Solar Energy Materials and Solar Cells,* vol. 90, no. 18-19, pp. 2968-2974, 2006.
[56] J. Chen, Z. Yan, and L. Wu, "The influence of Thomson effect on the maximum power output and maximum efficiency of a thermoelectric generator," *Journal of applied physics,* vol. 79, no. 11, pp. 8823-8828, 1996.
[57] K. A. Cook-Chennault, N. Thambi, and A. M. Sastry, "Powering MEMS portable devices—a review of non-regenerative and regenerative power supply systems with special emphasis on piezoelectric energy harvesting systems," *Smart Materials and Structures,* vol. 17, no. 4, 2008.
[58] S. W. Freiman and G. S. White, "Intelligent ceramic materials: issues of brittle fracture," *Journal of intelligent material systems and structures,* vol. 6, no. 1, pp. 49-54, 1995.
[59] S. Roundy, P. K. Wright, and J. Rabaey, "A study of low level vibrations as a power source for wireless sensor nodes," *Computer Communications,* vol. 26, no. 11, pp. 1131-1144, 2003.
[60] K. G. Chua, Y. F. Hor, and H. C. Lim, "Raindrop kinetic energy piezoelectric harvesters and relevant interface circuits: review, issues and outlooks," *Sensors & Transducers,* vol. 200, no. 5, pp. 1-15, 2016.
[61] T. Young, "Philosophical Transactions of the Royal Society," 1805.
[62] P. S. Laplace and P. Simon, "Théorie analytique des probabiletés," (in French), *Oeuvres de Laplace,* vol. 7, no. 6, 1847.
[63] J. S. Rowlinson and B. Widom, *Molecular Theory of Capillarity* Dover Publications, 2002.
[64] D. Quéré, "Non-sticking drops," *Reports on Progress in Physics,* vol. 68, no. 11, p. 2495, 2005.
[65] K. Y. Law, "Definitions for hydrophilicity, hydrophobicity, and superhydrophobicity: getting the basics right," *Physical Chemistry Letters,* vol. 5, no. 4, 2014.
[66] S. Wang and L. Jiang, "Definition of superhydrophobic states," *Advanced Materials,* vol. 19, pp. 3423-3424, 2007.
[67] K. Perera, B. Sampath, V. Dassanayake, and B. Hapuwatte, "Harvesting of kinetic energy of the raindrops," *International Journal of Energy and Power Engineering,* vol. 8, no. 2, pp. 325-330, 2014.
[68] M. Rein, *Drop-surface interactions*. Springer, 2014.
[69] C. Stow and M. Hadfield, "An experimental investigation of fluid flow resulting from the impact of a water drop with an unyielding dry surface," *Proceedings of the Royal Society of London A,* vol. 373, pp. 419-441, 1981.
[70] C. Mundo, M. Sommerfeld, and C. Tropea, "Droplet-wall collisions: experimental studies of the deformation and breakup process," *International journal of multiphase flow,* vol. 21, no. 2, pp. 151-173, 1995.

[71] C. Josserand and S. Zaleski, "Droplet splashing on a thin liquid film," *Physics of fluids,* vol. 15, no. 6, pp. 1650-1657, 2003.
[72] Š. Šikalo, M. Marengo, C. Tropea, and E. Ganić, "Analysis of impact of droplets on horizontal surfaces," *Experimental Thermal and Fluid Science,* vol. 25, no. 7, pp. 503-510, 2002.
[73] Š. Šikalo, C. Tropea, and E. Ganić, "Impact of droplets onto inclined surfaces," *Journal of Colloid and Interface Science,* vol. 286, no. 2, pp. 661-669, 2005.
[74] C. Josserand and S. T. Thoroddsen, "Drop impact on a solid surface," *Annual review of fluid mechanics,* vol. 48, pp. 365-391, 2016.
[75] S. Gart, J. E. Mates, C. M. Megaridis, and S. Jung, "Droplet impacting a cantilever: A leaf-raindrop system," *Physical Review Applied,* vol. 3, no. 4, p. 044019, 2015.
[76] P. B. Weisensee, J. Tian, N. Miljkovic, and W. P. King, "Water droplet impact on elastic superhydrophobic surfaces," *Scientific Reports,* vol. 6, p. 30328, 2016.
[77] J. Field, P. Davies, and M. Lesser, "Theoretical and experimental studies of two-dimensional liquid impact," in *5th International Conference on Erosion by Liquid and Solid Impact,* Cambridge, 1979.
[78] E. J. Davis, S. Zhang, J. H. Fulton, and R. Periasamy, "Measurement of the aerodynamic drag force on single aerosol particles," *Aerosol Science and Technology,* vol. 6, no. 3, pp. 273-287, 1987.
[79] D. G. Aboud and A. M. Kietzig, "Splashing threshold of oblique droplet impacts on surfaces of various wettability," *Langmuir,* vol. 31, no. 36, pp. 10100-10111, 2015.
[80] S. Warude, P. Unhale, S. Khandagale, A. Waykar, and S. Gaonkar, "Harnessing of Kinetic Energy of Raindrops," *International Journal of Recent Research in Civil and Mechanical Engineering,* vol. 2, no. 1, pp. 192-199, 2015.
[81] D. Soto, A. B. De Lariviere, X. Boutillon, C. Clanet, and D. Quéré, "The force of impacting rain," *Soft Matter,* vol. 10, no. 27, pp. 4929-4934, 2014.
[82] M. Nearing, J. Bradford, and R. Holtz, "Measurement of force vs. time relations for waterdrop impact," *Soil Science Society of America Journal,* vol. 50, no. 6, pp. 1532-1536, 1986.
[83] J. Li, B. Zhang, P. Guo, and Q. Lv, "Impact force of a low speed water droplet colliding on a solid surface," *Journal of Applied Physics,* vol. 116, no. 21, p. 214903, 2014.
[84] S. A. Orr and H. Viles, "Characterisation of building exposure to wind-driven rain in the UK and evaluation of current standards," *Journal of Wind Engineering and Industrial Aerodynamics,* vol. 180, pp. 88-97, 2018.
[85] R. A. Houze Jr, "Stratiform precipitation in regions of convection: A meteorological paradox?," *Bulletin of the American Meteorological Society,* vol. 78, no. 10, pp. 2179-2196, 1997.
[86] Y. Chen, J. L. An, H. Z. Liu, and J. Duan, "An observational study on vertical raindrop size distributions during stratiform rain in a semiarid plateau climate zone," *Atmospheric and Oceanic Science Letters,* vol. 9, no. 3, pp. 178-184, 2016.
[87] J. S. Mandeep, R. Nalinggam, and W. Ismai, "Cumulative distribution of rainfall data for tropical countries," *Scientific Research and Essays,* vol. 6, no. 2, pp. 447-452, 2011.
[88] H. Y. Lam, L. Luini, J. Din, C. Capsoni, and A. D. Panagopoulos, "Investigation of rain attenuation in equatorial Kuala Lumpur," *IEEE Antennas and Wireless Propagation Letters,* vol. 11, pp. 1002-1005, 2012.

[89] V. K. Wong, J. H. Ho, and A. B. Chai, "Performance of a piezoelectric energy harvester in actual rain," *Energy*, vol. 124, pp. 364-371, 2017.
[90] S. Lovejoy and D. Schertzer, "Fractals, raindrops and resolution dependence of rain measurements," *Journal of Applied Meteorology*, vol. 29, no. 11, pp. 1167-1170, 1990.
[91] C. Brown and L. Liebovitch, *Fractal analysis*. Sage, 2010.
[92] A. Clauset, C. R. Shalizi, and M. E. Newman, "Power-law distributions in empirical data," *SIAM review*, vol. 51, no. 4, pp. 661-703, 2009.
[93] M. E. Newman, "Power laws, Pareto distributions and Zipf's law," *Contemporary Physics*, vol. 46, no. 5, pp. 323-351, 2005.
[94] H. Bulut, Y. Pandir, and S. Tuluce Demiray, "Exact solutions of nonlinear Schrodinger's equation with dual power-law nonlinearity by extended trial equation method," *Waves in Random and Complex Media*, vol. 24, no. 4, pp. 439-451, 2014.
[95] C. M. Pinto, A. M. Lopes, and J. T. Machado, "Double power laws, fractals and self-similarity," *Applied Mathematical Modelling*, vol. 38, no. 15-16, pp. 4019-4026, 2014.
[96] J. Laherrere, "Parabolic fractal distributions in nature," *Academy of Sciences: Earth and Planetary Sciences*, vol. 322, pp. 535-542, 1996.
[97] S.-Y. Xie, Y.-G. Yang, Z.-Y. Bao, X.-Z. Ke, and X.-L. Liu, "Mineral resource analysis by parabolic fractals," *Mining Science and Technology (China)*, vol. 19, no. 1, pp. 91-96, 2009.
[98] B. Lavi and A. Marmur, "The exponential power law: partial wetting kinetics and dynamic contact angles," *Colloids and Surfaces A: Physicochemical and Engineering Aspects*, vol. 250, no. 1-3, pp. 409-414, 2004.
[99] L. Mattar and S. Moghadam, "Modified power law exponential decline for tight gas," in *Canadian International Petroleum Conference*, Calgary, 2009.
[100] Y. Chen, "Power-law distributions based on exponential distributions: Latent scaling, spurious Zipf's law, and fractal rabbits," *Fractals*, vol. 23, no. 02, p. 1550009, 2015.
[101] R. Guigon, J.-J. Chaillout, T. Jager, and G. Despesse, "Harvesting raindrop energy: theory," *Smart Materials and Structures*, vol. 17, no. 1, 2008.
[102] R. Guigon, J.-J. Chaillout, T. Jager, and G. Despesse, "Harvesting raindrop energy: experimental study," *Smart Materials and Structures*, vol. 17, no. 1, 2008.
[103] F. Viola, P. Romano, R. Miceli, and G. Acciari, "On the harvest of rainfall energy by means of piezoelectric transducer," in *2013 International Conference on Renewable Energy Research and Applications (ICRERA)*, Madrid, 2013: IEEE, pp. 1133-1138.
[104] F. Viola, P. Romano, R. Miceli, G. Acciari, and C. Spataro, "Piezoelectric model of rainfall energy harvester," in *2014 Ninth International Conference on Ecological Vehicles and Renewable Energies (EVER)*, Monte-Carlo, 2014, pp. 1-7.
[105] C. Spataro, F. Viola, P. Romano, and R. Miceli, "Performances of rainfall energy harvester," in *Proceedings of the 20th IMEKO TC4 International Symposium and 18th International Workshop on ADC Modelling and Testing Research on Electric and Electronic Measurement for the Economic Upturn, Benevento, Italy*, 2014, pp. 15-17.
[106] F. Viola, "Comparison among different rainfall energy harvesting structures," *Applied Sciences*, vol. 8, no. 6, p. 955, 2018.

[107] N. M. Nayan, M. F. Razaka, A. Ali, S. K. Mazalan, A. N. N. Abdullaha, and N. H. Rahmana, "Development of rain harvester using piezoelectric sensor," in *International conference on power, energy and communication systems, Perlis*, 2015.

[108] W. Chin-Hong, Z. Dahari, A. A. Manaf, O. Sidek, M. A. Miskam, and J. J. Mohamed, "Simulation of piezoelectric raindrop energy harvester," in *IEEE 2013 Tencon-Spring*, Sydney, 2013, pp. 465-469.

[109] V.-K. Wong, J.-H. Ho, E. H. Yap, and A. B. Chai, "Dynamics of a piezoelectric energy harvester in a simulated rain environment," *Proceedings of the Institution of Mechanical Engineers, Part C: Journal of Mechanical Engineering Science*, vol. 232, no. 15, pp. 2642-2654, 2018.

[110] X. Shan, R. Song, B. Liu, and T. Xie, "Novel energy harvesting: A macro fiber composite piezoelectric energy harvester in the water vortex," *Ceramics International*, vol. 41, pp. 763-767, 2015.

[111] R. Song, X. Shan, F. Lv, and T. Xie, "A study of vortex-induced energy harvesting from water using PZT piezoelectric cantilever with cylindrical extension," *Ceramics International*, vol. 41, pp. 768-773, 2015.

[112] M. Al Ahmad, "Piezoelectric water drop energy harvesting," *Journal of electronic materials*, vol. 43, no. 2, pp. 452-458, 2014.

[113] M. Lallart, S. Priya, S. Bressers, and D. J. Inman, "Small-scale piezoelectric energy harvesting devices using low-energy-density sources," *Journal of the Korean Physical Society*, vol. 57, no. 41, pp. 947-951, 2010.

[114] Y. Miao and Y. Jia, "Hybrid decentralised energy for remote communities: case studies and the analysis of the potential integration of rain energy," *Journal of Sustainable Development of Energy, Water and Environment Systems*, vol. 2, no. 3, pp. 243-258, 2014.

[115] A. Tinaikar, "Harvesting energy from rainfall," *International Journal of Sustainable and Green Energy*, vol. 2, no. 3, p. 130, 2014.

[116] Z. Lai *et al.*, "A hybrid piezo-dielectric wind energy harvester for high-performance vortex-induced vibration energy harvesting," *Mechanical Systems and Signal Processing*, vol. 150, p. 107212.

[117] A. S. Grinspan and R. Gnanamoorthy, "Impact force of low velocity liquid droplets measured using piezoelectric PVDF film," *Colloids and Surfaces A: Physicochemical and Engineering Aspects*, vol. 356, no. 1-3, pp. 162-168, 2010.

[118] D. Vatansever, R. Hadimani, T. Shah, and E. Siores, "An investigation of energy harvesting from renewable sources with PVDF and PZT," *Smart Materials and Structures*, vol. 20, no. 5, p. 055019, 2011.

[119] M. Al Ahmad and G. E. Jabbour, "Electronically droplet energy harvesting using piezoelectric cantilevers," *Electronics letters*, vol. 48, no. 11, pp. 647-649, 2012.

[120] T. Alkhaddeim, B. AlShujaa, W. AlBeiey, F. AlNeyadi, and M. Al Ahmad, "Piezoelectric energy droplet harvesting and modeling," in *SENSORS, 2012 IEEE*, 2012: IEEE, pp. 1-4.

[121] L. Valentini, S. B. Bon, and J. Kenny, "Liquid droplet excitation of freestanding poly (methyl methacrylate)/graphene oxide films for mechanical energy harvesting," *Journal of Polymer Science Part B: Polymer Physics*, vol. 51, no. 13, pp. 1028-1032, 2013.

[122] F. Viola, P. Romano, R. Miceli, and G. Acciari, "Harvesting rainfall energy by means of piezoelectric transducer," in *2013 International Conference on Clean Electrical Power (ICCEP)*, Alghero, 2013, pp. 634-639.

[123] M. A. Ilyas and J. Swingler, "Piezoelectric energy harvesting from raindrop impacts," *Energy*, vol. 90, pp. 796-806, 2015.
[124] M. A. Ilyas and J. Swingler, "Towards a prototype module for piezoelectric energy harvesting from raindrop impacts," *Energy*, vol. 125, pp. 716-725, 2017.
[125] D. Zakharov *et al.*, "Combined pyroelectric, piezoelectric and shape memory effects for thermal energy harvesting," in *Journal of Physics: Conference Series*, 2013, vol. 476, no. 1, p. 012021.
[126] A. Ballato, "Piezoelectricity: history and new thrusts," in *Proc.1996 IEEE Ultrasonics Symposium*, 1996, vol. 1: IEEE, pp. 575-583.
[127] C. Jacques and C. Pierre, "Development, via compression, of electric polarization in hemihedral crystals with inclined faces," *Bull. Soc. Minérologique Fr*, vol. 3, pp. 90-3, 1880.
[128] J. Curie and P. Curie, "Contractions and expansions produced by voltages in hemihedral crystals with inclined faces," *Comptes Rendus*, vol. 93, pp. 1137-1140, 1881.
[129] A. Arnau and D. Soares, "Fundamentals of piezoelectricity," in *Piezoelectric transducers and applications*: Springer, 2009, pp. 1-38.
[130] "Piezoelectric Fundamentals." Sensor Technology Ltd. https://sensortechcanada.com/technical-notes/piezoelectric-fundamentals/ (accessed 25 November, 2019).
[131] J. G. Rocha, L. M. Goncalves, P. Rocha, M. P. Silva, and S. Lanceros-Mendez, "Energy harvesting from piezoelectric materials fully integrated in footwear," *IEEE Transactions on Industrial Electronics*, vol. 57, no. 3, pp. 813-819, 2009.
[132] Measurements Specialties. "Piezo Film Sensors Technical Manual." https://www.sparkfun.com/datasheets/Sensors/Flex/MSI-techman.pdf (accessed 16 September, 2018).
[133] N. S. Shenck and J. A. Paradiso, "Energy scavenging with shoe-mounted piezoelectrics," *IEEE micro*, no. 3, pp. 30-42, 2001.
[134] "IEEE standard on piezoelectricity," in *ANSI/IEEE Std 176-1987*, 1988.
[135] G. H. Haertling, "Ferroelectric ceramics: history and technology," *Journal of the American Ceramic Society*, vol. 82, no. 4, pp. 797-818, 1999.
[136] A. Koszewnik, P. Grześ, and W. Walendziuk, "Mechanical and electrical impedance matching in a piezoelectric beam for energy harvesting," *The European Physical Journal Special Topics*, vol. 224, no. 14-15, pp. 2719-2731, 2015.
[137] G. L. Wojcik, D. Vaughan, N. Abboud, and J. J. Mould, "Electromechanical modeling using explicit time-domain finite elements," in *1993 Proceedings IEEE Ultrasonics Symposium*, Baltimore, 1993, vol. 2: IEEE, pp. 1107-1112.
[138] B. Malič, D. Kuščer, M. Vrabelj, and J. Koruza, "Review of methods for powder-based processing," in *Magnetic, ferroelectric, and multiferroic metal oxides*: Elsevier, 2018, pp. 95-120.
[139] Y. He, B. Bahr, M. Si, P. Ye, and D. Weinstein, "A tunable ferroelectric based unreleased RF resonator," *Microsystems & Nanoengineering*, vol. 6, no. 1, pp. 1-7, 2020.
[140] J. X. Zhang and K. Hoshino, "Chapter 6-Mechanical transducers: Cantilevers, acoustic wave sensors, and thermal sensors," *Molecular Sensors and Nanodevices Principles, Designs and Applications in Biomedical Engineering*, pp. 321-414, 2014.

[141] Y. Tian, G. Li, Z. Yi, J. Liu, and B. Yang, "A low-frequency MEMS piezoelectric energy harvester with a rectangular hole based on bulk PZT film," *Journal of Physics and Chemistry of Solids*, vol. 117, pp. 21-27, 2018.
[142] C. C. Bowland, M. H. Malakooti, and H. A. Sodano, "Barium titanate film interfaces for hybrid composite energy harvesters," *ACS applied materials & interfaces*, vol. 9, no. 4, pp. 4057-4065, 2017.
[143] G. D. Jones *et al.*, "Characterization, performance and optimization of PVDF as a piezoelectric film for advanced space mirror concepts," Citeseer, 2005.
[144] J. Y.-H. Kim, A. Cheng, and Y.-C. Tai, "Parylene-C as a piezoelectric material," in *2011 IEEE 24th International Conference on Micro Electro Mechanical Systems*, 2011: IEEE, pp. 473-476.
[145] A. Qaiss, H. Saidi, O. Fassi-Fehri, and M. Bousmina, "Cellular polypropylene-based piezoelectric films," *Polymer Engineering & Science*, vol. 52, no. 12, pp. 2637-2644, 2012.
[146] M. Ando, J. Endo, and H. Kawamura, "Display panel with pressure sensor and electronic device with pressing input function," US Patent 0338981, 2015.
[147] M. Ando. "Organic Piezoelectric Film Reshapes Sensor Features." Murata. https://www.murata.com/en-eu/about/newsroom/techmag/metamorphosis16/appnote/01 (accessed 2 January 2018).
[148] P. Ueberschlag, "PVDF piezoelectric polymer," *Sensor review*, 2001.
[149] B. Jaffe, *Piezoelectric ceramics*. Elsevier, 2012.
[150] H. J. Lee and D. A. Saravanos, "The effect of temperature dependent material nonlinearities on the response of piezoelectric composite plates," NASA, 1997. Accessed: 19 August 2018. [Online]. Available: https://ntrs.nasa.gov/citations/19980017194
[151] P. Weaver *et al.*, "The effects of porosity, electrode and barrier materials on the conductivity of piezoelectric ceramics in high humidity and dc electric field," *Smart Materials and Structures*, vol. 21, no. 4, p. 045012, 2012.
[152] C. A. Howells, "Piezoelectric energy harvesting," *Energy Conversion and Management*, vol. 50, no. 7, pp. 1847-1850, 2009.
[153] M. A. Ilyas, *Piezoelectric Energy Harvesting: Methods, Progress, and Challenges*. Momentum Press, 2018.
[154] S. Rajala and J. Lekkala, "Film-type sensor materials PVDF and EMFi in measurement of cardiorespiratory signals—A review," *IEEE Sensors Journal*, vol. 12, no. 3, pp. 439-446, 2010.
[155] A. Erturk and D. J. Inman, *Piezoelectric energy harvesting*. John Wiley & Sons, 2011.
[156] S. Mishra, L. Unnikrishnan, S. K. Nayak, and S. Mohanty, "Advances in piezoelectric polymer composites for energy harvesting applications: a systematic review," *Macromolecular Materials and Engineering*, vol. 304, no. 1, p. 1800463, 2019.
[157] J. Anjana, K. J. Prashanth, K. S. Asheesh, J. Arpit, and P. N. Rashmi, "Dielectric and piezoelectric properties of PVDF/PZT composites: a review," *Polymer Engineering & Science*, vol. 55, no. 7, pp. 1589-1616, 2015.
[158] B. Lin and V. Giurgiutiu, "Modeling and testing of PZT and PVDF piezoelectric wafer active sensors," *Smart Materials and Structures*, vol. 15, no. 4, p. 1085, 2006.
[159] L. Capineri, L. Masotti, V. Ferrari, D. Marioli, A. Taroni, and M. Mazzoni, "Comparisons between PZT and PVDF thick films technologies in the design of

low-cost pyroelectric sensors," *Review of scientific instruments*, vol. 75, no. 11, pp. 4906-4910, 2004.
[160] Y. Fenglin, M. Wengjun, Z. Jie, and Y. Hang, "Cantilver beam based piezoelectric energy harvester," *International Journal on Smart Sensing & Intelligent Systems*, vol. 8, no. 4, 2015.
[161] W. C. Young, R. G. Budynas, and A. M. Sadegh, *Roark's formulas for stress and strain*. McGraw-Hill New York, 2002.
[162] R. D. Blevins, "Formulas for natural frequency and mode shape," *The Journal of the Acoustical Society of America*, vol. 67, 1980.
[163] G. R. Prakash, M. V. Swamy, S. Huddar, and B. G. Sheeparamatti, "Study of Effect on Resonance Frequency of Piezoelectric Unimorph Cantilever for Energy Harvesting," in *Proceedings of the 2012 COMSOL*, Bangalore, 2012, vol. 2, no. 3, pp. 1-8.
[164] J. Y. Pyun, Y. H. Kim, S. W. Kwon, W. Y. Choi, and K. K. Park, "Comparison between Resonance and Non-Resonance type Piezoelectric Acoustic Absorbers," *Sensors*, vol. 20, no. 1, p. 47, 2020.
[165] R. Di Leo, M. Viscardi, G. Ferrini, and L. Lecce, "Preliminary theoretical study about a" Piezoelectric Shingle" for a piezoelectric energy harvesting system in presence of rain," in *Mathematical and Computational methods in Electrical Engineering "Proceedings of the 2th International Conference on Power and Energy, System, POES'15, Malta*, 2013.
[166] U. Tayyab and H. A. Alzaher, "A Self-Biased Active Voltage Doubler for Energy Harvesting Systems," *Active and Passive Electronic Components*, vol. 2017, 2017.
[167] A. A. Mustapha, K. Leong, and N. M. Ali, "Piezoelectric energy harvesting rectifying circuits comparison," *Journal of Engineering and Applied Sciences*, vol. 11, no. 10, pp. 6361-6365, 2016.
[168] D. Marinkovic, A. Frey, I. Kuehne, and G. Scholl, "A new rectifier and trigger circuit for a piezoelectric microgenerator," *Procedia Chemistry*, vol. 1, no. 1, pp. 1447-1450, 2009.
[169] Y. K. Ramadass and A. P. Chandrakasan, "An efficient piezoelectric energy harvesting interface circuit using a bias-flip rectifier and shared inductor," *IEEE Journal of Solid-State Circuits*, vol. 45, no. 1, pp. 189-204, 2009.
[170] B. F. Edwards, J. W. Wilder, and E. E. Scime, "Dynamics of falling raindrops," *European Journal of Physics*, vol. 22, no. 2, p. 113, 2001.
[171] Drinking Water Quality Regulator for Scotland. "Drinking Water Quality in Scotland 2012." Scottish Government. https://dwqr.scot/media/14226/dwqr-annual-report-2012.pdf (accessed 4 Feb, 2015).
[172] World Health Organization, "Nutrients in drinking water," Geneva, 7117242299, 2005. Accessed: 1 May 2019. [Online]. Available: https://www.who.int/water_sanitation_health/dwq/nutrientsindw.pdf
[173] N. Vargaftik, B. Volkov, and L. Voljak, "International tables of the surface tension of water," *Journal of Physical and Chemical Reference Data*, vol. 12, no. 3, pp. 817-820, 1983.
[174] S. Xu, J. Cui, and X. Ren, "Applied mechanics and engineering model on raindrops falling," in *2nd International Conference on Electronic & Mechanical Engineering and Information Technology (EMEIT)*, 2012, vol. 24.
[175] C. W. Chee, C.-H. Wong, and Z. Dahari, "An investigation of array of piezoelectric transducer for raindrop energy harvesting application," in *2016 IEEE Region 10 Conference (TENCON)*, Singapore, 2016: IEEE, pp. 3771-3774.

[176] C. H. Wong, Z. Dahari, M. H. Jumali, K. Mohamed, and J. J. Mohamed, "Simulation and fabrication of wagon-wheel-shaped piezoelectric transducer for raindrop energy harvesting application," *Journal of Electronic Materials,* vol. 46, no. 3, pp. 1587-1597, 2017.
[177] A. C. Turkmen and C. Celik, "Energy harvesting with the piezoelectric material integrated shoe," *Energy,* vol. 150, pp. 556-564, 2018.
[178] A. Jasim, H. Wang, G. Yesner, A. Safari, and A. Maher, "Optimized design of layered bridge transducer for piezoelectric energy harvesting from roadway," *Energy,* vol. 141, pp. 1133-1145, 2017.
[179] J. Kan, J. Fu, S. Wang, Z. Zhang, S. Chen, and C. Yang, "Study on a piezo-disk energy harvester excited by rotary magnets," *Energy,* vol. 122, pp. 62-69, 2017.
[180] X. Xie, A. Carpinteri, and Q. Wang, "A theoretical model for a piezoelectric energy harvester with a tapered shape," *Engineering Structures,* vol. 144, pp. 19-25, 2017.
[181] Z. Zhou, W. Qin, P. Zhu, and S. Shang, "Scavenging wind energy by a Y-shaped bi-stable energy harvester with curved wings," *Energy,* vol. 153, pp. 400-412, 2018.
[182] C.-H. Teoh, Z. Dahari, and I. Izrin, "A Study of the Output Voltage of the Asynchronous Raindrop for Piezoelectric Array Energy Harvester," in *10th International Conference on Robotics, Vision, Signal Processing and Power Applications*, 2019, pp. 327-332.
[183] A. Doria, C. Medè, D. Desideri, A. Maschio, L. Codecasa, and F. Moro, "On the performance of piezoelectric harvesters loaded by finite width impulses," *Mechanical Systems and Signal Processing,* vol. 100, pp. 28-42, 2018.
[184] A. Doria, G. Fanti, and F. Moro, "Response of a Piezoelectric Harvester to Impacts Generated by Rain-Drops," in *2019 Fourteenth International Conference on Ecological Vehicles and Renewable Energies (EVER)*, 2019: IEEE, pp. 1-9.
[185] T. R. Shrout and S. J. Zhang, "Lead-free piezoelectric ceramics: Alternatives for PZT," *Journal of Electroceramics,* vol. 19, no. 1, pp. 113-126, 2007.

APPENDICES

Appendix A

Distribution of events (power hits)

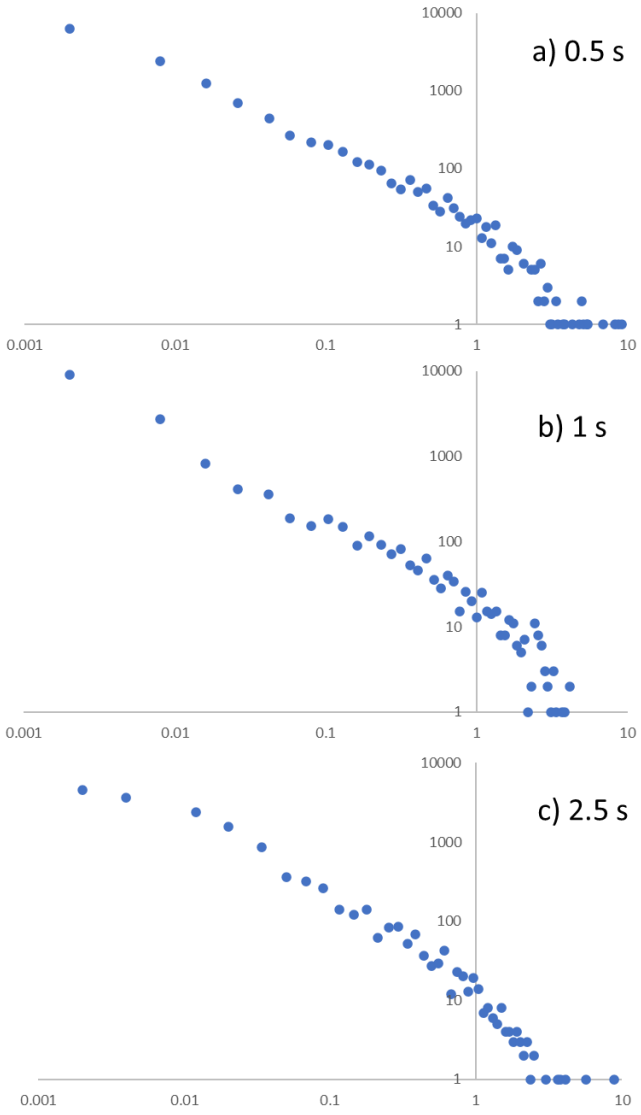

Distribution of power events